

Experimental study of hydrothermal alteration of volcanic rocks from the Volcanic Eifel

A. Abel¹, D. Sorger¹, T. Müller¹

¹*Geoscience Centre Göttingen, Georg-August-University, Germany
e-mail: angelina.abel@stud.uni-goettingen.de*

Hydrothermal alteration is known to cause intensive chemical and mineralogical changes in rocks driven by element fluxes between rock and infiltrating fluid depending on alteration conditions. Volume changes are commonly the result of mineral reactions associated with hydrothermal alteration and can lead to reaction-induced fracturing. In this experimental study we investigate the replacement of leucite by analcime in mafic rocks at near-surface hydrothermal conditions. The mineral reactions are shown to generate sufficient stresses to trigger fractures and even complete disintegration of the host rock depending on starting porosity and initial mineral modes. Tephritic and phonolitic foidites were collected in the Eifel Volcanic Fields in Western Germany. Both samples exhibit a porphyritic texture with clinopyroxene as dominant phenocrysts and a matrix consisting of clinopyroxene, feldspathoids and feldspar. The samples were reacted with a Na-K-Ca-Cl solution similar to seawater composition at 200 °C and 16 bars for intervals ranging from 1 to 8 weeks. Intact rock cores were placed into a batch reactor with fluid amounts twice their mass (W/R = 2). After the experiments, BSE and EDS measurements were used to identify and characterize reaction products and textures using a W-SEM. Samples were powdered and subsequently analysed with XRD including a Rietveld refinement for quantification. The cation concentrations in the reacted fluid were analysed by ICP-OES measurements. A replacement reaction of leucite by analcime was confirmed by both, SEM and XRD measurements. ICP-OES analyses reveal an increasing K^+ concentration in the fluid while Na^+ and Ca^{2+} concentrations decreased in contrast to the starting fluid. After 2 weeks of reaction, a steady state was reached for Na^+ , K^+ , and Ca^{2+} concentrations. No significant difference between the two starting materials could be measured for element fluxes between rock and fluid, but a variation in porosity increase was observed. In the phonolitic foidite, starting with lower porosity, complete disintegration of the rock formation was observed, while the tephritic foidite only showed reaction-induced fracturing. As the replacement reaction is associated with a 10 % increase in volume, crystallisation pressure lead to stresses that are potentially high enough for fracturing.

G.O.Joe: A new software for the evaluation and correction of LA-ICP-MS concentration data

F. Altenberger¹, T. Auer², J. Krause³, A. Auer², J. Berndt⁴

¹*Montanuniversität Leoben, Chair of Resource Mineralogy, Peter-Tunner-Straße 5, 8700 Leoben Austria*

²*Moonshot Pioneers GmbH, Dorfbeuern 35, 5152 Dorfbeuern, Salzburg, Austria*

³*Helmholtz Institute Freiberg for Resource Technology, Chemnitz Straße 40, 09599 Freiberg, Germany*

⁴*Westfälische Wilhelms-Universität Münster, Corrensstraße 24, 48149 Münster, Germany*

e-mail: florian.altenberger@unileoben.ac.at

Laser ablation-inductively coupled plasma-mass spectrometry (LA-ICP-MS) is widely used for spatially resolved measurements of the elemental and isotopic composition of solid materials. One of the problems of trace element analyses by LA-ICP-MS is the existence of interferences that cannot be resolved instrumentally. The software G.O.Joe was developed to calculate trace element concentrations in solid samples obtained by LA-ICP-MS analysis, offering several types of interference corrections. The software's algorithms are written in the Dart programming language within the Flutter programming environment and follow the procedure described in Jochum et al. (2006 and 2007). G.O.Joe operates online, allowing for immediate data evaluation. It efficiently processes large datasets, offering the flexibility to change parameters at any stage of the workflow. The software also includes features for uploading and storing multiple recovery files (.gojoe), thereby preserving the information from previously evaluated datasets.

A series of three self-instructive interfaces guide the user through a straightforward process of data evaluation. Clear visualization of raw data aids the evaluation of each measurement, facilitating the selection of background and sample signals. Concurrently, inclusions or mixed analyses can be excluded. The input of instrument settings and information about the reference material follows the data processing and is used to convert the isotope count rates to element concentrations. Importantly, advanced calculations can be applied to correct the measurements for isobaric or molecular interferences and abundance sensitivity. These essential advantages of G.O.Joe are demonstrated in different case studies that focus on the mineral chemistry of tungstates (i.e., scheelite) and silicates (e.g., garnet) including the relevant correction methods.

The exported result file (.xlsx) includes the calculated element concentrations, relevant statistical parameters, input data, and instrument settings, ensuring a transparent data processing. While G.O.Joe serves as a time-efficient, transparent, and easy-to-use tool for trace element analysis for experienced LA-ICP-MS users, it is also particularly appealing to newcomers to LA-ICP-MS data analysis. Notably, it is planned as non-commercial software and does not require installation. A first version of G.O.Joe is currently in the final stages of development and will be made available with further information at <https://www.gojoe.software>.

Jochum KP, Stoll B, Herwig K, Willbold M (2006): Improvement of in situ Pb isotope analysis by LA-ICP-MS using a 193 nm Nd:YAG laser. - J Analyt Atomic Spectrom 21, 666-675

Jochum KP, Stoll B, Herwig K, Willbold M (2007): Validation of LA-ICP-MS trace element analysis of geological glasses using a new solid-state 193 nm Nd:YAG laser and matrix-matched calibration. - J Analyt Atomic Spectrom 22, 112-121

Trace metals in hydrothermal magnetite – current knowledge, application, and experimental approaches

T. Angerer¹, R. Bakker², F. Melcher³

¹GeoSphere Austria, Department of Mineral Resources and Geoenery, Vienna

²Montanuniversität Leoben, Chair of Resource Mineralogy

³Montanuniversität Leoben, Chair of Geology and Economic Geology

e-mail: thomas.angerer@geosphere.at

Hydrothermal ore deposits host significant resources of iron and base, precious, and critical metals. In order to understand ore-forming hydrous fluid-rock interaction geoscientists analyse co-genetic mineral assemblages, fluid inclusions, elemental and isotopic geochemistry to approximate temperature, fO_2 , pH, and metal and ligand composition of hydrothermal fluids. Because the accessibility or applicability of measurable proxies is often limited in a given ore deposit, there is the need for other “recorders” of fluid-rock-interaction, preferentially ubiquitous, robust, and comfortably to analyse. In recent years, trace element abundances in magnetite have become a favourite study object due to its ability to robustly record complex fluid-rock interaction (Dupuis & Beaudoin 2011; Nadoll et al. 2014; Dare et al. 2014; Canil et al. 2016; Huang et al. 2018). The understanding of trace metal signatures has grown steadily, yet is far from being satisfactory. Here, the quantification of trace metal partitioning coefficients D between mineral and fluid as functions of system variables is a crucial requirement. For magnetite, empirical D' have been determined in numerous crystal/melt experimental studies, however, only a hand full of studies have dealt with trace metal partitioning in hydrothermal systems (e.g., Ilton & Eugster 1989; Lipko et al. 2020; Simon et al. 2006; Smagunov et al. 2021). In most published setups, experimental fluids were far away from representing natural ore-forming fluids, but designed to synthesise magnetite most efficiently. Metastudies for melt, metamorphic, or aqueous fluid systems reveal that magnetite D' values for given cations vary significantly (Dare et al. 2012; Dare et al. 2014; Nadoll et al. 2014; Nadoll et al. 2017). The present contribution provides an update on the use of magnetite chemistry, the present knowledge and experimental approaches, and introduces a new joint initiative to investigate hydrothermal magnetite.

In an FWF-funded 3-year postdoctoral project at GeoSphere Austria and Montanuniversität Leoben we are going to study systematically metal cation partitioning and fractionation in magnetite-rich high-T hydrothermal mineralisations. A multi-analytical approach will enable us to obtain and compare D' from hydrothermal magnetite from supercritical natural and synthetic samples. Magnetite synthesis from Fe-Si rich and trace metal doped chloride solutions can be archived in cold-seal Ni-steel autoclaves (Figure 1). Investigated systems comprise setups at ~1.5 kbar, 500-750 °C and various O_2 buffers (IM, MW, CCO, and MMO in outer capsules). Ore samples from similar systems will be selected to obtain complementary natural D' from magnetite and fluid inclusion chemistry in co-genetic transparent phases. To enhance the robustness of data, the competition for trace metals between magnetite and co-genetic phases such as silicates, sulfides, phosphates, and oxides will be considered, as well as any inter- and intra-grain chemical heterogeneity and solid inclusions at the micro- to nano-scale (Deditius et al. 2019, Verdugo-Ihl et al. 2021).

Building on the characterisation of co-existing mineral assemblages and fluid inclusions by petrography, EPMA, laser ablation ICPMS, microthermometry, and Raman spectroscopy, we plan following collaborative analyses: TEM petrography and ELNES with Liane Benning and Vladimir Roddatis from GFZ and Max Wilke from Uni Potsdam, SIMS O isotopes with

Etienne Deloule at CRPG-CNRS Nancy, fluid inclusion LA-ICPMS with Tobias Fußwinkel at RWTH Aachen, and alternative experimental setups with Bastian Joachim-Mrosko, Uni Innsbruck. We will select samples from own collections and from Robert Marschik, LMU Munich, and Christin Kehr, TU Freiberg.

Datasets from our holistic approach will provide an unprecedented, cross-validated, reservoir of quantitative information on the behaviour of cations in magnetite under distinct high-T hydrothermal conditions. New D’ datasets may allow calibrating thermometers and O₂-barometers and approximating hydrothermal fluid chemistries from mineral chemistry.

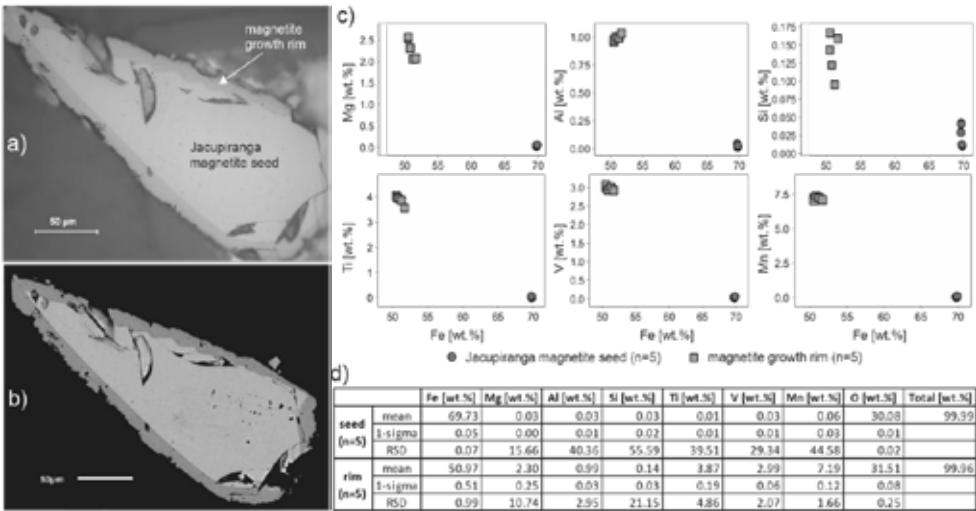


Figure 1. Magnetite seed with growth rim from a trial experimental run of 14 days at 600 °C and 1 kbar: (a) a plain polarized reflected light micrograph and (b) SEM backscatter image, both exposing a growth rim. (c, d) EPMA elemental analyses data show the distinct chemistry between seed and rim.

Canil D, Grondahl C, Lacourse T, Pisiak LK (2016): Trace elements in magnetite from porphyry Cu–Mo–Au deposits in British Columbia, Canada. - *Ore Geol Rev* 72, 1116-1128

Dare SA, Barnes S-J, Beaudoin G, Méric J, Boutroy E, Potvin-Doucet C (2014): Trace elements in magnetite as petrogenetic indicators. - *Mineral Deposita* 49, 785-796

Dupuis C, Beaudoin G (2011): Discriminant diagrams for iron oxide trace element fingerprinting of mineral deposit types. - *Mineral Deposita* 46, 319-335

Huang X-W, Boutroy É, Makvandi S, Beaudoin G, Corriveau L, De Toni AF (2018): Trace element composition of iron oxides from IOCG and IOA deposits: relationship to hydrothermal alteration and deposit subtypes. - *Mineral Deposita* 1-28

Ilton ES, Eugster HP (1989): Base metal exchange between magnetite and a chloride-rich hydrothermal fluid. - *Geochim Cosmochim Acta* 53, 291-301

Lipko S, Tauson V, Bychinskii V (2020): Gold partitioning in a model multiphase mineral-hydrothermal fluid system: Distribution coefficients, speciation and segregation. - *Minerals* 10, 890

Nadoll P, Angerer T, Mauk JL, French D, Walshe J (2014): The chemistry of hydrothermal magnetite: A review. - *Ore Geol Rev* 61, 1-32

Nadoll P, Mauk JL, Hayes TS, Koenig AE, Box SE (2017): Element partitioning in magnetite under low-grade metamorphic conditions – a case study from the Proterozoic Belt Supergroup, USA. - *Eur J Mineral* 29, 795-805

Simon AC, Pettke T, Candela PA, Piccoli PM, Heinrich CA (2006): Copper partitioning in a melt–vapor–brine–magnetite–pyrrhotite assemblage. - *Geochim Cosmochim Acta* 70, 5583-5600

Smagunov, N., Tauson, V., Lipko, S., Babkin, D., Pastushkova, T., Belozerovala, O. and Bryansky, N. (2021) Partitioning and Surficial Segregation of Trace Elements in Iron Oxides in Hydrothermal Fluid Systems. *Minerals* 11, 57

Deditius AP, Reich M, Simon AC, Suvorova A, Knipping J, Roberts MP, Rubanov S, Dodd A, Saunders M (2018): Nanogeochemistry of hydrothermal magnetite. - *Contrib Mineral Petrol* 173, 46

Verdugo-Ihl MR, Ciobanu CL, Cook NJ, Ehrig K, Slattery A, Courtney-Davies L, Dmitrijeva M (2021): Nanomineralogy of hydrothermal magnetite from Acropolis, South Australia: Genetic implications for iron-oxide copper gold mineralization. - *Amer Mineral* 106, 1273-1293

What does tourmaline reveal about the polymetamorphic evolution of the Matsch unit (Vinschgau, S-Tyrol, Italy)?

E. Bernabe¹, P. Tropper¹, C. Morelli², V. Mair²

¹University of Innsbruck, Institute of Mineralogy and Petrography, 6020 Innsbruck, Austria

²Amt für Geologie und Baustoffprüfung, Autonome Provinz Bozen - Südtirol

e-mail: peter.tropper@uibk.ac.at

The currently mapped sheet Schländers (Project CARG F012) offers the chance to carefully investigate the Austroalpine units in the Vinschgau and their tectonic contacts and to implement them into a tectonic model based on new petrological, geochronological and structural data. The Austroalpine nappe stack in the investigated area, located in the Vinschgau area (South Tyrol), comprises from bottom to top the Campo-Ortler-nappe, the Texel-unit, the Ötztal-nappe and the Matsch unit. The Matsch unit in the northern flank of the Vinschgau valley shows a clear polymetamorphic evolution history which can be well reconstructed using the spatial distribution of the aluminosilicates, the chloritoid-isograd and the observation of chemical zoning patterns in garnets, which, depending on the geographical position and the geological setting, exhibit single-phase, two-phase or even three-phase compositions. Geothermobarometry yielded a strong increase in eo-Alpine temperature conditions of 500 °C and 0.8 GPa to 650 °C and 1-1.2 GPa.

Tourmaline is especially well-suited as petrogenetic indicator owing to its expansive P - T stability, occurrence in rocks of widely varying composition, and settings ranging from sedimentary, to hydrothermal, metamorphic, and magmatic. Tourmaline composition varies systematically with changing P - T conditions in its host environment. A gradual increase in Al on the Y-site, the Mg/Fe-ratio, the vacancy content at the X site, accompanied by increasing Ca correlates with increasing metamorphic grade for metapelitic tourmalines.

Chemically the tourmalines are dravites. The tourmalines west of the chloritoid-isograd show a complex chemical zoning pattern with 3-5 zones, whereas east of the isograd only tourmalines with 2-4 zones occur. Chemical zoning within these western tourmalines reveals in the outermost rims a sharp increase in Ca(X), Al(Y), and the vacancy on X. The inner zones most likely represent stages of the pre-Alpine metamorphic evolution since the cores contain quite high Ca(X). The 3-zone eastern tourmalines show a clear prograde evolution with increasing Ca(X), Al(Y) and Mg/Fe. Overall, the Ca-content of tourmaline as indicator of increasing Eoalpine metamorphic conditions increases from the west (0.113 apfu) to the east (0.171 apfu).

The data show that most tourmalines in the western part of the Matsch nappe record mostly zones of pre-Alpine growth and only the outermost zone with sharp increases in Al, Ca and vacancy contents represents the Eoalpine growth stage. The eastern tourmalines on the other hand show almost no pre-Alpine growth stages (e.g., Ca-rich cores) and their zoning clearly shows the Eoalpine prograde metamorphic evolution.

Influence of deformation and fluids on Ti exchange in natural quartz

M. Bestmann¹, G. Pennacchioni², B. Grasemann¹, B. Huet², M.W.M Jones³, C.M Kewish⁴

¹*Department of Geology, University of Vienna, 1090 Vienna, Austria*

²*Department of Geosciences, University of Padova, 35131 Padova, Italy*

³*Department of Hard Rock Geology, Geological Survey of Austria, 1030 Vienna, Austria*

⁴*Central Analytical Research Facility, Queensland University of Technology, Brisbane, 4000, QLD, Australia*

⁵*Australian Synchrotron, ANSTO, Clayton, 3186, Vic, Australia*

e-mail: michel.bestmann@univie.ac.at

For over 10 years, the TitaniQ geothermometer has been used to constrain deformation temperatures in quartz-rich rocks. The calibration of the thermometer rests on the direct correlation of the titanium trace element concentration in quartz with respect to the ambient temperature. However, the processes and parameters which lead to re-equilibration of the Ti-in-quartz system during deformation are not yet fully understood. Here we analysed deformed quartz veins from the Eastern Alps (Prijakt Nappe) applying a combination of microstructural, spectroscopic, and geochemical analyses. In contrast to recent studies which highlight the importance of strain, we show that the availability of free grain boundaries, fluids, and their partitioning play the dominant role in Ti resetting towards lower concentrations in our studied case of retrograde deformation. We employ a robust analytical approach to investigate the interplay between grain-scale deformation, fluid-rock interactions, and geochemical exchange during increasing strain in the quartz mylonites. With this approach, the microstructures representing most re-equilibrated sites for the application of the titanium-in-quartz geothermometer can be readily identified, even at lower greenschist facies deformation conditions and a recrystallization regime dominated by subgrain rotation.

These coarse-grained quartz veins, that formed at amphibolite facies conditions, were overprinted by lower greenschist facies deformation to different degrees. During the overprint, subgrain rotation recrystallization was dominant during progressive deformation to ultramylonitic stages. The initial [Ti] (3.0-4.7 ppm) and cathodo-luminescence (CL) signature of the vein crystals decrease during deformation mainly depending on the availability of fluids across the microstructure. The amount of strain played a subordinate role in resetting to lower [Ti] and corresponding darker CL shades. Using a microstructurally-controlled analysis we find that the most complete re-equilibration in recrystallized aggregates ([Ti] of 0.2-0.6 ppm) occurred (i) in strain shadows around quartz porphyroclasts, acting as fluid sinks, and (ii) in localized microshear zones that channelized fluid percolation. [Ti] resetting is mainly observed along wetted high angle boundaries (misorientation angle >10-15°), with partial [Ti] resetting observed along dry low angle boundaries (<10-15°). This study shows for the first time that pure subgrain rotation recrystallization in combination with dissolution-precipitation under retrograde condition provide microstructural domains suitable for the application of titanium-in-quartz geothermobarometry at deformation temperatures down to 300-350 °C.

Evolution history of plagioclase hosted Fe-Ti oxides micro-inclusions from oceanic gabbros

G. Bian¹, O. Ageeva¹, A. Kovacs², G. Habler¹, R. Abart¹

¹University of Vienna, Department of Lithospheric Research

²Forschungszentrum Jülich, Ernst Ruska-Centrum für Mikroskopie und Spektroskopie mit Elektronen (ER-C)
e-mail: biang92@univie.ac.at

Fe-Ti oxides are commonly observed as oriented needle- and lath-shaped micro-inclusions in plagioclase. Our study focused on these inclusions in plagioclase from oceanic gabbros in the Mid-Atlantic ridge with distinct petrogenetic histories. Previous research indicates that the inclusions formed through precipitation from Fe-bearing plagioclase at temperatures ≥ 600 °C and low oxygen fugacity (Bian et al. 2021). They subsequently undergo a complex evolution, as determined through correlated polarisation microscopy, mineral chemical analysis by electron microprobe analyzer, scanning transmission electron microscopy and crystal orientation analyses.

Two evolutionary pathways are discerned. For both pathways, the Fe-Ti oxide micro-inclusions first formed as homogeneous titanomagnetite at ≥ 600 °C upon slow cooling and/or oxygen fugacity change. Such homogeneous titanomagnetite inclusions are rarely preserved.

Along pathway A, the inclusions experienced high temperature oxidation leading to formation of ilmenite-magnetite intergrowth. Ilmenite (Ilm) is typically present as lamellae in a matrix of magnetite (Mt) with $Mt\{111\} \parallel Ilm(0001)$. The magnetite still contains a small amount of Ti. As temperature decreases $< \sim 600$ °C, the Ti-bearing magnetite exsolves into ulvospinel (Usp) and magnetite. These inclusions thus contain ilmenite lamellae and extremely fine ulvospinel lamellae within a matrix of Ti-poor magnetite.

Along pathway B, high temperature oxidation did not occur, and the inclusions are devoid of ilmenite lamellae. This indicates comparatively low fO_2 at the early stage. When cooling below ~ 600 °C, titanomagnetite exsolves forming magnetite-ulvospinel intergrowth with a significant proportion of ulvospinel. At a later stage, ulvospinel may be oxidised into secondary magnetite (Mt_s) and ilmenite (Ilm_s) which tend to form aggregates along the contacts between exsolved ulvospinel and magnetite. The oxidation is likely linked to relatively low-temperature hydrothermal activity.

Inclusions in both pathways may form plate shaped Ilm or relics of ilmenite particles due to preferential dissolution of magnetite. The crystallographic orientation relationships (COR) of ilmenite inclusions to the plagioclase are determined by the COR between ilmenite lamellae and the dissolved magnetite hosting the ilmenite in the first place.

Two pathways represent different cooling conditions, with the key distinction being high-temperature oxidation during early hydrothermal alteration in A, which is absent in B. Path A is typical for non-altered oceanic gabbros (Ageeva et al. 2020; Bian et al. 2021), but was also revealed in the oceanic gabbro that was affected by felsic magmatism and high temperature hydrothermal overprint (Ageeva et al. 2016).

Path B was revealed in the plagioclase of gabbroic rocks from the Vema lithospheric section, the petrogenetic history of which shows several stages (Pertsev et al. 2015). Stage I: early magmatic crystallization of coarse-grained pyroxene-plagioclase assemblage. Stage II: late magmatic syn-deformation interaction between the crystal aggregate and residual melt with local magmatic-aqueous fluid at 800-900 °C. Stage III: local high temperature (about 600 °C) reducing hydrothermal alterations as a result of interaction with brine (20-21 % NaCl) remained after low temperature (< 500 °C) interaction of seawater with mantle peridotites. Stage IV: low temperature hydrothermal alteration associated with the infiltration of seawater derivatives with salinity (< 7 wt% NaCl) during tectonic exhumation of the lithospheric section.

The microstructural and textural evolution of the Fe-Ti oxide micro-inclusions can be linked to the main events in the petrogenetic history of the gabbro. In particular, the late magmatic stage with magmatic-aqueous fluid at the Stage II catalysed precipitation of Fe-Ti oxides from plagioclase forming the micro-inclusions. The ulvospinel-magnetite inclusions appeared as a result of exsolution of titanomagnetite during the reducing hydrothermal alterations (Stage III). Likely, this process was preceded by recrystallization of primary inclusions, because in these gabbros only micro-inclusions elongated parallel to the [001] direction of plagioclase are present, which is typical for recrystallized inclusions (Bian et al. 2023). The Ilm_s-Mt_s micro-inclusions are related to water-rock interaction during the low temperature hydrothermal stage (Stage IV).

The magnetic signals recorded by plagioclase with oriented Fe-Ti oxide micro-inclusions may exhibit differing biases for pathway A and B. Consequently, comprehending the evolution of these micro-inclusions is crucial for paleomagnetic reconstructions.

- Ageeva O, Habler G, Pertsev A, Abart R (2016): Orientation relationships of Fe-Ti-oxide micro-inclusions and their hosts in the oceanic gabbro. - EMC-2016. Minerals, rocks and fluids: alphabet and words of planet Earth. Book of Abstract. p. 218
- Ageeva O, Bian G, Habler G, Pertsev A, Abart R (2020): Crystallographic and shape orientations of magnetite micro-inclusions in plagioclase. - Contrib Mineral Petrol 175, 95
- Bian G, Ageeva O, Recnik A, Habler G, Abart R (2021): Formation pathways of oriented magnetite micro-inclusions in plagioclase from oceanic gabbro. - Contrib Mineral Petrol 176, 1–21
- Bian G, Ageeva O, Roddatis V, Habler G, Schreiber A, Abart R (2023): Oriented secondary magnetite micro-inclusions in plagioclase from oceanic gabbro. - Amer Mineral, doi: 10.2138/am-2022-8784
- Pertsev AN, Aranovich LY, Prokofiev VY, Bortnikov NS, Cipriani A, Simakin SS, Borisovskiy SE (2015): Signatures of Residual Melts, Magmatic and Seawater-Derived Fluids in Oceanic Lower-Crust Gabbro from the Vema Lithospheric Section, Central Atlantic. - J Petrol 56, 1069-1088

Matching crystal structure plots to “atomic-resolution” HR-TEM images

J. Birkenstock¹, S. Pokhrel^{2,3,4}, L. Mädler^{2,3,4}

¹University of Bremen, FB5-GEO/Crystallography & Geomaterials, Klagenfurter Straße 2-4, 28359 Bremen

²Faculty of Production Engineering, University of Bremen, Badgasteiner Straße 1, 28359 Bremen

³Leibniz Institute for Materials Engineering IWT, Badgasteiner Straße 3, 28359 Bremen

⁴MAPEX Center for Materials and Processes, University of Bremen, 28359 Bremen

e-mail: jbirken@uni-bremen.de

High-resolution TEM images of single crystals, oriented with a prominent zone axis [uvw] parallel to the electron beam, display periodic arrangements of light and dark contrast. Considering that modern TEM instruments are claimed to supply sub-Ångström ($< 10^{-10}$ m) resolution one would expect that the interpretation should be easy, assuming that the light or dark contrast represent single atoms or voids. However, only in rare cases, e.g., using deep learning algorithms, automatic recognition has been applied to simple structures like graphene layers (Madsen et al. 2018) where the orientation of the layer with respect to the beam is previously known. If certain features like open, void channels exist and the channels are oriented parallel to the beam, recognizing the orientation of the crystal structure from its observed pattern is also quite easy, as e.g., shown by MacLaren & Ramasse (2014).

For complex structures without such features, determining the orientation of the crystal structure for an observed periodic pattern of dark and light contrasts presents a more difficult task. The reasons for this are manifold: It starts with noting that the observed image usually does not represent an atomic monolayer but results from transmission through a more or less thick stack of material. Accordingly, the observed pattern is a projection of the crystal structure, which can be more or less complex in terms of the number of independent crystallographic sites, involving chemical complexes in different orientations, solid solution sites etc. Thus, a single light or dark feature in the resulting HR-TEM image may represent any of these stacked on top of each other along the viewing direction, perfectly aligned or offset by fractions of an atomic diameter. On the other hand, some atoms may “invisible” in the respective image. Furthermore, light and dark contrast may be interchanged depending on the actual settings of the microscope, e.g., with respect to focus. Accordingly, even if the crystal structure is comprehensively known, interpretation of the observed dark and light contrast in the HR-TEM image in terms of a given crystal structure can be a major challenge.

The procedure presented here for matching a certain crystal structure to an observed periodic HR-TEM pattern relies on these steps:

- 1) Measurements of d-spacings d_{obs} via normal distances between parallel “rows” of either light or dark contrast in several directions in the observed patterns and determination of the angle(s) between pairs of normal distance directions (i.e., between their d-spacing vectors \mathbf{d}_{obs}). Notes: 1. Two directions will usually be sufficient since they define a plane in space, 2. d-spacings from HR-TEM images may suffer from systematic errors (often several percent) which should be considered by a standard uncertainty (of several percent) in observed d-spacings.
- 2) Comparison of observed d-spacings with a list of d-spacings calculated from the crystal structure and identification of potential hkl planes matching them.
- 3) Calculation of angles between the \mathbf{d}_{hkl} vectors of the identified lattice planes to find matches for the angles, too. Notes: 1. To find matches in the angles symmetrically equivalent hkl planes may have to be considered, too, 2. one pair of two lattice planes matching a single observed angle is usually sufficient.

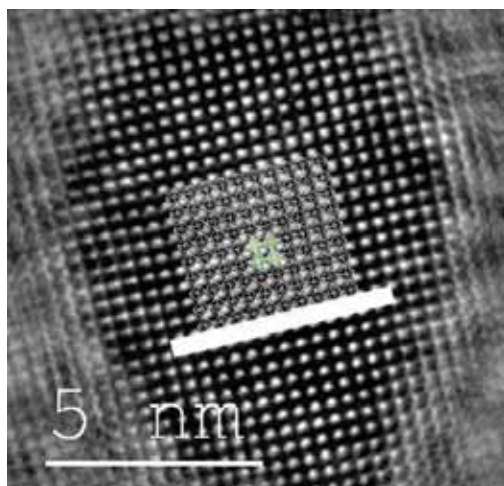


Figure 1. Crystal structure of WO_3 (monoclinic) matched onto the HR-TEM of nanoparticles of WO_3 which displays a pseudo-cubic arrangement when projected along $[001]$ direction ($[010]$ and $[100]$ similar). The scale bar in the crystal structure is 5 nm, too.

- 4) If a match of two hkl planes and their angle is found, calculate the zone axis to identify the crystallographic direction $[uvw]$ that was parallel to the beam on measurement.
- 5) In the software used for displaying the crystal structure (e.g. VESTA, Momma & Izumi, 2011), create a structure model with a sufficiently large number of unit cells, set the viewing direction to $[uvw]$ from step 5. Add a scale bar matching that of the HR-TEM image.
- 6) Copy the crystal structure plot in semi-transparent mode onto the HR-TEM image, resize the crystal structure image to match the two scale bars.
- 7) Match the crystal structure to the dark and light contrast by translations and rotations of the crystal structure image on top of the HR-TEM image.

Further notes: If the identification of hkl was correct some details in the periodic motifs of the crystal structure or in the observed

periodic dark and light contrast may be left unmatched. As a result, modifications in the crystal structure plot may have to be considered: 1) small scaling of the plot (a few percent only!), 2) display of selected crystallographic sites only since some (groups of) atoms may be missing in the contrast details, 3) as noted above, a single light or dark contrast may represent a single atom or groups of atoms from different crystallographic sites, potentially offset by fractions of an atomic diameter. Accordingly, highlighting groups of atoms, e.g., via polyhedral representation, may be indicated as well.

In this contribution we will show some well-documented, previously published examples which were taken from Pokhrel et al. (2023), Li et al. (2021), Dreyer et al. (2016), Kemmler et al. (2012), Pokhrel et al. (2009, see Figure 1).

- Momma K, Izumi F (2011): VESTA3 for three-dimensional visualization of crystal, volumetric and morphology data. – J Appl Cryst 44, 1272-1276
- Madsen J, Liu P, Kling J, Wagner JB, Hansen TW, Winther O, Schiøtz J (2018): A deep learning approach to identify local structures in atomic-resolution transmission electron microscopy images. – Adv Theory Simul 1, 1800037
- MacLaren I, Ramasse QM (2014): Aberration-corrected scanning transmission electron microscopy for atomic-resolution studies of functional oxides. – Int Mater Rev 59, 115-131
- Dreyer JAH, Pokhrel S, Birkenstock J, Hevia MG, Schowalter M, Rosenauer A, Urakawa A, Teoh WY, Mädler L (2016): Decrease of the required dopant concentration for $\delta\text{-Bi}_2\text{O}_3$ crystal stabilization through thermal quenching during single-step flame spray pyrolysis. – Cryst Eng Comm 18, 2046-2056
- Kemmler JA, Pokhrel S, Birkenstock J, Schowalter M, Rosenauer A, Bärnsan N, Weimar U, Mädler L (2012): Quenched, nanocrystalline $\text{In}_4\text{Sn}_3\text{O}_{12}$ high temperature phase for gas sensing applications. – Sens Actuators B Chem 161, 740-747
- Li H, Erinmwingbovo C, Birkenstock J, Schowalter M, Rosenauer A, La Mantia F, Mädler L, Pokhrel S (2021): Double flame-fabricated high-performance $\text{AlPO}_4/\text{LiMn}_2\text{O}_4$ cathode material for Li-ion batteries. – ACS Appl Energy Mater 4, 4428-4443
- Pokhrel S, Birkenstock J, Schowalter M, Rosenauer A, Mädler L (2009): Growth of ultrafine single crystalline WO_3 nanoparticles using flame spray pyrolysis. – Cryst Growth Des 10, 632-639
- Pokhrel S, Stahl J, Groeneveld JD, Schowalter M, Rosenauer A, Birkenstock J, Mädler L (2023): Flame aerosol synthesis of metal sulfides at high temperature in oxygen-lean atmosphere. – Adv Mater 2023, 2211104

Assessing enrichment efficiency: A study of mineralogical and physical characteristics of Pb-Zn ore from Erzgebirge, Germany

A. Bravo¹, O. Popov¹, H. Lieberwirth¹

*¹Institute for Minerals Processing Machines and Recycling Systems Technology (IART),
Technische Universität Bergakademie Freiberg, Germany
e-mail: bravo@iart.tu-freiberg.de*

The mineralogical and physical properties of minerals play a crucial role in understanding their behaviour during the comminution process, where materials are reduced into different sizes. Accurate determination of the characteristics of mineral phases present in the materials is essential to assess their potential selectivity during comminution. Then differences in the physical properties of gangue and ore minerals can be exploited. As a result, the valuable minerals appear in a different particle size than the gangue material and can be separated by classifying techniques.

In this study, an integrated assessment was conducted on samples of Pb-Zn ore from Reiche Zeche, located in Saxony's prominent mining district in Germany, the Ore Mountains, Erzgebirge Region. The Ore Mountains are mainly composed of metasediments (grey gneisses) and metamagmatites (red and grey gneisses) and exhibit hydrothermal polymetallic mineralisation including lead, zinc and silver. The veins are commonly categorised based on their orientation and mineral associations.

Smaller vein-like deposits along with the typical host rock gneiss from Freiberg, have been chosen as research environment for evaluating the enrichment of different sieve classes before and after undergoing jaw crusher and cross Beater mill processes. The mineralogical characterisation was performed using automated mineralogy through Mineral Liberation Analysis (MLA). The material's properties, such as the Point Load strength index, Vickers Hardness Number, and fracture toughness, were determined. MLA provided information on particle size distribution, liberation degree, association, and modal mineralogy for each fraction. The preliminary results showed an enrichment of smaller sieve classes for specific phases, including chalcopyrite, galena, sphalerite, and pyrite. These results were correlated with the rock's physical properties, including textural observations, as well as the behaviour of grains and grain boundaries within the rock.

Reviewing the formation and transformation behaviour of amorphous calcium carbonate: implications for environmental proxies

J-M. Brazier^{1,2}, M. Pettau¹, K.E. Goetschl¹, M. Dietzel¹

¹*Graz University of Technology, Institute of Applied Geosciences, Rechbauerstraße 12, 8010 Graz, Austria*

²*Current address: University of Bern, Institute of Geological Sciences, Baltzerstraße 1+3, 3012 Bern, Switzerland*

e-mail: michael.wedenig@tugraz.at

The elemental and isotopic compositions of CaCO₃ minerals are commonly used as proxies to reconstruct the (paleo)environmental conditions that existed during their formation. Amorphous calcium carbonate (ACC) is known to be a metastable phase and a precursor to crystalline phases within the so-called "non-classical" nucleation pathway. Various factors can influence its formation, lifespan, structure, and transformation pathways, raising questions regarding the reliability of the crystalline phase resulting from precursor transformation as an archive for (paleo)environmental conditions. Evaluating the elemental and isotopic composition of such crystalline phases requires considerations of the specific pathways of CaCO₃ formation and transformation, as well as the system conditions, such as reaction kinetics versus equilibrium. In this review, we discuss the elemental and isotopic fractionations between ACC/crystalline CaCO₃ and the precipitating solution, focusing on structural characterization, ion exchange behaviour, precipitation kinetics, and transformation behaviour in open versus closed systems.

Pressure-Temperature structure of the Makbal UHP complex (NW Kyrgyzstan)

D. Brunner¹, E. Skrzypek¹, S. Schorn¹, C. Hauzenberger¹, K. Stüwe¹, R. Orozbaev²

¹*Institute of Earth Sciences, University of Graz*

²*Institute of Geology, Kyrgyz National Academy of Sciences
e-mail: danie.brunner@edu.uni-graz.at*

The Makbal ultra-high-pressure (UHP) complex in NW Kyrgyzstan is one of several (ultra-)high-pressure [(U)HP] – low temperature (LT) complexes in the western part of the Tianshan mountain range. It is mainly composed of continental material and can be divided into a ultra-high, high (HP) and medium pressure (MP) unit. The UHP unit is located in the core of the complex and consists of quartzite, garnet-quartz-phengite schist and garnet-chloritoid-talc schist. UHP conditions were inferred from coesite inclusions in garnet from garnet-chloritoid-talc schist (Tagiri et al. 2010). The UHP unit is surrounded by the HP unit, which consists mainly of garnet-phengite±chloritoid schist. The outermost MP unit comprises greenschist facies phyllite and marble.

For HP and UHP unit samples, a maximum temperature of $510\text{--}530\text{ }^{\circ}\text{C} \pm 30\text{ }^{\circ}\text{C}$ was determined using graphite thermometry. Thermodynamic modelling based on garnet and phengite composition yields a prograde P-T path leading from ~ 15 kbar and $\sim 450\text{ }^{\circ}\text{C}$ to peak conditions of ~ 18.5 kbar and $\sim 510\text{ }^{\circ}\text{C}$ for a HP sample located close to the MP unit. The HP sample collected at the boundary to the UHP unit indicates P-T conditions of ~ 19 kbar at $\sim 470\text{ }^{\circ}\text{C}$ for garnet core and ~ 23 kbar at $\sim 510\text{ }^{\circ}\text{C}$ for peak metamorphism. Electron probe microanalyzer monazite dating in the HP sample near the MP unit yields 488 ± 5.76 Ma ($n = 34$; MSWD = 0.48) and is interpreted as recording retrograde metamorphism. A garnet-chloritoid-talc schist sample from the UHP unit indicates P-T conditions of ~ 23.5 kbar and $\sim 520\text{ }^{\circ}\text{C}$ for garnet core and peak conditions of ~ 29 kbar and $\sim 580\text{ }^{\circ}\text{C}$.

Our data reveal a continuous increase in P-T conditions towards the core of the UHP complex. This suggests that at least the UHP and HP unit could represent a continuous continental section that was subducted and also exhumed “en masse” as a single block.

Tagiri M, Takiguchi S, Ishida C, Noguchi T, Kimura M, Bakirov A, Sakiev K, Takahashi M, Takasu A, Bakirov A, Togonbaeva A, Suzuki A (2010): Intrusion of UHP metamorphic rocks into the upper crust of Kyrgyzian Tien-Shan: P-T path and metamorphic age of the Makbal Complex. - J Mineral Petrol Sci, 105, 233-250

Accessory minerals in the Isua Supracrustal Belt

H. Brüscke¹, D. Sorger¹, A. Kronz¹, A.A.G. Webb², T. Müller¹

¹*Geoscience Center Göttingen, Georg-August-University Göttingen, Germany*

²*Department of Earth Sciences, The University of Hong Kong, Hong Kong, China
email: h.brueschke@stud.uni-goettingen.de*

The Isua supracrustal belt (ISB) is an example of Archean crustal evolution and well-known as it hosts Earth's oldest 10s-of-km scale supracrustal rocks. However, the conditions and timing of its metamorphic evolution are controversially debated. Most importantly, this knowledge is underpinning the different existing hypothesis of Eoarchean vs. Neoproterozoic tectono-metamorphic events and geodynamic models of horizontal vs. vertical tectonic evolution. Recent studies have shed light on the metamorphic conditions based on geothermobarometry and phase equilibria modeling of major rock forming minerals. However, data from accessory minerals in the ISB have only been sparsely studied despite their potential to better constrain the metamorphic evolution of the belt. In this work, we study structure, composition, and its spatial variation of the accessory phases, especially their rare earth element (REE) contents.

A total of 5 samples with bulk composition resembling so-called "mafic pelites" have been investigated. The typical mineral assemblage comprises garnet porphyroblasts, biotite, quartz and chlorite being the major rock forming phases. Garnet porphyroblasts indicate two stages of garnet growth marked by an inclusion-rich core (M1) and inclusion-poor overgrowth rim (M2). Zircon, monazite, rutile and ilmenite are the most prominent accessory minerals present in the studied lithology.

Backscattered electron images and polarization microscopy were used to petrographically describe the textural context. Major and trace elements have been analyzed using an electron microprobe.

Preliminary results reveal that zircons occur as 5 to 10 microns inclusions within garnet (both core and rim), biotite and chlorite. No visible CL pattern could be found in any of the studied grains indicating substantial metamictization. Despite the presence of zircons in the rocks, Zr-in-Rutile measurements of matrix grains are often below or around detection limit of the electron microprobe, resulting in unresolvable low temperature estimates.

Monazite grains occur as individual grains in the matrix and as inclusions in both, rim and core of garnet porphyroblasts. Rare earth element analysis indicates the absence of an Eu-anomaly in all types of monazites, suggesting growth in the absence of feldspar. Monazite inclusions in garnet cores exhibit slightly higher Sm, Gd and Y contents compared to monazite grains in garnet rims and matrix. One possible reason for the higher content of MREE is that this type of monazite was formed in absence of a competitor phase such as garnet or apatite. If true, this possibly indicates a monazite formation either before the first M1 garnet growth stage or in a different environment.

The preliminary results highlight the potential to reconstruct the metamorphic evolution of the belt in more detail. For example, variations in the REE content of accessory phases potentially shed light on the presence or absence of metamorphic index minerals during formation of accessory phases. Such knowledge provides additional information on the timing of the major tectonometamorphic event (M1) and thus feeds into the interpretation of the geodynamic evolution of the ISB.

Annealing of metamict minerals – spectroscopic study

C. Chanmuang N.¹, M. Zeug^{1,2}, A. Erlacher¹, K.A.G. Sameera^{3,4}, L. Nasdala¹

¹*Institut für Mineralogie und Kristallographie, Universität Wien, 1090 Vienna, Austria*

²*Landesamt für Geologie und Bergwesen Sachsen-Anhalt,
An der Fliederwegkaserne 13, 06130 Halle (Saale), Germany*

³*Postgraduate Institute of Science, University of Peradeniya, P.O. Box 25, Peradeniya 20400, Sri Lanka*

⁴*Geological Survey and Mines Bureau, 569 B120, Sri Jayawardenepura Kotte 10100, Sri Lanka
e-mail: lutz.nasdala@univie.ac.at*

In the country of Sri Lanka, efforts were recently undertaken to survey the occurrence of radioactive phases (Kuruppu et al. 2020; Sameera et al. 2020), among others as potential Th sources. However, phase identification is hampered in many cases because corpuscular self-irradiation over geologic periods of time, caused by the radioactive decay of Th and U and their instable daughter products, may cause these phases to undergo crystalline-to-aperiodic transition. The final, glassy state is referred to as *metamict* (Brøgger 1893).

Metamict minerals are difficult to identify, as structural analysis techniques cannot yield specific information. For instance, X-ray powder diffraction patterns of metamict aeschynite-(Y), euxenite-(Y), fergusonite-(Y), polycrase-(Y), pyrochlore, and samarskite-(Y) are widely similar (Erlacher 2021; and references therein). Similarly, Raman spectra of metamict minerals are extremely broadened and hence cannot be reliably distinguished from each other. The initial, crystalline mineral phase may in some cases be identified using annealing experiments. This, however, is only possible if upon dry annealing, the phase under discussion undergoes structural reconstitution but does not decompose. An example for the latter are allanite-group minerals: Already at temperatures as low as ca. 300 °C, potential dehydrogenation and Fe²⁺ oxidation need to be considered (Sobek et al. 2023; and references therein).

The heating-induced recovery of radiation-damaged minerals may be vastly different, depending on the degree of damage. If a specimen consists of aperiodic and remnant crystalline domains, moderate-T growth of the latter may contribute substantially to the reconstitution. In contrast, the recovery of metamict (that is, fully radiation-damaged) phases requires random nucleation in the glassy bulk and, therefore, typically requires more elevated T.

We present herein the identification of two metamict mineral species whose occurrence on the island of Sri Lanka was hitherto unconfirmed, gadolinite-(Y) (Y₂Fe²⁺Be₂Si₂O₁₀) and fergusonite-(Y) (YNbO₄). Stepwise annealings of multiple chips of samples was undertaken to study the recovery processes. Metamict gadolinite-(Y) recovers its initially monoclinic structure at above ca. 800 °C. Our Raman spectrum (Fig. 1), obtained after oxidising heating at 1150 °C, matches well with spectra of natural non-metamict (Allaz et al., 2020) and heated gadolinite-(Y) (Gorelova et al. 2021). Annealing of fergusonite-(Y) involves an $\alpha \rightarrow \beta$ transition: At ca. 550–600 °C, tetragonal fergusonite-(Y) forms and at ca. 750 °C and above, monoclinic clinofergusonite-(Y) is present. The Raman spectrum in Fig. 1 was obtained after oxidising annealing at 1000 °C (Erlacher et al. 2021); it matches well the reference spectrum of Ruschel et al. (2010). We can of course not retrace whether fergusonite-(Y) of clinofergusonite-(Y) were initially present. Independent from that, further Raman analysis of annealed heavy minerals from “*katta*” (local name for the dark and radioactive fraction of heavy mineral concentrates) may help to widen our knowledge of metamict phases occurring in Sri Lanka. Photoluminescence spectroscopy might have similar potential; however, it is currently less suitable, because of the lack of a database of reference spectra.

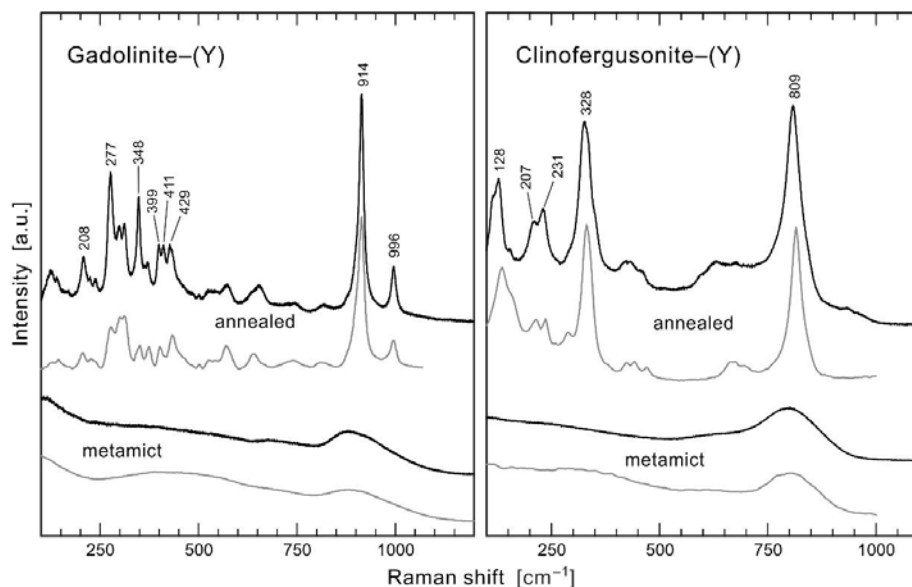


Figure 1. Raman spectra of metamict gadolinite-(Y) and metamict fergusonite-(Y) and their annealed analogues (black), in comparison with reference spectra (grey). Reference spectrum of metamict gadolinite-(Y) extracted from Tomašić et al. (2020); reference spectrum of annealed gadolinite-(Y) extracted from Gorelova et al. (2021); reference spectra of metamict and annealed clinofergusonite-(Y) extracted from Ruschel et al. (2010).

- Allaz JM, Smyth JR, Henry RE, Stern CR (2020): Beryllium-silicon disorder and rare earth crystal chemistry in gadolinite from the White Cloud pegmatite, Colorado, USA. - *Canad Miner* 58, 829-845
- Brøgger WCA (1893): *Salmonsens Store Illustrerede Konversationsleksikon* 1. - Brødrene Salmonsens, København, 742
- Erlacher A, Zeug M, Škoda R, Sameera KAG, Nasdala L (2021): Metamict fergusonite from Kolonna and Masimbula, Sri Lanka. - *J Geol Soc Sri Lanka* 22, 1-14
- Gorelova LA, Panikorovskii TL, Pautov LA, Vereshchagin OS, Krzhizhanovskaya MG, Spiridonova DV (2021): Temperature-versus compositional-induced structural deformations of gadolinite group minerals with various Be/B ratio. - *J Solid State Chem* 299, 122187
- Kuruppu KADDN, Hewathilake HPTS, Illangasinghe IKMSCK, Ranasinghe RANC, Jayasinghe N, Dharmaratne TS (2020): Radioactivity survey on Godakawela gem field in Sri Lanka; to identify the origin of the unknown radioactive mineral. - *J Geol Soc Sri Lanka* 21, 57-65
- Ruschel K, Nasdala L, Rhede D, Wirth R, Lengauer CL, Libowitzky E (2010): Chemical alteration patterns in metamict fergusonite. - *Eur J Mineral* 22, 425-433
- Sameera KAG, Wickramasinghe WAGK, Harankahawa SB, Welikanna CR, de Silva KTUS (2020): Radiometric surveying for Th and U mineralization in southwestern, Sri Lanka: radiological, mineralogical and geochemical characteristics of the radioactive anomalies. - *J Geol Soc Sri Lanka* 21, 57-80
- Sobek K, Losos Z, Škoda R, Hola M, Nasdala L (2023): Crystal chemistry of ferriallanite-(Ce) from Nya Bastnäs, Sweden: Chemical and spectroscopic study. - *Mineral Petrol* 117, 345-357
- Tomašić N, Škoda R, Bermanec V, Šoufek M (2020): Crystal chemistry and microfeatures of gadolinite imprinted by pegmatite formation and alteration evolution. - *Amer Mineral* 105, 1647-1655

Speciation of La^{3+} in Cl-bearing hydrothermal fluids: Development of a new polarizable force field

R. Chattopadhyay¹, S. Jahn¹

¹*Institute of Geology and Mineralogy, University of Cologne, Zùlpicher StraÙe 49b, Cologne, Germany
e-mail: rchattop@uni-koeln.de*

The Rare Earth Elements (REEs) are an important group of elements both geologically as well as economically. REEs find important applications in the fields of green energy, electric vehicles and electronics. They are also important tracers for geological processes under hydrothermal /high grade metamorphic conditions. The ability of fluids to mobilize the REEs depend on the chemical composition and the presence of suitable ligands such as chloride and fluoride. *Ab initio* molecular dynamics simulations (AIMD) have been used to predict stability constants of various REE complexes and REE speciation under hydrothermal conditions (Stefanski & Jahn 2020; Guan et al. 2022). However, AIMD simulations often suffer from significant finite time and size effects.

The development of classical force fields for ions in aqueous solutions is essential in the field of hydrothermal geochemistry. The reliability and accuracy of classical force fields not only depends on its representation of effects of ionic size but also on polarization of solvent and solute charge densities. The latter many-body term becomes important particularly when dealing with highly charged ions (Piquemal et al. 2009) in concentrated solutions (Tribello et al. 2009) and in interfacial environments (Jungwirth & Tobias 2006). Many different polarizable force fields exist, each having a different representation of polarizability. Here, we choose the point polarizability model of Dang & Chang (1997) for H_2O , which was specifically parameterized to describe gas-liquid interface (Dang & Chang 1997).

We develop a new polarizable forcefield for La^{3+} in Cl-bearing hydrothermal fluids. The forcefield has been fitted to snapshots of AIMD simulations of La^{3+} and Cl^- ions in water at hydrothermal conditions (773 K, 5 kbar). We used Maximally Localized Wannier Functions (MLWFs) along with force and dipole matching techniques to fit the parameters of the potential (Tazi et al. 2012). We used the technique of Madden and co-workers to calculate the ionic polarizabilities of the charged ions (Salanne et al. 2012). Experimental and AIMD data (wherever available) were used to test the validity of this new potential by comparing structural and thermodynamic properties. We also investigate the speciation of La^{3+} in highly concentrated hydrothermal brines for which no experimental/AIMD data exists.

Stefanski J, Jahn S (2020): Yttrium speciation in subduction-zone fluids from *ab initio* molecular dynamics simulations. - Solid Earth 11, 767–789

Guan Q, Mei Y, Etschmann B, Louvel M, Testemale D, Spezia R, Brugger J (2022): Speciation and thermodynamic properties of La(III)-Cl complexes in hydrothermal fluids: A combined molecular dynamics and in situ X-ray absorption spectroscopy study. - Geochim Cosmochim Acta 330, 27–46

Piquemal J-P, Perera L, Cisneros GA, Ren P, Pedersen LG, Darden TA (2006): Towards accurate solvation dynamics of divalent cations in water using the polarizable amoeba force field: From energetics to structure. - J Chem Phys 125, 054511

Tribello GA, Bruneval F, Liew C, Parrinello M (2009): A molecular dynamics study of the early stages of calcium carbonate growth. - J Phys Chem B 113(34), 11680–11687, PMID: 19650654

- Jungwirth, P. and Tobias, D. J. (2006). Specific ion effects at the air/water interface. - Chem Rev 106(4), 1259–1281. PMID: 16608180
- Dang LX, Chang T-M (1997): Molecular dynamics study of water clusters, liquid, and liquid–vapor interface of water with many-body potentials. - J Chem Phys 106(19), 8149–8159
- Tazi S, Molina JJ, Rotenberg B, Turq P, Vuilleumier R, Salanne M (2012): A transferable *ab initio* based force field for aqueous ions. – J Chem Phys 136(11), 114507
- Salanne M, Rotenberg B, Jahn S, Vuilleumier R, Simon C, Madden PA (2012): Including many-body effects in models for ionic liquids. - Theoret Chem Accounts 131, 1143

Al, Si interdiffusion under lower mantle conditions

L. Czekay¹, N. Miyajima¹, C. McCammon¹, D. Frost¹

¹ Bayerisches Geoinstitut, University of Bayreuth
e-mail: laura.czekay@uni-bayreuth.de

The diffusion of atoms in minerals at high temperatures and pressures influences Earth's lower mantle dynamic processes. This study aims to better understand the physical behaviour of Earth's most abundant mineral with implications for lower mantle viscosity. Previous studies that measured Si-self diffusion coefficients in bridgmanite (Brg) showed a value at 25 ± 1 GPa and 1800 °C of $\text{Log}_{10}(D_{\text{Si}}) = -18 \pm 0.5$ (based on units of m^2/s ; relevant information can be found by Yamazaki et al. 2000; Dobson et al. 2008; Xu et al. 2011). Our study revealed a significantly slower diffusion coefficient that may challenge previous calculations of lower mantle viscosity. We investigated Al, Si interdiffusion in Brg experimentally at 24 GPa and 1750 to 2000 °C using a multi-anvil apparatus using diffusion couples composed of bridgmanites that were pre-synthesised from 0-5 mol.% Al_2O_3 -bearing MgSiO_3 enstatite. The Al diffusion profiles were analysed across the diffusion interface in the recovered samples using a scanning transmission electron microscope equipped with an energy-dispersive X-ray spectrometer. The obtained diffusion coefficient for interdiffusion (volume diffusion) at 24 GPa and 1800 °C was $\text{Log}_{10}(D_{\text{Al,Si}}) = -20.1 \pm 0.7$. The resulting data can be used to estimate deformational strain rates of Brg in the lower mantle from viscosity based on different creep mechanisms.

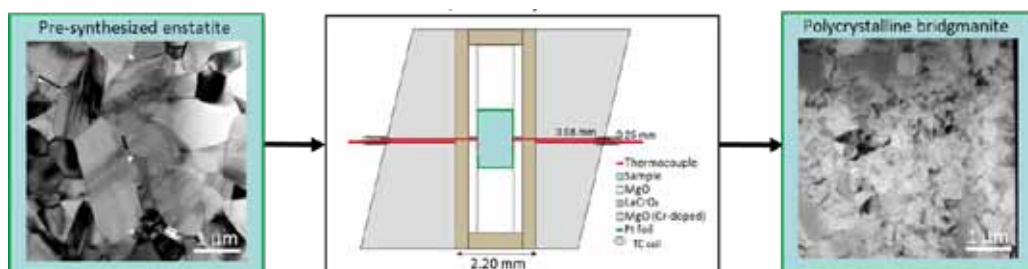


Fig. 1: Experimental setup of the 7/3 assembly and schematic drawing of the experimental path from the pre-synthesized enstatite to the polycrystalline bridgmanite for the diffusion experiments.

- Dobson DP, Dohmen R, Wiedenbeck M (2008): Self-diffusion of oxygen and silicon in MgSiO_3 perovskite. - Earth Planet Sci Lett 270, 125-129
- Xu J, Yamazaki D, Katsura T, Wu X, Remmert P, Yurimoto H, Chakraborty S (2011): Silicon and magnesium diffusion in a single crystal of MgSiO_3 perovskite. - J Geophys Res: Solid Earth 116(B12)
- Yamazaki D, Kato T, Yurimoto H, Ohtani E, Toriumi M (2000): Silicon self-diffusion in MgSiO_3 perovskite at 25 GPa. - Phys Earth Planet Inter [Internet] 119, 299–309

The lower Permian basalt - rhyolite - carbonatite magmatic activity in the Kvetnica volcanic area, Western Carpathians

R. Demko

*Turzovka, Stred 373, 023 54, Slovakia
rastislav.demko@geology.sk*

The Western Carpathians crystalline basement is built by granite–metamorphic rock complexes, covered by sedimentary sequences tectonically arranged into Alpine nappe structures. The Hronic Unit is one of the most spatially extended tectonic upper Alpine nappe structure in the Western Carpathians. The lithology of the Hronic Unit represents a record of volcanic and sedimentary rocks from the Upper Carboniferous to Upper Triassic and Jurassic period. The volcanism operated in parental Hronic area forming two main volcanic phases in the Lower and the Upper Permian with massive production of basalts, basaltic andesites, basaltic trachyandesites and their pyroclastics.

The presented results focus on news from the Kvetnica quarry near Poprad city in the Low Tatras, which belongs to the well-known locality of Maluzina Fm. During field research, I have identified intrusions of younger basalt accompanied by rhyolite, penetrating a set of older horizontally layered older basaltic lavas.

Based on the TAS classification, it is an intrusion of alkaline basaltic trachyandesite BTA and subalkaline rhyolite with a high SiO₂ content (76.5 wt.%). BTA has a porphyritic amygdaloid texture dominated by zonal plagioclases and quartz-calcite amygdales. The rhyolite rock is black, aphanitic, with an association of small phenocrysts: quartz, albite, plagioclase, biotite, garnet, Fe-Ti oxides with accessory zircon and monazite. Garnet contains inclusions of orthopyroxene and ilmenite. The rhyolite rock itself is combined by inserted / mingled rhyolite and carbonatite magma, the relationship of which is determined by their mutual immiscibility, see Figure 1.

This is the first detection of rhyolite rock in the Hronicum unit, directly intruding a thick cover of basaltic effusions. The special composition of the rhyolite rock, made it possible to determine magmatic age of rhyolite as the Lower Permian (Kungurian) 278±6.2 Ma., using U-Th-Pb EPMA of monazites. The identified age is the first analytical geochronological data that assigns age of the Kvetnica paleovolcanic activity to the Lower Permian!

Thermobarometric study of Qtz+Pl+Bt+Grt phenocryst association of rhyolite provides PT data 800-750 °C at 135-200 MPa, indicating the depth of magma chamber emplacement, where BTA magma had differentiated to form rhyolite.

The K₂O (1.5 wt.%) and Fe₂O₃/FeO (0.51) content of the rhyolite rock is very similar to the host alkaline BT-andesite with K₂O (1.74 wt.%) and Fe₂O₃/FeO (0.63). Geochemical analyzes show significant REE fractionate during differentiation of basaltic parental magma, whose La/Yb_{C1} (4.64) and Eu/Eu* (0.82) fractionate toward rhyolitic magma with La/Yb_{C1} (18.43) and Eu/Eu* (0.58). REE modelling of basaltic rocks from the Hronic Unit shows that the first volcanic products (lower Permian) are result of lower melting degree 1.1% melt grt-peridotite & 14% melt of sp-peridotite mixed in mass (1/1.7) with continuous increase to melting of 1.9% melt Grt-peridotite & 13% melt of sp-peridotite mixed in mass 1/2.8 (fractional cumulated melting, McKenzie & O'Nions 1991). BTA composition from Kvetnica, as a parental analogue of rhyolite magma, shows a similarity with other Lower Permian basalts generated by lower degree of melting, which agrees with obtained magmatic age.

Petrographic observations and EPMA study showed existence of interstitial or droplet calcite, which represent a carbonatite melt in the host silicate magma. Their mutual spatial relationships indicate interaction of two immiscible liquids. For the first time in the evolution of BTA-rhyolite differentiation, a carbonatite melt is observed in a sample of BTandesite in form of spirally shaped carbonate globules, inclusions in plagioclase, and thin bounded zones of albite enclosed in intermediate plagioclases (56-54 anorthite mol.%). Thermodynamic MELTS modelling (Gualda et al., 2012; Ghiorso & Gualda 2015), focused on BTA fractionation and composition of feldspars, suggest highly oxidizing conditions in magma chamber. Observed composition of feldspars phenocrysts were reached in 1060-1050 °C and $\Delta QFM = +2$ or 1040-1030 °C and $\Delta QFM = +3$. The evolution of observed carbonatite melts is connected with degassing of released CO₂, which interacted with host silicate melt to form carbonatite.



Figure 1: Fragments of rhyolite melt "frozen" between carbonatite immiscible liquid and phenocrysts of quartz, plagioclases, biotite, Fe-Ti oxides and garnet. Photography in polarized light.

Ghiorso MS, Gualda GAR (2015): An H₂O - CO₂ mixed fluid saturation model compatible with rhyolite-MELTS. - *Contr Miner Petrol*, doi:10.1007/s00410-015-1141-8

Gualda GAR, Ghiorso MS, Lemons RV, Carley TL (2012): RhyoliteMELTS: A modified calibration of MELTS optimized for silica-rich, fluid-bearing magmatic systems. - *J Petrol* 53, 875-890

McKenzie D, O'Nions RK (1991): Partial Melt Distributions from Inversion of Rare Earth Element Concentrations. - *J Petrol* 32, 1021-1091

Fingerprinting graphite: The development of a three-step approach to differentiate between natural graphite deposits

V. Dietrich¹, R. Arató¹, F. Melcher¹

¹Montanuniversität Leoben, Department of Applied Geosciences and Geophysics,
Peter-Tunner-Straße 5, 8700 Leoben
e-mail:valentina.dietrich@unileoben.ac.at

Graphite is considered as a critical raw material due to its significant importance in various industrial applications, such as the steel and refractories industry, but energy storage being the most important industrial sector. Graphite is a vital component in lithium-ion batteries, which are widely used in electric vehicles and other electronic devices. The demand for lithium-ion batteries has been rapidly increasing, driving the demand for graphite and therefore also the interest in the origin of this raw material. Embedded in a framework project aimed at traceability of battery raw materials, this project aims to reinforce transparency, reliability and sustainability of complex critical raw material supply chains.

This study shows an innovative multi-parameter analytical approach in order to differentiate between graphite samples from different locations. Stable carbon isotopes offer a parameter to differentiate between different sources of carbon. The initial carbon in flake and amorphous graphite is of organic origin, whereas carbon in hydrothermal graphite deposits is inorganic and mostly originates from CO₂ or CH₄ rich fluids (Luque 2013). This distinction can be constrained via carbon isotopy and serves as the first step in distinguishing natural graphite deposits. The Raman spectrum of graphite is characteristic for its microstructural state and serves as a basis for estimating peak metamorphic temperatures during graphite formation (Lünsdorf et al. 2016; Rantitsch et al. 2016). As such, it provides a further means to distinguish different deposits. The third part for proving the origin of graphite is provided by trace element analysis. Given that the formation temperature of many flake graphite deposits is similar within error, the geographical origin of individual deposits can be traced only by means of characteristic trace elements. Research is still underway to find a suitable analytical method for this purpose (e.g., ICP-MS, LIBS, XRF). Solution-based analysis (e.g. via ICP-MS), however, proved to be unsuitable, as the complete dissolution of graphite is notoriously difficult, due to the carbon layers being very challenging or even impossible to break up. The digestions and their analytical results are therefore not consistently reproducible and also too costly to withstand routine application as a fingerprinting technology for industry purposes. LA-ICP-MS proved to be much more suitable also due to simpler sample preparation. Although the ablation of very fine-grained material in compressed form also poses challenges, pathfinder elements that allow a geographical differentiation of origins, could be found by LA-ICP-MS. ETV-ICP-OES serves as another potential methodology for discrimination of graphite deposits, especially as an approved methodology for analysis of trace elements in carbon-rich materials (Vogt et al. 2015). However, this methodology for graphite must first be evaluated to prove its suitability. Analytical proof of origin (APO) methods in general are regarded as the least corruptible methods, as they directly relate to the chemical composition of the raw material (Melcher et al. 2021). Other methods such as conventional documents, tracers, QR codes and barcodes can be outmanoeuvred in one way or another.

- Lünsdorf NK, Lünsdorf JO (2016): Evaluating Raman spectra of carbonaceous matter by automated, iterative curve-fitting. - *Int Jour Coal Geol* 160-161, 51-62
- Luque FJ, Huizenga JM, Crespo-Feo E, Wada H, Ortega L, Barrenechea JF (2014): Vein graphite deposits: geological settings, origin, and economic significance. - *Miner Deposita* 49, 261-277
- Melcher, F., Dietrich, V., Gäbler, H.-E. (2021): Analytical Proof of Origin for Raw Materials. - *Minerals* 11, 461
- Rantitsch G, Lämmerer W, Fisslthaler E, Mitsche S, Kaltenböck H (2016): On the discrimination of semi-graphite and graphite by Raman spectroscopy. - *Int Jour Coal Geol* 159, 48-56
- Vogt T, Bauer D, Neuroth M, Otto M (2015): Quantitative multi-element analysis of Argonne Premium Coal samples by ETV-ICP OES – A highly efficient direct analytical technique for inorganics in coal. – *Fuel* 152, 96-102

New applications for digitised historical collections as teaching materials for special mineralogy and petrography

A. Duriagina¹, C. Kehrer², G. Heide¹

¹ TU Bergakademie Freiberg, Institute for Mineralogy, Brennhausgasse 14, 09599 Freiberg

² TU Bergakademie Freiberg, Geoscientific Collections, Brennhausgasse 14, 09599 Freiberg

e-mail: Asiia.Duriagina@mineral.tu-freiberg.de

The Geoscientific Collections of the TU Bergakademie Freiberg are among the most extensive and diverse of their kind. Since the founding of the Bergakademie, they have been created in the context of teaching and further education of students as well as for research purposes and have been continuously expanded ever since. Today, the collections still form an important cornerstone within the education of students and specialist staff. In the emerging age of digital media and virtual realities, as well as against the background of an ever-increasing pool of historical collection material, the aim is to present, archive and use these objects appropriately.

Since the teaching collections and their objects are only accessible to a limited extent within the framework of courses, it is necessary, among other things, to digitise them so that they can be made available in interactive teaching formats. Especially in the field of mineralogy, crystallography and petrology, it is particularly important for students to deal with the greatest possible variety of different objects within the teaching collections. This can be optimally realised through the additional digitised content and thus complement conventional teaching. The digital and visualised collection recording is thus indispensable for a location-independent and cross-thematic use in teaching. Through digital recording, background knowledge on the exhibits is prepared in multimedia form, thus making a greater variety of knowledge accessible to the student in addition to classroom studies.

Digitisation also allows us to use other very interesting objects as teaching aids. For example, historical collection of decorative stones from the Altai Mountains (stone-cutting workshop in Kolywan) is usually not suitable for student work due to its rarity and uniqueness, but once it is digitised, it offers enormous potential for study.

The collection, compiled by Bernhard von Cotta (1808-1879) during his journey to Altai (Cotta et al. 1871), comprises 70 hand specimens and 40 thin sections and is housed in the Geosciences Collections of the TU Bergakademie Freiberg. Each rock slab is 8 x 4.5 cm, ground and polished on one side as well as on the edges, the other main side has a fresh fracture. They are mainly granites, felsic igneous rocks with porphyritic structure, marbles and various schists, as evidenced by a post-determination (Weber, 2019). In 2021, the samples were also digitally recorded using multi- and hyperspectral photography to provide reference data for the non-destructive analysis of museum objects. Furthermore, the historical thin sections were microscopically scanned with linear and cross polarised light and matched with the historical images.

Acknowledgements: We would like to thank the foundation "Innovation in der Hochschullehre" for the financial support and Mr. G. Sacher from "Fokus GmbH" for the discussions and talks.

Cotta B von, Teplouchow TA, Geinitz HB, Stelzner AW (1871): Der Altai: Sein geologischer Bau und seine Erzlagerstätten. - Leipzig: Weber JJ

Weber A (2021): Bernhard von Cottas historische Sammlung polierter Gesteinstafeln aus der russischen kaiserlichen Steinschleiferei zu Kolyvan' im Altai. - Perspektive des Sammlungswissens, Humboldt-Universität zu Berlin 48-56, doi.org/10.18452/23914

Fused beads for the analysis of Li bearing samples by LIBS and XRF

D. Ebert¹, R. Möckel¹, A.D. Renno¹, A. Schneider^{1,2}, T. Dittrich³

¹Helmholtz-Zentrum Dresden-Rossendorf; Helmholtz-Institute Freiberg for Resource Technology,
Chemnitz Straße 40, 09599 Freiberg

²TU Bergakademie Freiberg, Institut für Organische Chemie, Leipziger Straße 29, 09599 Freiberg

³Deutsche Lithium GmbH, Am Junger-Löwe-Schacht 10, 09599 Freiberg

e-mail: d.ebert@hzdr.de

In recent decades, it has become apparent that due to the increasing complexity of deposits, the complexity of ore samples is also increasing. At the same time, the need for detailed geological and mineralogical information also increased. Therefore, it is important to combine methods in order to obtain more comprehensive conclusions.

We present a method of combining WDXRF (wavelength dispersive X-ray fluorescence) analyses with a wide spectrum of elements and pLIBS (portable laser induced breakdown spectroscopy, see Fig. 1) with a likewise spectrum and the additional possibility to detect light elements such as Li. Nevertheless, the representativeness of LIBS analyses is significantly smaller compared to XRF. To overcome this and effectively combine both methods, we designed and produced fused beads using $\text{Na}_2\text{B}_4\text{O}_7$ as flux. Unfortunately, such beads are transparent to the laser which makes LIBS analysis almost impossible, therefore, we tested two different approaches: 1) dying the bead by adding CuO to the flux and 2) roughen the beads surface. We used a mixture of $\text{Na}_2\text{B}_4\text{O}_7$ (+ CuO) + KI as matrix. Potassium iodide (KI) was added as a releasing agent. We used Greisen rocks from the Altenberg-Zinnwald district with known composition – including Li – and LiBO_2 in different concentration ratios to adjust the Li content.

To produce crack-free beads, we had to adapt the melting process in the fully automatic melting furnace TheOx (CLAISSE). For the analytical work, we use a portable LIBS instrument manufactured by SciAps (Z-300, laser wavelength 1064 nm) and a PANalytical Axiosmax minerals XRF spectrometer.

The fused beads will now serve as calibration samples for both XRF and LIBS measurements (see Fig. 2). Samples with unknown composition will be analysed by XRF first. It turned out that roughening the beads has no significant influence on the XRF-spectra as revealed in before and after scan measurements. In a second step the LIBS analysis is performed in particular for light element determination such as Li. Furthermore, adding a dying component such as Cu might be suitable as a robust internal standard for both LIBS and XRF.



Fig. 1: pLIBS measurement on a fused bead containing Cu as dying agent.

The obvious disadvantage of the method is that neither Cu, K nor Na can be included in the quantitative analysis. De-pending on the analytical problem, they would have to be determined in a preceding step (e.g. via a conventional Li-borate melt and XRF).

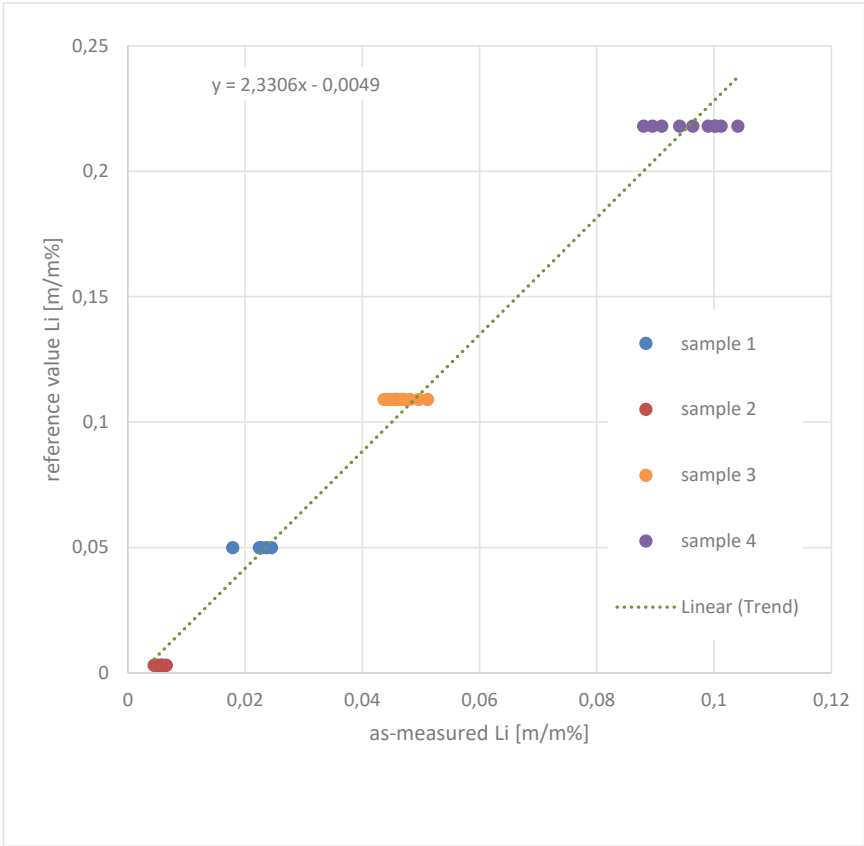


Fig. 2: Calibration factor derived from the initial fused beads, showing robust data on each sample.

CuSeO₄ and Cu(SeO₃OH)₂·6H₂O: A tribute to the enlightenment of the stereochemistry of Cu²⁺ ions by Josef Zemann (1923–2022)

H.S. Effenberger¹, G. Giester¹, M. Wildner¹

¹Institut für Mineralogie und Kristallographie, Universität Wien
herta.silvia.effenberger@univie.ac.at

In the middle of the last century the stereochemistry of divalent copper atoms was mostly unknown. Crystal structure investigations of trippkeite, azurite, linarite, or teinite led Josef Zemann (1923–2022) to understand the coordination figures controlled by the Jahn-Teller-effect. In contrast to the earlier thought CuO₆ octahedra, he described the coordination figures as planar [4], tetragonal pyramidal [4+1], and tetragonal *dipyramidal* [4+2] (Zemann 1961; 1972). The additional ligands have none or only a minor influence on the geometry of the CuO₄ square. In honour to these pioneering investigations, two further compounds with Cu²⁺ ions are presented here: Cu(SeO₄) and Cu(SeO₃OH)₂·6H₂O. They were synthesized at low-temperature hydrothermal conditions (220 °C) and room temperature, respectively.

Snyman & Pistorius (1964) described two modifications of CuSeO₄: one crystallises in the structure type of ZnSO₄ (mineral name zincosite, space group *Pnma*), the high-pressure

form in the NiSO₄-structure type (space group *Cmcm*). The new Cu(SeO₄) modification presented here adopts the MnAsO₄-structure type (space group *P2₁/n*), it represents a monoclinic distortion form the *Pnma* modification.

Mn³⁺ ions exhibit a pronounced [4+2] coordination due to the Jahn-Teller effect. Therefore, the substitution Cu²⁺ ↔ Mn³⁺ is not surprising. The coupled substitution Mn³⁺ + As⁵⁺ ↔ Cu²⁺ + Se⁶⁺ enables isotypy between CuSeO₄-*P2₁/n* and MnAsO₄.

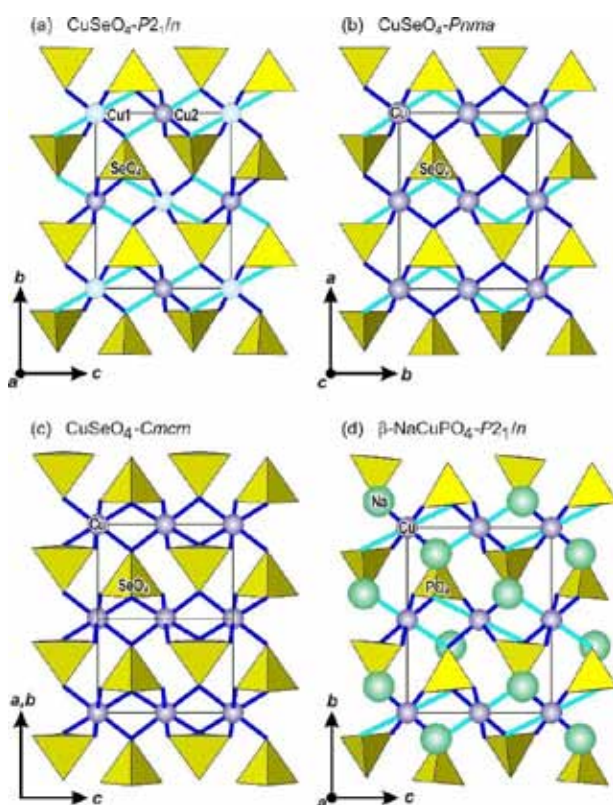


Fig. 1 The crystal structures of
(a) Cu(SeO₄)-*P2₁/n* (structure type MnAsO₄),
(b) Cu(SeO₄)-*Pnma* (structure type ZnSO₄),
(c) Cu(SeO₄)-*Cmcm* (structure type NiSO₄,
and
(d) β-NaCuPO₄-*P2₁/n* (Kawahara et al. 1993).

The crystal structure of $\text{Cu}(\text{SeO}_3\text{OH})_2 \cdot 6\text{H}_2\text{O}$ crystallizes in a new structure type. It is characterized by three structural units (i.e., $[\text{Cu}^{[4+2]}(\text{H}_2\text{O}_w)_4\text{O}_2]$, $[\text{SeO}_3(\text{O}_h\text{H})]$, and $[\text{H}_2\text{O}_w7]$). They are connected mainly by hydrogen bonds (Fig. 2). The $\text{Cu}^{[4+2]}\text{O}_6$ polyhedron forms a quite regular tetragonal *dipyramid* with site symmetry $\bar{1}$. The two pairs of independent $\text{Cu}—\text{O}_w$ bonds within the CuO_4 square are nearly identical and vary only by 0.0016 Å; $\text{O}—\text{Cu}—\text{O}$ bond angles deviate up to 2° from the ideal value. Hence, the $\text{Cu}^{[4+2]}\text{O}_6$ *dipyramid* adopts a nearly regular shape, obviously due to the rather soft connection among the structural units. The bond valence sum calculated for the Cu atom is unexpectedly large (2.26 v.u.). It is a general experience that for coordination polyhedra loosely bound to further structural units the cation—anion distances are shortened to compensate for the under-saturation of the anions. Consequently, the bond valence sums are over-estimated. Blocksatz

During the final refinement cycles, anisotropic displacement parameters of the Se, Cu, and O atoms as well as isotropic ones for the H atoms were refined. Only for the atom $\text{Ow}7$ the displacement parameters of the two H ligands were constrained to equal values during the structure refinement. The protonated selenate(VI) group exhibits $\text{Se}—\text{O}$ bonds of 1.614 to 1.626 Å (to the atoms O1 , O2 , and O3) whereas the $\text{Se}—\text{O}_h$ bond is extended to 1.695 Å. This environment is in agreement with the average $\text{Se}—\text{O}_h$ value in *monoprotonated selenate(VI)* groups of 1.71 Å as compiled by Ferraris and Ivaldi (1984).

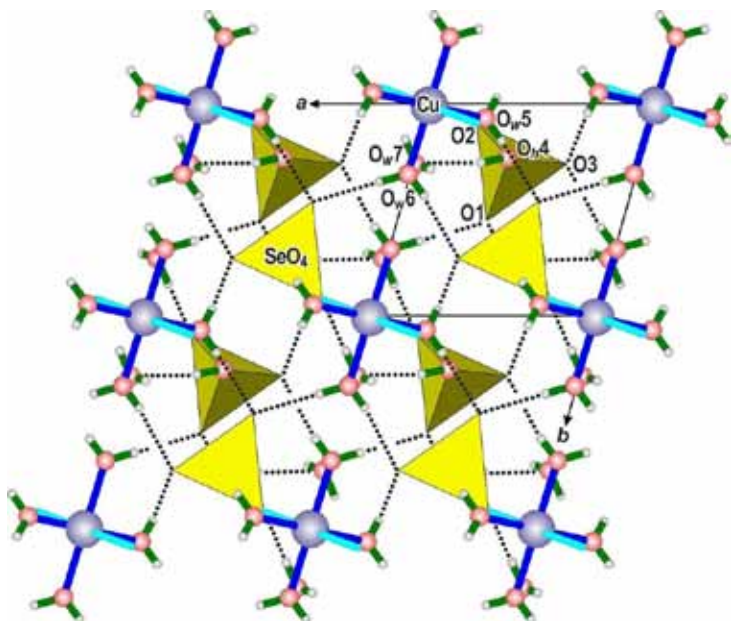


Fig. 2 The crystal structure of $\text{Cu}[\text{SeO}_3(\text{OH})]_2 \cdot 6\text{H}_2\text{O}$ in a projection parallel to $[001]$ on (110) . "Short" and "long" $\text{Cu}—\text{O}$ bond lengths are indicated in dark blue respectively turquoise colour.

- Ferraris G, Ivaldi G (1984): X—OH and O—H···O bond lengths in protonated oxoanions. — Acta Cryst B40, 1–6
- Kawahara A, Kageyama T, Watanabe I, Yamakawa J (1993): Structure du monophosphate synthétique de cuivre et de sodium. — Acta Cryst C49, 1275–1277
- Snyman HC, Pistorius CWFT (1964): Polymorphism in the selenates of Mg, Mn, Co and Cu at high pressures. — Z Krist 120, 317–322
- Zemann J (1961): Die Kristallchemie des Kupfers. — Fortschr Miner 39, 59–68
- Zemann J (1972): Copper. 29-A, Crystal chemistry. — Handbook of Geochemistry, Vol. 11/3, Berlin-Heidelberg-New York: Springer

Mechanisms of calcium carbonate mineral formation in a Roman aqueduct near Cologne (Germany) - A microstructural and geochemical approach

I. Egartner¹, R. Boch¹, K. Grewe², M. Dietzel¹, D. Hippler¹

¹*Graz University of Technology, Institute of Applied Geosciences, Rechbauerstraße 12, Graz, 8010, Austria*

²*Tannenstraße 18, 53913 Swisttal-Morenhoven, Germany*

e-mail: egartner@student.tugraz.at

A special case of freshwater carbonate deposits in man-made settings are calcium carbonate (CaCO_3) scale deposits in aqueducts and water conduits of the Roman times. They occur across the ancient expansion of the Roman Empire and therefore in different climate zones, from maritime to continental mid-latitude regions. Such scale deposits can serve as an archive, for the reconstruction of the physico-chemical environmental conditions, the palaeoclimate and the hydrogeology of the catchment and the aquifer. This study therefore aimed to investigate the ancient environmental physico-chemical conditions of the scale deposits of a Roman aqueduct channel, the so called „Eifel-Wasserleitung“, that supplied water from the Eifel mountains to the Roman city of Cologne, Germany, by microstructural and geochemical proxies. In order to reveal the meso- and microstructural fabric as well as geochemical and stable isotope compositions of the CaCO_3 scale deposits, petrographic, mineralogical and geochemical analyses have been applied (e.g., light microscopy, XRD, Raman spectroscopy and LA-ICP-MS).

First results revealed differences in carbonate mineral nucleation and growth dynamics that are indicated by individual crystal shapes, arrangements and scale textures. The polished hand specimen of the investigated CaCO_3 scale deposit shows mesofabric characteristics of individual horizons ranging from 1 to 5 mm in size and low porosity. At the microfabric level, the calcite, which forms the individual laminae, shows different growth types, occurring as microsparit, elongated columnar calcite crystals and thin micritic layers. These growth types are well comparable to other investigations of CaCO_3 scale deposits in aqueducts of the Roman Empire, but they are also frequently found in freshwater carbonate deposits in man-made settings as well as in natural environments, like speleothems. The results of the macro- and microstructural characterization, major/trace element distributions (e.g., Mg, Ca, Sr, Ba) will be discussed in respect to reaction mechanisms and mineral growth rates, potential microorganic influence, and (water) discharge.

Ammonium-iron-sulfites from a burning coal-mine dump

B. Fehér¹, S. Szakáll², M. Ende³, H.S. Effenberger³, J. Mihály⁴, I. Sajó⁵,
L. Kótai⁴, D. Szabó⁶

¹Department of Mineralogy, Herman Ottó Museum, Miskolc, Hungary

²Institute of Mineralogy and Geology, University of Miskolc, Hungary

³Institut für Mineralogie und Kristallographie, Universität Wien, Austria

⁴Institute of Materials and Environmental Chemistry, Research Centre for Natural Sciences, Budapest, Hungary

⁵Szentágotthai Research Centre, University of Pécs, Hungary

⁶Department of Mineralogy, Eötvös Loránd University, Budapest, Hungary

e-mail: herta.silvia.effenberger@univie.ac.at

Three ammonium-iron-sulfites from a burning coal dump in an abandoned open coal pit at Pécs-Vasas (Mecsek Mountains, South Hungary) were identified. They were formed by the interaction of decomposing iron sulfides and ammonia released from organic matter. For synthetic analogues to these natural phases see Erämetsä (1943); Erämetsä & Valkonen (1972); Kocsis et al. (2018).

$(\text{NH}_4)_9\text{Fe}^{3+}(\text{SO}_3)_6$ is metastable and decomposes quickly. Larsson & Niinistö (1973) performed a crystal-structure investigation in space group $P\bar{3}$ from powder X-ray data. Identity with the natural samples was proved. Isolated Fe^{2+}O_6 polyhedra are corner-connected to sulfite anions. Each corner is shared with an O atom of a $(\text{SO}_3)^{2-}$ group forming $[\text{Fe}^{3+}(\text{SO}_3)_6]^{9-}$ clusters (Fig. 1). Thus, only one O atom of the sulfite group links to a FeO_6 octahedron; the others are acceptor atoms of the hydrogen bonds.

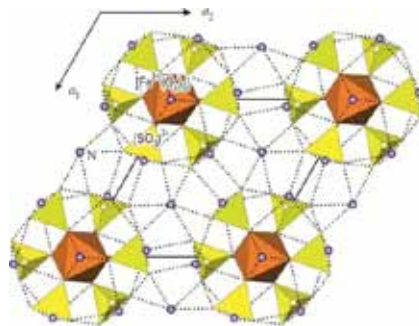


Figure 1. The crystal structure of $(\text{NH}_4)_9\text{Fe}^{3+}(\text{SO}_3)_6$.

$(\text{NH}_4)_2\text{Fe}^{2+}(\text{SO}_3)_2$ (AIS-2) crystallizes in space group $R\bar{3}m$ and is characterized by a 2D net with composition $[\text{Fe}^{2+}(\text{SO}_3)_2]^{2-}$ (Fig. 2). All three O atoms belonging to the sulfite group represent corners in FeO_6 octahedra. Thereby two layers of O atoms are parallel to (0001) and in a close packed arrangement. 1/4 of the octahedral voids in this double layer are filled by Fe^{2+} ions.

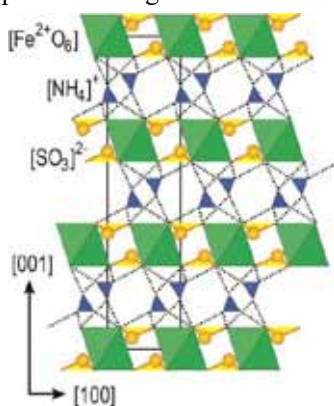


Figure 2. The crystal structure of $(\text{NH}_4)_2\text{Fe}^{2+}(\text{SO}_3)_2$.

The apical S atom points into the 2D net, the lone-electron pairs are centred in the $[\text{Fe}(\text{SO}_3)_2]^{2-}$ layer.

The crystal structure is topologically equivalent to the buetschliite-type selenites $\text{K}_2\text{Mn}(\text{SeO}_3)_2$ and $\text{K}_2\text{Co}(\text{SeO}_3)_2$ (Wildner 1992a,b). Also carbonates like eitelite and buetschliite $[\text{Na}_2\text{Mg}(\text{CO}_3)_2, \text{K}_2\text{Ca}(\text{CO}_3)_2]$, are representatives belonging to this connection schema; here the C atom of the CO_3 triangles are close to the O atom layers as only minor but significant aplanarities of the carbonate groups are verified (Knobloch et al. 1980; Effenberger & Langhof 1984). Like for in the sulfites and selenites, the apex of the carbonate points towards the octahedral layer; as pointed out by Zemmann (1981) towards the smaller and higher charged cations where one expects stronger covalent contributions to the chemical bonds between the cations and oxygen atoms.

$(\text{NH}_4)_2\text{Fe}^{3+}(\text{OH})(\text{SO}_3)_2 \cdot \text{H}_2\text{O}$ (Fig. 3) crystallizes in space group $Cmcm$ and exhibits $[\text{Fe}^{3+}(\text{OH})(\text{SO}_3)_2]^{2-}$ chains. The Fe^{3+} ions are octahedrally coordinated to four O atoms belonging to sulfite groups (O_s atoms) and to two oxygen atoms belonging to hydroxyl groups (O_h atoms). These FeO_6 octahedra are corner linked to buckled chains; each two *trans*-arranged O_h atoms are shared and represent the backbone of the $[\text{Fe}^{3+}(\text{OH})(\text{SO}_3)_2]^{2-}$ chains. The shape of these chains is related to a wind wheel with the selenite groups pointing off the $[\text{Fe}(\text{O}_s)_4\text{O}_h]^{2-}$ columns. About 8 % of the Fe^{2+} ions are displaced along the c axis (the Fe' position is 0.64 Å apart from the Fe atom).

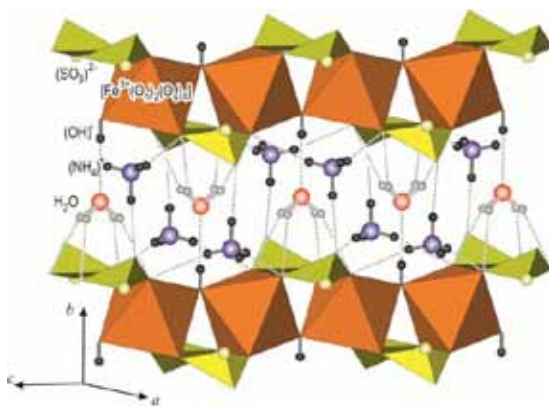


Figure 3. The crystal structure of the new mineral kollerite, $(\text{NH}_4)_2\text{Fe}^{3+}(\text{OH})(\text{SO}_3)_2 \cdot \text{H}_2\text{O}$

Intercalated between the $[\text{Fe}^{3+}(\text{OH})(\text{SO}_3)_2]^{2-}$ chains are the water molecules and the ammonium cations. Linkage is achieved by hydrogen bonds only. Despite this loose connection, the $(\text{NH}_4)^+$ group is ordered and forms clearly defined hydrogen bonds. As the O_w atom has site symmetry $m2m$, the water molecules exhibit a site disorder with respect to the H atoms at least for the structure model in space group $Cmcm$. As only two H atoms per formula unit are affected, order (neither by a reduction of symmetry nor by an enlargement of the unit cell) could be proved.

It is remarkable that for a crystal size of $6 \times 7 \times 65 \mu\text{m}^3$ it was possible to refine the half occupied H atom position without any restrictions (*i.e.*, with variable atomic coordinates and a variable isotropic displacement parameter). The H_2O molecules – like the Fe' atoms – exhibit an orientational disorder violating at least locally the *centro*-symmetry. X-ray data were collected at 220 K using a Stoe-StadiVari diffractometer equipped with a Dectris Pilatus 300 K pixel detector. It was operated with monochromatized $\text{MoK}\alpha$ radiation from a 100 W air-cooled Incoatec $\text{I}\mu\text{S}$ micro-focus X-ray tube (50 kV, 1 mA).

- Effenberg H, Langhof H (1984): On the aplanarity of the CO_3 group in buetschliite, dipotassium calcium dicarbonate, $\text{K}_2\text{Ca}(\text{CO}_3)_2$. A further refinement of the atomic arrangement. - Acta Cryst C40, 1299-1300
- Erämettä O (1943): Über Ammonisulfitoferriate. - Ann Acad Sci Fenn Ser A LIX, 5-30
- Erämettä O, Valkonen J (1972): Ammonium ferric sulfites. Suomen Kemistilehti 45, 91–94
- Knobloch D, Pertlik F, Zemann J (1980): Crystal structure refinements of buetschliite and eitelite: a contribution to the stereochemistry of trigonal carbonate minerals. N Jb Mineral Mh 1980 230-236
- Kocsis T, Magyari J, Sajó IE, Pasinszki T, Homonnay Z, Szilágyi IM, Farkas A, May Z, Effenberg H, Szakáll S, Pawar RP, Kótai L (2018): Evidence of quasi-intramolecular redox reactions during thermal decomposition of ammonium hydroxodisulfitoferriate(III), $(\text{NH}_4)_2[\text{Fe}(\text{OH})(\text{SO}_3)_2] \cdot \text{H}_2\text{O}$. - J Therm Anal Calorim 132, 493–502
- Larsson LO, Niinistö L (1973): The crystal structure of ammonium hexasulphito-ferrate(III), $(\text{NH}_4)_9[\text{Fe}(\text{SO}_3)_6]$. - Acta Chem Scand 27, 859–867
- Wildner M (1992a): Structure of $\text{K}_2\text{Mn}(\text{SeO}_3)_2$, a further buetschliite-type selenite. - Acta Cryst C48, 595
- Wildner M (1992b): Isotypism of a selenite with a carbonate: structure of the buetschliite-type compound $\text{K}_2\text{Co}(\text{SeO}_3)_2$, a further selenite. - Acta Cryst C48, 410-412
- Zemann J (1981): Zur Stereochemie der Karbonate. - Fortschr Mineral 59 95–116

Petrology and geochemistry of the Haddo House – Arnage district contact aureole, Aberdeenshire / Scotland

A. Fehleisen¹, C.A. Hauzenberger¹, J. Booth¹

*¹University of Graz, Department of Earth Sciences, Universitätsplatz 2, 8010 Graz
e-mail: anna.fehleisen@edu.uni-graz.at*

In Aberdeenshire, NE Scotland, a suite of gabbroic intrusions was intruded roughly contemporaneous to peak regional metamorphism during the middle Ordovician Grampian orogenic event. This study is based on samples collected from the Belhelvie, Haddo House, Arnage and Huntly gabbro intrusions, their metamorphic aureoles and zones of contact anatexis. The intrusions are classified as various types of gabbro and norite, composed of anorthite-rich plagioclase, olivine (usually partially or completely altered) and pyroxenes. Many samples collected at the boundary of the intrusions are norites, with significant amounts of cordierite and biotite, indicating they probably formed from magma mixing with partial melts produced by anatexis of the country rocks. The parageneses of the overprinted metapelites of the country rock range from high grade hornfels within a few meters of the gabbro contact, with Opx+Grt+Sp+Plg+Bt+Crd+Cor assemblages, transitioning further out into middle-high grade Sill+Grt+Bt and calc-silicate rich assemblages, overprinting previous regional metamorphic assemblages that contained And+Cor. The high grade hornfels often contain thin, wispy, more leucocratic veinlets thought to be produced by partial melting. These mineral paragenesis, whole rock and mineral chemistry have been used to reconstruct PT-conditions. Preliminary geothermobarometric calculations indicate that the highest grade hornfels experienced peak conditions of around 900 °C and 4-6 kbar. Further studies are being conducted using trace elements distribution help to understand the role and origins of fluids involved in the metamorphism of the aureole and related anatexis. U-Pb age dating on zircons and monazites extracted from many samples will help constrain the absolute ages of both the gabbro intrusions and the adjacent regionally metamorphosed rocks. This range of methods should deliver new insights on the causal and temporal relationship between these intrusions and the regional metamorphic events (see Droop et al. 2003; Pattison et al. 2022).

Droop GTR, Clemens JD, Dalrymple DJ (2003): Processes and conditions during contact anatexis, melt escape and restite formation: the Huntly Gabbro Complex, NE Scotland. - J Petrol 44, 995-1029

Pattison DR, Goldsmith SA (2022): Metamorphism of the Buchan type-area, NE Scotland and its relation to the adjacent Barrovian domain. - J Geol Soc 179, <https://doi.org/10.1144/jgs2021-040>

P-T-t evolution of the Pulkau and Pleiſing Nappes from the Moravo-Silesian Thaya Window, Lower Austria

M.J. Findl¹, C.A. Hauzenberger¹, E. Skrzypek¹, D. Gallhofer¹, M. Linner²

¹*Department of Earth Sciences - NAWI Graz Geocenter,
University of Graz, Universitätsplatz 2, 8010 Graz, Austria*

²*Department of Hard Rock Geology, GeoSphere Austria, Neulinggasse 38, 1030 Vienna, Austria
e-mail: martin.findl@edu.uni-graz.at*

The Moravo-Silesian Zone in the Bohemian Massif is a ~300 km long deformation zone that formed through underthrusting of the Brunia microcontinent beneath the Moldanubian–Lugian domain. The Moravo-Silesian zone crops out in three tectonic windows which are from north to south: (1) the Silesian zone, (2) the Svratka and (3) the Thaya windows, the last two being known as the Moravian zone *sensu stricto*. The Svratka and Thaya windows consist of a parautochthonous basement, a ~7 km thick pile of two nappes (the Lower and Upper Moravian Nappes) (Štípská et al. 2015). In relation to local ductile and brittle-ductile shear zones, only one major regional thrust runs through the Thaya Window, which separates the tectonically upper Pleiſing (Lower and Upper Moravian Nappes) from the tectonically lower Pulkau Nappe (basement) (Linner et al. 2021). The research area is located in the Austrian part of the Thaya Window.

Samples taken along two SE-NW trending profiles (A and B) were used to constrain the P-T-t evolution of the Thaya Window using petrological modelling together with U-Pb zircon and Th-U-Pb monazite dating. Profile A, northern Thaya window: P-T estimates for the Pulkau Nappe are ~600 °C and 6.5-7.5 kbar and for the Pleiſing Nappe slightly higher conditions of 550 °C up to 630 °C and 11 kbar. Graphite thermometry indicates 550±30 °C for the Pleiſing Nappe. Two phase garnets can be clearly recognised in one sample. Inner garnet cores indicate P-T conditions of ca. 550 °C/5 kbar and inner garnet rims ca. 630 °C and 6 kbar.

Profile B, central Thaya Window: P-T estimates for the Pulkau Nappe are 600 °C and 8 kbar. Temperature is estimated to 603±30 °C (graphite thermometry) and 606±15 °C (Zr in rutile thermometry). The Pleiſing Nappe exhibits 650-660 °C and 10.5-11 kbar, while graphite thermometry points to lower temperatures of 570±30 °C and 530±30 °C.

The Ky-Grt micaschists from Meiseldorf (Upper Moravian Nappe after Štípská et al. (2015); northwestern part of the Pleiſing Nappe after Linner et al. (2021)) indicate 680-720 °C and 8-8.5 kbar based on petrological modelling and Zr in rutile thermometry.

Zircon dating by LA-MC-ICP-MS yields a weighted mean protolith ²⁰⁶Pb/²³⁸U age of 588±7.8 Ma for a metatuffite belonging to the Pleiſing Nappe (profile A) and 592±7.8 Ma for a metatuffite from the Pulkau Nappe (profile B). Monazite commonly occurs in metapelite with grain sizes from 10-50 µm. In rare cases monazite can reach up to 100 µm. Th-U- total Pb chemical dating of monazite by EPMA yields 301-344 Ma in the Pleiſing Nappe. ²⁰⁶Pb/²³⁸U monazite dates by LA-MC-ICP-MS range from 312 to 356 Ma.

We provide the first evidence for Ediacarian magmatism and coeval sedimentation for the protoliths of the Moravian zone. We confirm the occurrence of regional metamorphism from lower amphibolite to lower granulite facies conditions in the Austrian part of the Moravian zone and propose that peak P-T conditions were attained between 312 and 356 Ma based on monazite dating.

- Linner M, Rötzel R, Huet B, Hintersberger E (2021): A new subdivision for the Moravian Superunit - The redefined Pleißing and the newly defined Pulkau nappe. – In: Proceedings of the 4th Friends of the Bohemian Massif Meeting, October 7-10, Freistadt, Austria, 10
- Štípská P, Hacker BR, Racek M, Holder R, Kylander-Clark ARC, Schulmann K, Hasalová P (2015): Monazite dating of prograde and retrograde P–T–d paths in the Barrovian Terrane of the Thaya Window, Bohemian Massif. - J Petrol 56, 1007–1035, url: <https://doi.org/10.1093/petrology/egv026>

Twinning of götzenite and wöhlerite from the Fohberg phonolite, Kaiserstuhl

R.X. Fischer¹, J. Birkenstock¹, G. Biskup², L.A. Fischer³, W.-A. Kahl⁴, A. Klügel¹, S. Spürgin⁵

¹FB 5 Geowissenschaften, Universität Bremen, Klagenfurter Straße, 28359 Bremen, Germany

²Breslauer Straße 6a, 75181 Pforzheim, Germany

³Institut für Geo- und Umweltwissenschaften, Geochemie, Albert-Ludwigs-Universität Freiburg, Germany

⁴MAPEX Center for Materials and Processes, University of Bremen, 28359 Bremen, Germany

⁵Hans G. Hauri KG, Mineralstoffwerke, Bergstraße 114, 79268 Bötzingen, Germany

e-mail: rfischer@uni-bremen.de

Götzenite and wöhlerite were found as part of a fissure assemblage in the Fohberg phonolite (Kaiserstuhl, SW Germany), in close association with natrolite and clinopyroxene (aegirine-augite). Both minerals have a similar appearance with yellowish brown prismatic crystals as shown in Fig. 1. Single species were separated and investigated by single-crystal X-ray diffraction (SXRD), electron probe microanalyzer (EPMA), laser ablation inductively coupled plasma mass spectrometry (LA-ICP-MS), and X-ray diffraction contrast tomography (DCT) showing the presence of two different phases, götzenite and wöhlerite.



Figure 1. Yellowish brown crystals of götzenite and wöhlerite in association with natrolite (white) and clinopyroxene (black). Widths of figures are 11 cm (top) and 5.7 mm (bottom), respectively.

Götzenite has a chemical composition of $\text{Na}_{1.5}\text{Ca}_{5.1}\text{Sr}_{0.1}\text{Zr}_{0.1}\text{Ti}_{0.8}\text{Nb}_{0.2}(\text{Si}_2\text{O}_7)_2\text{O}_{0.4}\text{F}_{3.7}$ with additional $\text{Fe}+\text{Mn}+\text{REE} < 0.3$. SXR D revealed rotation twinning on [001] (twin matrix -**a**-1/2**c**, -**b**, **c**; twin components 40:60) with lattice parameters $a = 9.6191(3) \text{ \AA}$, $b = 5.7342(2) \text{ \AA}$, $c = 7.3386(2) \text{ \AA}$, $\alpha = 89.986(1)^\circ$, $\beta = 101.040(1)^\circ$, $\gamma = 100.485(1)^\circ$, triclinic, space group $P\bar{1}$, refined to $R1 = 3.4 \%$.

Wöhlerite has a chemical composition of $\text{Na}_{1.6}\text{Ca}_{4.4}\text{Fe}_{0.2}\text{Mn}_{0.1}\text{Zr}_{0.6}\text{Ti}_{0.2}\text{Nb}_{0.8}(\text{Si}_2\text{O}_7)_2\text{O}_{2.4}\text{F}_{1.4}$ with additional $\text{Sr} + \text{REE} < 0.05$. SXR D revealed rotation twinning on [001] (twin matrix -**a**-**c**, -**b**, **c**; twin components 31:69) with lattice parameters $a = 10.842(1) \text{ \AA}$, $b = 10.249(1) \text{ \AA}$, $c = 7.2673(8) \text{ \AA}$, $\beta = 109.344(4)^\circ$, monoclinic, space group $P2_1$, refined to $R1 = 1.3 \%$.

The crystal structures closely resemble those of untwinned götzenite (Christiansen et al. 2003; Bellezza et al. 2004) and untwinned wöhlerite (Mellini et al. 1979; Biagoni et al. 2012), respectively.

Bellezza M, Merlino S, Perchiazzi N (2004): Chemical and structural study of the Zr,Ti-disilicates in the venanzite from Pian di Celle, Umbria, Italy. – *Europ J Mineral* 16, 957-969

Biagoni C, Merlino S, Parodi GC, Perchiazzi N (2012): Crystal chemistry of minerals of the wöhlerite group from the Los Archipelago, Guinea. – *Canad Mineral* 50, 593-609

Christiansen CC, Johnsen O, Makovicky E (2003): Crystal chemistry of the rosenbuschite group. – *Canad Mineral* 41, 1203-1224

Mellini M, Merlino S (1979): Refinement of the crystal structure of wöhlerite. – *Tschermaks Mineral Petrogr Mitt* 26, 109-125

Extreme chemical disequilibrium patterns in hydrothermal vein minerals – a case study from Columbian emeralds

G. Franz¹, V. Khomenko^{1,2}, F. Schiperski¹, U. Gernert³, J. Nissen³

¹*Institut für Angewandte Geowissenschaften, Technische Universität Berlin*

²*Institute of Geochemistry, Mineralogy and Ore Formation, Academy of Sciences, Kyiv*

³*Zentraleinrichtung Elektronenmikroskopie Technische Universität Berlin*

e-mail: gefra548@gmail.com; gerhard.franz@tu-berlin.de

Chemical zoning in metamorphic and igneous minerals has been shown to be a very powerful tool for reconstruction of pressure-temperature-time condition of growth of minerals. Vein minerals have also been in the focus because of their common occurrence with economically interesting mineralizations. Columbian emeralds formed in veins in low-grade metamorphic black shales; they are known as highly-prized gemstones and have been studied extensively over the years (e.g., Pignatelli et al. 2015; Schmetzer & Martyan 2023). We present data about their growth phenomena, from combined element distribution mappings with μ -XRF and the electron microprobe EMPA in oriented thin sections, and from scanning electron microscopy SEM.

External growth phenomena are small indentations on the basal plane (0001), which are interpreted as an expression of skeletal growth along the *c*-axis of the beryl, and rare sceptre growth. Chemical zoning shows very unusual patterns with sector zoning, which is however variable for different elements in different crystals. Sector boundaries are in some

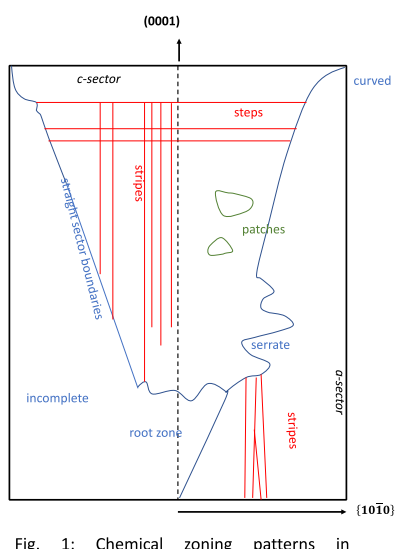


Fig. 1: Chemical zoning patterns in Columbian emerald

instances straight, or curved, or serrate (Fig. 1). In addition to sector zoning, stripes in the *a*- and *c*-sector were observed with alternating chemical composition. Most unusual are chemical patterns produced by the substitution $\text{Al} + \square(\text{channel}) = \text{Mg} + \text{Na}$, with straight borders, but neither parallel nor perpendicular to the *c*-axis (Fig. 2). Another unusual feature was observed in the root zone of the crystals with cone-shaped structures extending in *c*-direction from a homogeneous zone.

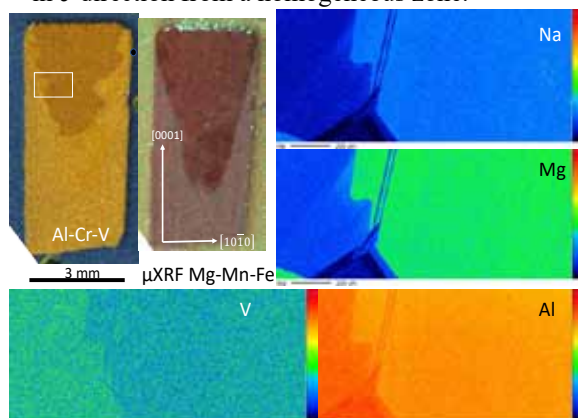


Fig. 2: Element distribution maps for crystal no. 2; left part shows combined intensities for μ -XRF for the whole crystal, other images results from EMPA mapping of a selected area (white frame in Al-Cr-V-mapping).

Freely grown crystals, such as beryls in open veins are often characterized by dissolution-formed etch pits. The Columbian emeralds also show such etch pits, with different shapes (rectangular, diamond-shaped), originating from point- as well as line-defects. They are typically arranged in chains, parallel and oblique to the beryl's *c*-axis (Fig. 3), what has not been observed in pegmatitic beryls (Kurumathoor & Franz 2018). These chains of etch pits point to screw-dislocation arrays and are another indication for rapid growth of the crystals. In summary, both features of growth and dissolution phenomena point to extreme disequilibrium.

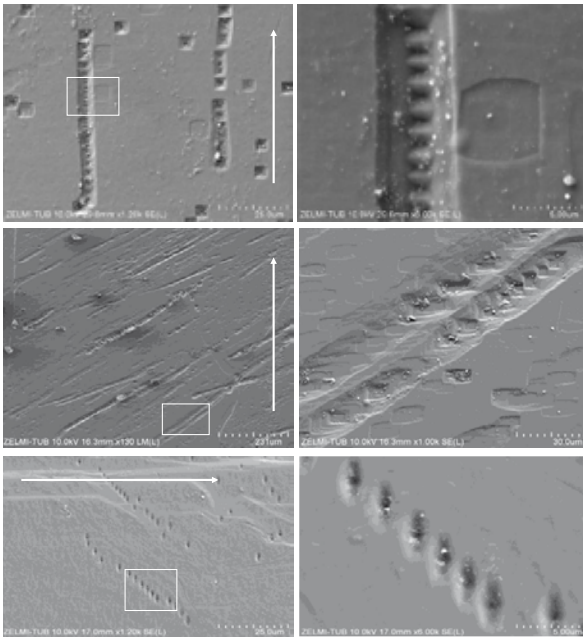


Fig. 3: SEM images of the first-order prism face of Columbian emeralds. Etch pits are arranged in chains, indicating dislocation arrays. Direction of *c*-axis is indicated by the arrow.

- Kurumathoor R, Franz G (2018): Etch pits in beryl as indicators for dissolution behaviour. – *Eur J Miner* 30, 107-124
- Pignatelli I, Giuliani G, Ohnenstetter D, Agrosi G, Mattheu S, Moriot C, Branquet Y (2015): Colombian trapiche emeralds: Recent advances in understanding their formation. - *Gems & Gemology* 51, 222-259
- Schmetzer K, Martayan G (2023): Morphology of Columbian emerald: some less-common cases and their growth and dissolution history. – *Gems & Gemology* 59, 46-71

High-Ti Paleozoic basalts in NE Bavaria

G. Franz¹, F. Lucassen², F. Schiperski¹, M. Kutzschbach¹

¹*Institut für Angewandte Geowissenschaften, Technische Universität Berlin*

²*MARUM-Center for Marine Environmental Sciences-Universität Bremen*

e-mail: gefra548@tu-berlin.de; gerhard.franz@tu-berlin.de

The Paleozoic sedimentary rocks, surrounding the Münchberg Massif with its relict high-pressure nappe pile in NE Bavaria, host Ordovician to Devonian mafic volcanic and subvolcanic rocks (commonly named diabase in the German literature) that formed timely close to the deposition of the sediments. In the W and SW of the Münchberg Massif, these rocks were previously studied for age, structure and chemical composition by Höhn et al. (2018); similar rocks can be found in the E of the Münchberg Massif. Late Carboniferous granites of the Fichtelgebirge represent the next magmatic pulse, and post-Variscan mafic dikes intruded these granites as well as the metamorphic series of the Münchberg Massif.

The focus of this study is the elemental composition of stratigraphically well-defined mafic volcanic rocks from the (meta)sedimentary Thuringian facies E of the Münchberg Massif (E-domain) and post-Variscan mafic dikes from this Massif, and the Sr, Nd, and Pb isotope compositions of these mafic volcanic rocks and comparison with previously studied mafic rocks from the W domain (Höhn et al. 2018). Of special interest are the unusually high Ti-contents.

The Ordovician diabase rocks from the E and the Devonian rocks from the W are characterized by high TiO₂-contents up to almost 6 wt%, accompanied by high Fe₂O_{3(tot)}-contents of up to almost 20 wt%. The initial ⁸⁷Sr/⁸⁶Sr_i of E Ordovician samples are variable (0.7031 to 0.7107) and most initial εNd_i (+2.8 to +6.3) closely scatter around +5 irrespective the locality and without covariation of Nd and Sr isotopes. The E post-Variscan dikes show a similar range of ⁸⁷Sr/⁸⁶Sr_i (0.7052 to 0.7081) but, compared with E Ordovician, much lower εNd_i between -1.3 and +0.9. The W Ordovician-Silurian samples show only a small variation ⁸⁷Sr/⁸⁶Sr_i (0.7033 to 0.7039) and εNd_i (+2.8 to +3.4). The ⁸⁷Sr/⁸⁶Sr_i (0.7042 to 0.7046) of the W Devonian rocks is rather uniform, but εNd_i is variable in two clusters, +4.8 to +6.1 and +2.3 to +2.5, that resemble the εNd_i of E and W Ordovician rocks. Initial uranogenic Pb isotope compositions of most Ordovician and Devonian samples from both domains plot in overlapping arrays above or near the crustal Pb-evolution line (Stacey and Kramers, 1975). The W Silurian rocks are different and show the highest ²⁰⁷Pb/²⁰⁴Pb_i and ²⁰⁶Pb/²⁰⁴Pb_i of the whole sample suite. The initial ²⁰⁸Pb/²⁰⁴Pb of all sample groups plot in a similar array except the Silurian samples with the two the highest and the lowest ²⁰⁸Pb/²⁰⁴Pb_i values. The E post Variscan dikes have a chemical signature which is clearly different from the Ordovician rocks.

The data are discussed in the context of the paleotectonic position of the rocks, the southern passive margin of the Rheic ocean bordering northern Gondwana or alternatively a separate Saxo-Thuringian Ocean between a Gondwana derived microcontinent and Gondwana.

Höhn S, Koglin N, Klopff L, Schüssler U, Tragelehn H, Frimmel H, Zeh A, Brätz H (2018): Geochronology, stratigraphy and geochemistry of Cambrian, Ordovician, Silurian and Devonian volcanic rocks of the Saxothuringian in NE Bavaria (Germany). – *Int J Earth Sci* 107, 359-377

Stacey JS and Kramers JD (1975): Approximation of terrestrial lead isotopic evolution by a two-stage model. – *Earth Planet Sci Lett* 26, 207-221

Mineral assemblage, geochemistry and geochronology of the Kawisigamuwa carbonatite, Sri Lanka

D. Gallhofer¹, E. Skrzypek¹, C.A. Hauzenberger¹, G. Auer¹, G.W.A.R. Fernando²

¹*Institute for Earth Sciences, University of Graz*

²*Department of Physics, The Open University of Sri Lanka*

e-mail: daniela.gallhofer@uni-graz.at

The Kawisigamuwa and Eppawala carbonatites in Sri Lanka are located within upper amphibolite to granulite facies metasedimentary and metaigneous rocks of the Wann Complex. Both occurrences have previously been interpreted as mantle-derived carbonatites, however, a recent study has shown that the Eppawala carbonatite was derived from melting of a sedimentary carbonate protolith (Wang et al. 2021). Since the origin and formation of the Kawisigamuwa carbonatite is still unclear, this study investigates its mineral paragenesis, geochemistry (XRF, EPMA, IRMS), and geochronology (LA-ICPMS).

Textural relationships indicate the following sequence of mineral formation: 1) calcite, olivine, zircon 1, phlogopite, apatite, baryte, celestine, and spinel (?) form the primary mineral assemblage, 2) dolomite, monazite, zircon 2, baddeleyite, magnetite, spinel, ilmenite, and sulfides, 3) zirconolite, allanite, and Th-rich phases and a late stage of 4) serpentinization of olivine and weathering products of Fe-oxides and other minerals.

The Kawisigamuwa carbonatite is dominated by calcite (48-51.7 wt.% CaO), has low SiO₂ (<2.3 wt.%) and P₂O₅ (<0.14 wt%) and elevated Sr (4497-4930 µg/g), La (56-188 µg/g), and Ce (164-422 µg/g) contents. Olivine has moderately high x_{Mg} (0.85-0.91) and is surrounded by reaction coronae of tremolite and/or diopside and dolomite. Phlogopite has x_{Mg} ranging from 0.88 to 0.92, elevated Ba (0.04-0.19 apfu) and moderate F (0.35-0.56 apfu) contents. Oxygen ($\delta^{18}\text{O}_{\text{VSMOW}} = 13.75$ to 14.14) and carbon ($\delta^{13}\text{C}_{\text{VPDB}} = -2.73$ to -2.52) isotopes of calcite from Kawisigamuwa overlap those of Eppawala and are slightly lower than those of Sri Lankan marbles. Fractionation of oxygen isotopes between calcite and zircon indicate an equilibrium temperature of ~850 °C.

Geochronological data support a multi-stage evolution of the mineral assemblage at Kawisigamuwa: 1) oscillatory zoned zircon 1 yields the crystallisation age of 532.39 ± 0.66 Ma, 2) recrystallisation lead to partial resetting of U-Pb ages and formation of zircon 2 at 518 Ma or later and 3) a late stage of (re-)crystallisation is recorded by allanite (U-Pb ca. 474 Ma).

While the Kawisigamuwa carbonatite shows mineral assemblages and some geochemical characteristics consistent with mantle-derived carbonatites, the mineral chemical and isotopic characteristics do not support a mantle origin. We suggest that the Kawisigamuwa carbonatite is another example of a crustal-derived anatectic carbonate body.

Wang J, Su B-X, Chen C, Ferrero S, Malaviarachchi, SPK, Sakyi, PA, Yang Y-H, Dharmapriya, PL (2021): Crustal Derivation of the ca. 475 Ma Eppawala Carbonatites in Sri Lanka. – J Petrol 62, 11, 1-18

Relationships between fluid-flow, fluid-rock-interaction, and evolving microstructures in a polyphase system – results from experimental approaches using synthetic impure carbonates

J. Gärtjen¹, B. Rose¹, D. Sorger¹, S. Piazzolo², T. Müller¹

¹*Geoscience Centre Göttingen, Georg-August-University, Germany*

²*School of Earth and Environment, The University of Leeds, United Kingdom
e-mail: jochen.gaetjen@uni-goettingen.de*

In polyphase materials (e.g., porous rocks), fluid-mineral-reactions typically result in complex microstructural changes □ including a spatial and temporal evolution of fluid pathways. However, a full quantitative understanding of the accompanied processes governing the development of such microstructures remains elusive. In this experimental study, we focus on the wollastonite forming reaction in a synthetic impure carbonate system with two reactants (calcite + quartz) and two products (wollastonite + CO₂) phases. This decarbonation reaction causes a negative 33 % volume change of the solid phase.

The experiments were carried out using a rapid quench cold seal apparatus. In a first step, a CaCO₃-SiO₂-mixture (~ 7:3) was pressurized to 0.2 GPa together with a fluid phase (~ 5 wt% H₂O, initial $X(\text{CO}_2) = 0.5$) and heated to 600 °C for one week allowing the powder to recrystallize and anneal prior to overstepping of the reaction (initial porosity = ~ 13 vol%). In a second step, we increased the temperature (700 °C or 800 °C) to trigger the decarbonation reaction for an additional week.

Preliminary results indicate that variations in the reaction affinities govern the resulting microstructures. Experiments with conditions close to the equilibrium state ($T = 700\text{ °C}$, final $X(\text{CO}_2) = 0.56$, final porosity = ~ 20 vol%) exhibit low nucleation rates in combination with relative high growth rates resulting in a slightly more porous microstructure with a few idiomorphic wollastonite grains growing in the pore space. Here, only a small amount of SiO₂ and CaCO₃ reacted to form CaSiO₃ and CO₂ as the system reached the equilibrium state due to the evolving $X(\text{CO}_2)$ fluid composition in the internally buffered system. Experiments conducted at conditions far away from the equilibrium state ($T = 800\text{ °C}$, final $X(\text{CO}_2) = 0.86$) exhibit very high nucleation rates combined with comparatively low growth rates. Here, the reaction went to completion consuming all of the SiO₂ without reaching the equilibrium state. The remaining CaCO₃ grains are interconnected by a very porous (~ 35 vol%) nano- to microcrystalline mass of wollastonite.

Future experimental work will include piston cylinder experiments, fluid-flow experiments and time series. Quantitative orientation analysis using EBSD (Electron Backscatter Diffraction) will provide information about the micro/nano-structure of the material while serial sectioning within an SEM or NanoCT scanning will allow for porosity and permeability assessment. The experimental setup will be extended to include a mineral reaction with positive volume change (periclase + H₂O = brucite) □ as well as a combination of both reaction types.

Real structure of mineral kenyaite, $\text{Na}_2\text{Si}_{20}\text{O}_{40}(\text{OH})_2 \cdot 8 \text{H}_2\text{O}$

I. Grosskreuz¹, B. Marler¹

¹Dept. of Geology, Mineralogy and Geophysics, Ruhr University Bochum; Germany
e-mail: isabel.grosskreuz@rub.de

Only very few natural occurrences of the rare mineral kenyaite are known. Named after Kenya, the country where the first sample had been discovered, kenyaite is known since 1967 with a composition of the type material $\text{NaSi}_{11}\text{O}_{20.5}(\text{OH})_4 \cdot \text{H}_2\text{O}$ according to Hans Eugster [1]. Different compositions, however, have been determined due to the fact that i) a part of the sodium cations can easily be leached from the structure with water and ii) the content of structural water seems to depend on the relative humidity and temperature of the environment and/or the pre-treatment of the sample prior to chemical analysis. The structure of kenyaite remained hidden for a long time because of very small crystals, a complex structure and a certain degree of structural disorder. Only in 2021, the crystal structure of synthetic kenyaite was published [2]. Kenyaite is a layered silicate and belongs to the group of Hydrrous Layer Silicates (HLSs) [3] similar to minerals kanemite [4], $\text{Na}_4[\text{H}_4\text{Si}_8\text{O}_{20}] \cdot 12 \text{H}_2\text{O}$, magadiite [5], $\text{Na}_2[\text{Si}_{14}\text{O}_{26}(\text{OH})_6] \cdot 6 \text{H}_2\text{O}$, and makatite [6], $\text{Na}_8[\text{Si}_{16}\text{O}_{32}(\text{OH})_4] \cdot 16 \text{H}_2\text{O}$.

Experimental data: Natural kenyaite samples from Lake Magadi were kindly provided by K. Beneke and G. Lagaly, Kiel, Germany. In all samples, kenyaite was associated with either magadiite, quartz or both phases. For structure analysis, a fairly well crystalline sample (Fig. 1) was chosen which contained quartz as an impurity. Powder XRD data were recorded in modified Debye-Scherrer geometry using $\text{CuK}\alpha_1$ radiation. The average structure of kenyaite was refined using the FullProf 2K program [7].

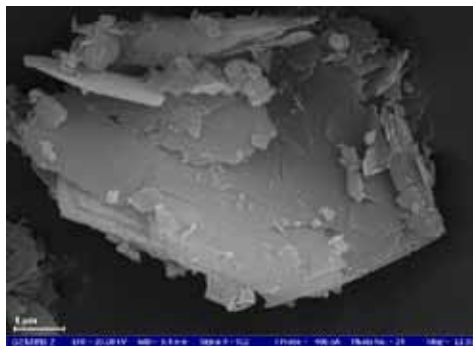


Fig. 1: Plate-like morphology of kenyaite crystals.

Subsequently, the disordered real structure was studied by comparing experimental powder XRD patterns with simulated ones calculated with the program DIFFaX [8]. In order to simulate the broadened reflections in the XRD powder diagram illustrating the disorder, various structure models were constructed based on a stacking disordered arrangement of layers.

The average structure

Nearly identical to synthetic kenyaite, the structure of the kenyaite mineral contains thick silicate layers (thickness: 15.9 Å) and bands of edge-sharing $[\text{Na}(\text{H}_2\text{O})_{6/1.5}]$ octahedra which are intercalated between these layers (Fig. 2). The dense layers (six layers [3]) have the same topology as the layers of RUB-6 [9] and synthetic kenyaite and possess a high silicon Q^4 to Q^3 ratio of 4.0. One half of the terminal $\equiv\text{Si-O}$ units form silanol groups ($\equiv\text{Si-OH}$) while the other half forms siloxy groups ($\equiv\text{Si-O}^-$) to compensate the charge of the sodium cations. Interestingly, quite strong hydrogen bonds ($d(\text{O} \cdots \text{O}) = \text{approx. } 2.5 \text{ Å}$) exist (confirmed by ^1H MAS NMR spectroscopy) between the terminal silanol/siloxy groups themselves as intra-layer interactions, but also between the silanol/siloxy groups and water molecules of the octahedra. The kenyaite mineral crystallizes with space group symmetry $F2dd$ (No. 43, setting 3) and lattice parameters $a = 10.604(1) \text{ Å}$, $b = 10.080(1) \text{ Å}$, $c = 79.383(8) \text{ Å}$.

Analysis of the real structure

The structure of kenyaite is slightly disordered typical for hydrous layer silicates which possess only weak ionic interactions between the alternating blocks of silicate layers and cations (in this case: $\text{Na}(\text{H}_2\text{O})_{6/1.5}$ octahedra). The silicate layers of kenyaite (six layers) and inter-layer regions containing the octahedra are stacked perpendicular to the *ab*-plane.

The type of stacking disorder was investigated in detail by calculating hypothetical powder diagrams corresponding to various stacking sequences. The regular (average) structure of kenyaite possesses an ordered ABCD... stacking sequence of identical six layers with a sequence of shift vectors of $0.5a + 0.5b \Rightarrow -0.5a + 0.5b \Rightarrow 0.5a + -0.5b \Rightarrow 0.5a + 0.5b$ between successive layers. In addition, successive layers are rotated by 90° against each other (Fig. 2). However, other shift vectors are also possible (e.g., $0.25a + 0.25b$ or $-0.25a + 0.25b$) without distortion of structural building blocks. Figure 3 shows a comparison between the experimental PXRD diagram and simulated diagrams.

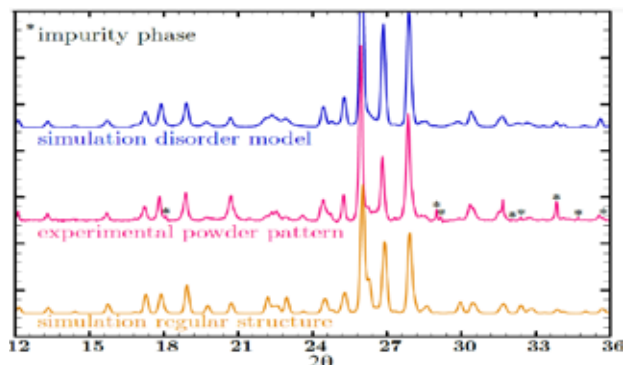


Fig. 3: Section of the experimental PXRD diagram of mineral kenyaite (quartz subtracted) and the simulated diagrams of the regular and disordered structure.

* indicate reflections of the impurity phase Trona.

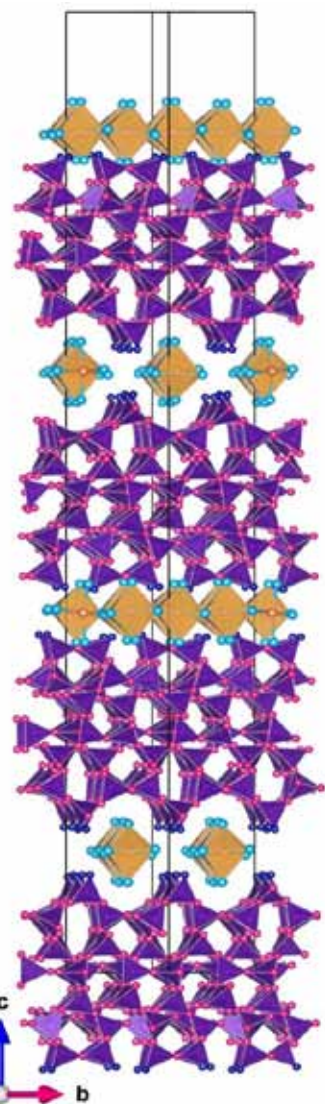


Fig. 2: Average structure of mineral kenyaite.

- [1] Eugster HP (1967): Hydrous sodium silicates from Lake Magadi, Kenya: precursors of bedded chert. - Science 157 (3793) 1177–1180
- [2] Marler B, Großkreuz I, Gies H (2021): The crystal structure of synthetic kenyaite, $\text{Na}_2\text{Si}_{20}\text{O}_{40}(\text{OH})_2 \cdot 8\text{H}_2\text{O}$. - J Solid State Chem 300, Article No. 122215
- [3] Marler B, Grünewald-Lücke A, Ikeda T, Zuber P, Heimes H, Gies H: Database of hydrous layer silicates - <https://www.hls-database.com>
- [4] Vortmann S, Rius J, Marler B, Gies H (1999): Structure solution from powder data of the hydrous layer silicate kanemite, a precursor of the industrial ion exchanger SKS-6. - Eur J Mineral 11 125–134
- [5] Marler B, Krysiak Y, Grosskreuz I, Gies H, Kolb U (2022): The crystal structure of mineral magadiite, $\text{Na}_2\text{Si}_{14}\text{O}_{28}(\text{OH})_2 \cdot 8\text{H}_2\text{O}$. - Amer Mineral 107, 211–2110
- [6] Annehed H, Faehl L, Lincoln LJ (1982): Crystal structure of synthetic makatite $\text{Na}_2\text{Si}_4\text{O}_8(\text{OH})_{2.4} \cdot \text{H}_2\text{O}$. - Z Kristallogr 159, 203–210
- [7] Rodríguez-Carvajal J (1993): Recent advances in magnetic structure determination by neutron powder diffraction. - Physica B: Condensed Matter 192, 55–69
- [8] Treacy MMJ, Deem MW, Newsam JM: *DIFFaX*, <https://www.public.asu.edu/~mtreacy/DIFFaX.html>
- [9] Krysiak Y, Marler B, Barton B, Plana-Ruiz S, Gies H, Neder RB, Kolb U (2020): New zeolite-like RUB-5 and its related hydrous layer silicate RUB-6 structurally characterized by electron microscopy. - IUCr J 7, 522–534

“Nothing is more important than health“ Eduard Suess (1831-1914)
Eduard Suess was a leading contributor to the
city of Vienna's projects of the century:
the 1st Vienna spring-water pipeline and the regulation of the Danube

M. Hamilton¹

*¹Geological Archive, Department of Geology, University of Vienna
e-mail: margarete.hamilton@univie.ac.at*

E. Suess not only played an important role as a professor of paleontology and geology at the University of Vienna, but as a member of the Vienna City Council he also submitted his expertise on the two century projects of the city of Vienna.

In the Archive of the Geological Institute at the University of Vienna exist handwritten notes by E. Suess between 1861 and 1869 dealing with the meetings of the Vienna City Council with regard to the quality of the water for the city and, as a result, the health of the population.

In his memoirs, which were published posthumously in 1916, Suess points out in an essential conversation with the then mayor Cajetan Felder (1814-1894) that "nothing is more important than the health" of the population of Vienna. The rapid population increase, the infections with dysentery, typhus and cholera in 1855 were a significant problem, also poor water quality and a lack of sewerage.

Between 1869 and 1873 a 90 km long canal was built from the springs in the foothills of the Eastern Alps via tunnels and aqueducts to the water tanks of the city of Vienna. This first Vienna high spring water pipeline was officially opened on October 24, 1873 with the commissioning of the high jet fountain on Schwarzenbergplatz in the presence of Emperor Franz Josef I. There also exist a copy of the piano piece "Die Hochquelle" composed by Eduard Strauss (1835-1916) in 1911. The piece is dedicated to the initiator of the first Vienna spring-water pipeline Eduard Suess.

The second major project to improve water quality and thus improve the health of Vienna's population was the regulation of the Danube bed. With the Danube Regulation Commission created in 1868, not only should the devastating floods of the Danube river be prevented, but also new facilities for the creation of shipping and trade should be made possible. Work began on May 14, 1870 in the presence of Emperor Franz Josef I, and just 5 years later, on April 15 and 16, 1875, the two breakthroughs were made on the north and east of the Danube.

In the geological archive exist three soil maps of Vienna from the years 1873-1875 showing the course of the Danube in the old and new beds. A copy of a letter from the Emperor to E. Suess from 1911 has also survived, in which the Emperor praised E. Suess for his achievements for the benefit of the people of Vienna.



Figure 1. Stadler R Lithographie: Der neue Springbrunnen vor dem Schwarzenberg-Palais (1873)



Figure 2. Plan der Donauregulierung in Wien. Donauregulierungskommission (1875). Geological Archive, KS ¼

- Drenning A (1973): Die 1. Wiener Hochquellenleitung. - Festschrift aus Anlaß der 100-Jahr-Feier am 24. Oktober 1973
- NN (1875): „Die Donau-Regulierung bei Wien“. - Herausgegeben aus Anlaß der feierlichen Eröffnung der Schifffahrt im neuen Strombette am 30. Mai 1875 von der Donau-Regulierungs-Commission in Wien
- Stadler R (1873): Die Wasserversorgung der Stadt Wien in ihrer Vergangenheit und Gegenwart. Denkschrift zur Eröffnung der Hochquellenwasserleitung im Jahr 1873. 296 pp
- Suess E (1916): Erinnerungen. 154 p

Compressibility of pearceite-polybasite group minerals

C. Hejny¹

¹University of Innsbruck, Innrain52, 6020 Innsbruck, Austria

e-mail: Clivia.hejny@uibk.ac.at

Pearceite-polybasite group minerals (PPGM), [(Ag,Cu)₆(As,Sb)₂S₇][Ag₉CuS₄], display Ag⁺ fast ion conduction character. The crystal structure is described as being composed of two different layers: layer A with general composition [(Ag,Cu)₆(As,Sb)₂S₇]²⁻ and layer B with general composition [Ag₉CuS₄]²⁺. Ionic conductivity is observed in layer B (Bindi et al. 2007). The root-name *pearceite* is given to minerals where As is dominant over Sb and the root-name *polybasite* for Sb-dominant phases. A suffix attached to the root-name stands for the superstructure variant, the three most common ones are (1) trigonal with lattice parameters $a \approx 7.5$, $c \approx 12.0$ Å, PPG-*Tac*, trigonal with lattice parameters $a \approx 15.0$, $c \approx 12.0$ Å, PPG-*T2ac* and monoclinic with $a \approx 26.0$, $b \approx 15.0$, $c \approx 24.0$ Å, $\beta \approx 90^\circ$, PPG-*M2a2b2c*, although a number of different crystal structures and their temperature-induced phase transitions are known (e.g., Bindi et al. 2006).

In-situ single-crystal diffraction experiments of PPGMs in a diamond anvil cell were performed to test the possibility of using pressure as a switch for the ionic conductivity. Initial experiments have indeed shown that it is possible to induce phase transitions from the ionic conduction form with the aristotype crystal structure PPG-*Tac* to an ordered or partially ordered superstructure form with Ag ions “frozen-up” into fixed atomic positions. In this way a crystal of pearceite-*Tac* transformed to the -*T2ac* crystal structure at a pressure of 0.5(1) GPa and a crystal of polybasite-*T2ac* showed a phase transition to the -*M2a2b2c* superstructure variant at 4.5(2) GPa. In both cases the compressibility is significantly larger along the *c*-direction, i.e. perpendicular to the layered structure, which is in accordance with a reduction of the size for the ionic conductivity pathways. The limited number of datapoints within the small pressure range from AP to 5.4GPa and without considering phase transitions only allows for an estimation of the bulk modulus, which, with a value of $K = 48(1)$ GPa, is well in accordance of other sulphosalt materials.

Bindi L, Evain M, Pradel A, Albert S, Ribbs M, Menchetti S (2006): Fast ion conduction character and ionic phase-transitions in disordered crystals: the complex case of the minerals of the pearceite–polybasite group. - Phys Chem Miner 33, 677-690

Bindi L, Evain M, Spry PG, Menchetti S (2007): The pearceite-polybasite group of minerals: Crystal chemistry and new nomenclature rules. - Amer Miner 92, 918-925

Research insights based on documents from the Geological Archive of the University of Vienna

M. Heninger¹, B. Holly², P. Nagl³, R. Wohlschlägl¹, M. Hamilton⁴

¹Institut für Geologie, Universität Wien

²Institut für Mineralogie und Kristallographie, Universität Wien

³Department für Lithosphärenforschung, Universität Wien

⁴Geologisches Archiv, Universität Wien

e-mail: margarete.hamilton@univie.ac.at

The main task of the Geological Archive is the acquisition, evaluation, order, description, preservation, and utilization of written material, audiovisual material, and collections that are created in the institute and above all by the academic people working there. Of course, archiving is always linked to librarianship; nevertheless, in the present case, it is a special archive that deals with the preservation not of specialized library literature, but of documents and objects of geological research, whose historical significance is undisputed, but goes beyond literature.

In today's age of digitization and the new technical possibilities, an important aspect is making the holdings accessible via electronic media (Hamilton 2021). Furthermore, in accordance with the educational mandate of archiving, interested students are offered the opportunity to get to know the history of geosciences in detail in a special course and also to establish a connection to current research and to present it in seminars. The works presented here give an insight into specially selected documents from the Geological Archive and show their diversity.

Otto Ampferer (1875-1947) - The theory of the undercurrent: Plate tectonics and the name "Alfred Wegener" (1880-1930) are almost inextricably linked. Ships, research centers and asteroids have been named after the German explorer. Otto Ampferer and his undercurrent theory, which he presented as early as 1906, are less well known. He developed this theory in the course of his alpine research and mapping work. Remarkably, it comes very close to today's concept of "seafloor spreading".

Perhaps because his contributions were difficult for laypeople to read, the Austrian geologist is far less known as the godfather of institutions and sites than his German colleague. However, the interested reader soon notices his pictorial and skilful use of language as well as the high scientific quality of his contributions - reason enough to take a closer look at the researcher.

Historical personnel files of assistants and demonstrators: The present personnel files include documents from the period 1873 to 1945, which were first written in current, later in cursive handwriting and typewritten. In addition to letters that deal directly with the employment and salary of people, there are also ministerial decrees and documents that are directly or indirectly related to the military service of employees in the First and Second World Wars. The existing documents not only reflect the drastic change in correspondence, but also the special challenges for the University of Vienna in this very special time.

Historical geological maps - their origin and preservation: One of the oldest surviving maps in the Geological Archive of the Institute for Geology at the University of Vienna is the "Geognostic Map of the Areas of Krems and Manhardsberge" (1848). Based on this geological map, the author deals with the life and work of the map author Johann Baptist Cžjžek (1806-1855) and gives an overview of the creation and preservation of historical geological maps. Furthermore, the creation of geological maps in the past and present is examined.

Walter Medwenitsch - Expedition to East Africa in 1971: Walter Medwenitsch (1927-1992), whose numerous study trips took him halfway around the world, undertook a 15-day expedition to East Africa in February 1971. Driven by a broad interest in all natural sciences - but especially in geology (doctorate 1949 at the University of Vienna) - during these two weeks he visited cyanite and carbonatite deposits in Kenya, studied the young volcanism of the East African Rift Valley and dealt with the glaciology of the Kilimanjaro massif. His curiosity also led him to the extinct volcano Mount Kenya and its glaciers and to the Pleistocene fossils of Tanzania's Olduvai Gorge, considered part of the 'Cradle of Mankind'.

In the geological archive of the University of Vienna there is a comprehensive geological report by W. Medwenitsch ("Notes on the geological excursion to East Africa") on this wide-ranging expedition, as well as numerous maps and excerpts from reports that contain additional information on the areas visited.



Figure 1: Insights into the newly organized Geological Archive of the University of Vienna. Left: History of the Geological Institute, Box 1; Center top: geological maps, map box 1; Right: Walter Medwenitsch, box 5; center bottom: Otto Ampferer, Box 3 (Photos: M Hamilton)

Hamilton M (2021): The collections of the Archive of the History of Geology at the University of Vienna. - In: 15th International ERBE-Symposium, Eggenburg 2021. Proceedings, 58-74.

Using combined C, Cd, Ba, and Ni isotopes as novel biomarkers to decipher Archean microbial metal cycling

S.V. Hohl¹, Y. Lv², S. Viehmann³, Yi-bo Lin⁴, Y. Zhang⁵, Y. Jiang¹

¹State Key Laboratory of Marine Geology, Tongji University, Shanghai; P.R. China

²State Key Laboratory of Geological Processes and Mineral Resources, China University of Geosciences, Beijing, P.R. China

³Department of Mineralogy, University of Hannover, Germany

⁴State Key Laboratory of Minerals Resources Research, Nanjing University, Nanjing, PR China

⁵Key State Laboratory of Palaeobiology and Stratigraphy (LBS)

Nanjing Institute of Geology and Palaeontology (NIGPAS)

e-mail: sv_hohl@tongji.edu.cn

Stromatolitic carbonates are geochemical archives that allow studying the long-term interplay of the biosphere, atmosphere, and hydrosphere through deep-time, with the unique potential to also investigate early life environments and the evolution of the metallome. Recently non-traditional stable isotopes of bioactive metals emerged as novel proxies to reconstruct the micronutrient cycling in stromatolitic microbial habitats.

In this study, we use stromatolites from the ~2.95 billion-year-old Pongola Supergroup (South Africa) as field laboratory for combined in-situ trace metal mapping and layer-specific novel stable metal isotope compositions to determine biogeochemical metal cycling in early Earth microbial habitats. LA ICP-MS maps reveal intrinsic bio-sedimentary enrichments of Ni and Cd in laminae; in contrast, Ba shows a more heterogeneous distribution throughout the stromatolite. Intra-laminae $\delta^{60}\text{Ni}$ and $\delta^{112}\text{Cd}$ follow typical kinetic isotopic fractionation, i.e., the isotopic composition of Cd and Ni evolves to heavier values with decreasing respective element concentrations arguing for carbonate precipitation from a fractionated Ni and Cd pool heavier than ambient silicate rocks. Further correlations with $\delta^{13}\text{C}$ and macronutrient P argue for co-existing methanogenetic, and photogenetic metal uptake responsible for pronounced isotopic fractionation. In contrast, $\delta^{138}\text{Ba}$ records isotope fractionation related to variable aragonite precipitation rates in the stromatolite, i.e., Ba evolves to isotopically heavier values with increasing concentrations under variable alkalinity in microbial habitats.

We show that the combination of Cd and Ni isotopes has a unique potential as novel isotope biomarker for early Earths bio-chemical sediment record of where traditional biomarkers are not applicable due to fragmentary preservation of organic material.

From allanite to monazite and back: a complex polymetamorphic REE-phase evolution

M. S. Hollinetz¹, B. Huet², C. McFarlane³, D. Schneider⁴, B. Grasemann¹

¹⁾ Department of Geology, University of Vienna

²⁾ Department of Hard Rock Geology, GeoSphere Austria

³⁾ Department of Earth and Environmental Sciences, University of Ottawa

⁴⁾ Department of Earth Sciences, University of New Brunswick

e-mail: marianne.sophie.hollinetz@univie.ac.at

REE-bearing minerals (e.g. allanite / epidote, monazite, xenotime) are suitable targets for in-situ U-Th-Pb geochronology, thus it is essential to understand their stabilities during metamorphism for bringing the age data into any tectonic framework. At lower greenschist facies conditions, allanite / REE-rich epidote forms from the breakdown of detrital or low-grade metamorphic REE-bearing phosphates (e.g., monazite, xenotime). Depending on the bulk rock chemistry, the reverse reaction can occur at the greenschist – amphibolite facies transition or allanite remains stable at amphibolite facies conditions (e.g., Janots et al. 2008).

In this contribution, we present complex allanite – monazite – xenotime phase relations in chloritoid- and staurolite-bearing micaschist sampled at the base of the Schöckel Nappe (Austroalpine Unit, Eastern Alps). The samples contain large chloritoid, staurolite and retrogressed plagioclase porphyroblasts in a matrix of white mica, ilmenite, rutile and quartz. We distinguish two rock types that exhibit different REE-bearing minerals assemblages. Type 1 samples exhibit a simple REE-mineralogy that consist of a LREE-rich allanite core, which is overgrown by chemically zoned REE-rich epidote rim. U-Th-Pb dating using laser-ablation ICPMS yields an age of 275.2 ± 6.2 Ma (MSWD: 2.2, n: 45). In type 2 samples, the REE-phase relationships are much more complex. Few mm-scale LREE-rich allanite porphyroblasts possessing relicts of HREE-rich epidote rims are observed. Another generation of chemically zoned REE-epidote formed in fractures crosscutting both zones. Small (20–50 μm) REE-rich epidote blasts with a similar chemical composition occur in the vicinity of the large porphyroblasts. Additionally, up to 1 mm long aggregates consisting of small (10–20 μm) highly zoned, REE-rich epidote crystals intergrown with apatite are abundant. BSE imaging reveals highly irregular, micron-scale chemical zoning within the REE-epidote aggregate, resulting in a patchy appearance. In these aggregates small (<10 μm) monazite inclusions are typical. Small (<10 μm) xenotime crystals surrounding both the LREE-rich allanite and the REE-epidote aggregate also occur. U-Th-Pb dating that targeted the LREE-rich allanite was unsuccessful due to its high common Pb concentration. The zoned REE-rich epidote (overgrowth, blasts and aggregates) yield an age of 108.8 ± 6.2 Ma (MSWD: 3.1, n: 13).

Combining petrography, chemical composition and geochronological data from both sample types, we interpret LREE-rich allanite growth followed by formation of REE-rich epidote during prograde metamorphism in the Permian. Due to different bulk rock compositions, this assemblage remained stable at peak metamorphic conditions in type 1 samples, but was replaced by clusters of small monazite and xenotime crystals. During the Early Cretaceous metamorphic overprint in the allanite stability field, Permian monazite was destabilized and replaced by REE-rich epidote and apatite.

Janots, E, Engi, M, Berger, A, Allaz, J, Schwarz, JO, Spandler, C (2008): Prograde metamorphic sequence of REE minerals in pelitic rocks of the Central Alps: implications for allanite–monazite–xenotime phase relations from 250 to 610 °C. - J Metam Geol 26, 509-526

Raman spectroscopy of calcium oxalate hydrates from plant leaves

N. Horáková¹, J. Cempírek¹

¹Department of Geological Sciences, Masaryk University, Brno, Czech Republic
e-mail: nice.horak@gmail.com

There are several types of biominerals in plants; the most common are crystals and aggregates of calcium oxalate (CaOx), calcium carbonate (amorphous CaCO_3 or calcite) and amorphous silica. Ca-oxalates are represented by three hydrated forms of CaC_2O_4 : whewellite (monohydrate; COM), weddellite (dihydrate; COD), and caoxite (trihydrate; COT). The most common mineral is COM whereas COD and COT are considered to be metastable phases; on the other hand, they are assumed to be precursor phases during COM or COD formation (Conti et al. 2015). Plant crystals are formed from endogenously synthesized oxalic acid which combines with calcium from the environment (Franceschi & Nakata, 2005).

We used synthetic analogues of CaOx hydrates to acquire high-resolution reference Raman spectra (Fig. 1). Consequently, we identified different CaOx hydrates in leaves of five different species of the *Araceae* family.

In the studied plants, the most common phase is COM in the form of needles (raphids), or crystalline sand; COD more commonly forms druses, dipyrramids or crystal twins, and COT is usually in the form of prisms or rounded aggregates. All three CaOx hydrates were found in 3 plant species, only COD in 4 plants and COM as the most common form in all five plants. COM is widespread, it is contained in all parts of the plant, mostly in the form of long needles stored in idioblasts, whereas the COD is in most cases in petiole in the form of druses. COT as the least stable phase is present only in rare cases in the leaves, its crystals were found in a large amount especially in *Alocasia macrorrhiza* Stingray.

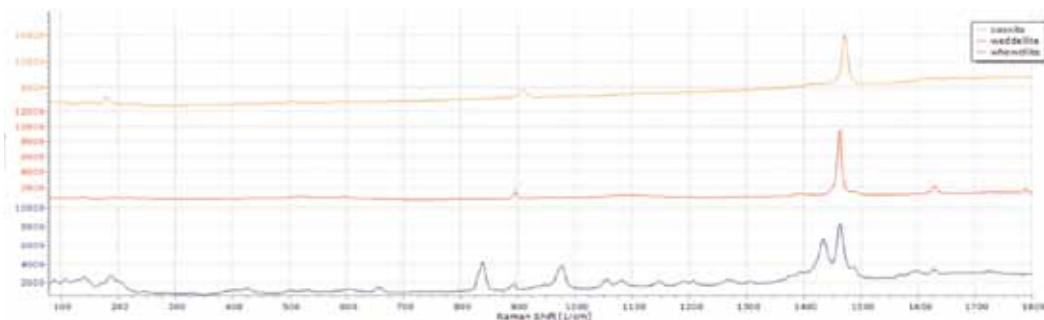


Figure 1 Raman spectra of COM, COD, and COT. - Foto: N. Horáková

Conti C, Casati M, Colombo C, Possenti E, Realini M, Gatta GD, Zerbi G (2015): Synthesis of calcium oxalate trihydrate: New data by vibrational spectroscopy and synchrotron X-ray diffraction. - *Spectrochimica Acta A, Molecular and Biomolecular Spectroscopy* 150, 721-730

Franceschi VR, Nakata PA (2005): Calcium oxalate in plants: formation and function. - *Annu Rev Plant Biol* 56, 41-71

Mineralogy and geochemistry of the Majala and Chacarilla Formations in Northern Chile (Atacama Desert): Implications for provenance, tectonic setting and paleoenvironmental conditions

N. Hurem¹, J. Méndez², V. Gesualdi³, M. Yurac⁴, M. Belvedere^{3,5}, C. Salazar², C. A. Meyer⁶, D. Hippler¹

¹Graz University of Technology, Institute of Applied Geosciences, 8010 Graz, Austria

²Universidad Mayor, Escuela de Geología, 7500000 Providencia, Santiago de Chile, Chile

³Università degli Studi di Firenze, Dipartimento di Scienza della Terra, 50121 Firenze, Italy

⁴Unidad de Patrimonio Paleontológico, Consejo de Monumentos Nacionales 7500000 Providencia, Santiago de Chile, Chile

⁵NBFC, National Biodiversity Future Center, Piazza Marina 61, Palermo 90133, Italy

⁶University of Basel, Department of Environmental Sciences, 4056 Basel, Switzerland
e-mail: nejla.hurem@student.tugraz.at

The Mesozoic sedimentary record of the northern Atacama and Tarapacá region in Chile is still to be fully explored. Mineralogical and geochemical studies as well as dating methods have never been carried out in this region, even though numerous and well-preserved Late Jurassic to Early Cretaceous dinosaur tracksites have been found recently. A pioneer field campaign was therefore carried out in 2022 in the Quebrada Huatacondo followed by a second campaign in 2023 in the Quebrada Arca. At both sites, Late Jurassic to Early Cretaceous sedimentary rocks of the Majala and Chacarilla Formations are well-exposed and constitute a promising geological archive. We sampled the sedimentary rocks, mainly fine-grained sandstones and siltstones, along the lithological sections in order to investigate the depositional and paleo-environmental conditions, provenance and tectonic setting as well as paleo-weathering and climate. In order to achieve our goals, we performed mineralogical and geochemical analysis using XRD and XRF in combination with high-resolution photogrammetry of the outcrops.

Preliminary results indicate that most of the fine-grained sandstones and siltstones can be classified as (sub-) litharenites mainly consisting of quartz and minor to accessory contributions of alkali feldspar, illite and chlorite. Finely-disseminated magnetite and pyrite produce the dark fresh-cut color and the reddish weathering color. Calcite and/or quartz constitute the main cementing phases. The geochemical composition of the sampled sedimentary rocks equals an almost upper crustal composition with distinct formation-specific differences between sand- and siltstones of the Majala and Chacarilla Formations: Rocks of the Majala Fm are slightly enriched in Cr, Ni and Cu, whereas rocks of the Chacarilla Fm show slight differences in elemental composition between the base and the top part. Summarizing the preliminary results, changes in the geochemistry between the two formations can already be clarified. With the complementary new data of the Quebrada Arca, the paleo-environmental conditions of the region can be reconstructed in a promising way. Additional U-Pb dating of the formations will provide desirable age constraints of deposition and provenance to set up an overall picture of the Late Jurassic to Early Cretaceous paleo-environment in Northern Chile.

Melting experiments reproducing early differentiation in primitive achondrites

S. Iannini Lelarge¹, M. Masotta^{1,2}, L. Folco^{1,2}, T. Ubide³, M.D. Suttle^{1,4}, W.N. Wegner⁵,
L. Pittarello⁵

¹*Università di Pisa, Italy*

²*Centro per l'Integrazione della Strumentazione Università di Pisa (CISUP), Pisa, Italy*

³*The University of Queensland, Brisbane, Australia*

⁴*The Open University, Milton Keynes, United Kingdom*

⁵*Naturhistorisches Museum, Vienna, Austria*

e-mail: lidia.pittarello@nhm.at

Even small planetary bodies can have experienced internal differentiation, i.e., separation of the metal-sulphur components from the silicates forming a core and a mantle, respectively. In the meteorite record, primitive and anomalous achondrites represent a puzzle for scientists, as they seem to result from a differentiation process, but contain some primitive characteristics. Dedicated heating experiments in a piston-cylinder at 1 GPa and temperature steps from 1050 °C to 1400 °C, for 24h, have been performed to understand the uncomplete differentiation occurring on the parent body(ies) of such meteorites. As starting material, chondrites representative of specific early chemical settings were chosen: a) shocked L6 (DAV 01001), for intermediate redox state among the ordinary chondrites, b) carbonaceous chondrite (CM2, MCY12002), for oxidised parent bodies, and c) enstatite chondrite (EL6, MCY14005), for the reduced material in the Solar System. The resulting samples have been investigated with scanning electron microscope, electron microprobe analyser, laser ablation inductively coupled plasma mass spectrometry, Raman spectroscopy, and synchrotron radiation-micro computed tomography.

The experiments with the L6 chondrite resulted in non-eutectic melting of a small percent of the sample, with the metal and sulphide phases being mobilised first, already for the lowermost heating temperatures, and the silicates melting according to the sequence plagioclase-Ca-pyroxene-low Ca-pyroxene-olivine. This melting sequence affects the composition of the first melt produced, which evolves from trachyandesitic to more andesitic terms for increasing vol% of melting. Despite the fast quenching, crystallisation of olivine dendrites could not be avoided. The chemical composition of the produced melt shows similarities with that of some andesitic to trachyandesitic anomalous achondrites, such as NWA 11119, EC002, GRA 60128/9, Almahata Sitta clast ALM-A, NWA 6698, and NWA 11575. This suggests that these anomalous achondrites could have formed by incipient melting of chondritic material under fast heating conditions, like due to planetary collisions.

In the case of the CM2 carbonaceous chondrite as starting material, the obliteration of the initial texture is immediate. The melt produced has a composition ranging from microbasaltic to basaltic-andesite, but already at the “low” temperature experiments several phases crystallises from the melt, such as Ca-rich olivine, pyroxene, spinel, kirschsteinite, and Ca-phosphates. The composition of the newly formed phases and the melt closely recall those found in angrites, some rare and peculiar basaltic achondrites, which likely have an impact origin (Rider-Stokes et al., 2023), where one of the bodies had a carbonaceous composition.

The analyses of the experiments with the enstatite chondrite are still ongoing. However, this work shows the importance of an experimental petrologic approach in constraining magmatic processes in the early Solar System.

Rider-Stokes BG, Greenwood RC, Anand M, White LF, Franchi IA, Debaille V, Goderis S, Pittarello L, Yamaguchi A, Mikouchi T, Claeys P (2023): Impact mixing among rocky planetesimals in the early Solar System from angrite oxygen isotopes. - Nat Astron, <https://doi.org/10.1038/s41550-023-01968-0>

Calorimetric characterisation of the alkali feldspar binary

F. Ingegneri¹, E. Dachs², R. Abart¹

¹ Department of Lithospheric Research, University of Vienna

² Department of Chemistry and Physics of Materials
Section Materials Science and Mineralogy, Salzburg University
e-mail: flora.ingegneri@univie.ac.at

The thermodynamic study of materials is vital as thermodynamic data such as Gibbs energy are of pivotal importance for modelling phase equilibria and processes in both nature and industry. This work aims at contributing to the thermodynamic characterisation of the most common mineral group in Earth's crust, namely feldspar. The focus is on the alkali feldspar solid solution, the endmembers of which are Albite ($\text{NaAlSi}_3\text{O}_8$) and Orthoclase (KAlSi_3O_8), and on the quantification of its molar heat capacity c_p and vibrational entropy S^{vib} as functions of composition X_{Or} .

Gem quality sanidine from Volkesfeld, Germany, with a composition of $X_{\text{Or}} = 0.85$ was used as starting material for cation exchange with a (Na,K)Cl salt melt. A total of 14 feldspar samples together with different (Na,K)Cl salt mixtures were held at 900 °C for a duration of 30 to 45 days in order to reach equilibrium. The resulting series was analysed on the EPMA Cameca SX Five FE at the University of Vienna and represents the composition of the whole binary.

10 of these samples have already been analysed via heat pulse calorimetry using the Physical Property Measurement System (PPMS) by Quantum Design at Salzburg University. C_p data were obtained for the temperature range from 2 to 300 K. S^{vib} was subsequently calculated by numerical integration of c_p/T and is shown in Tab. 1. The corresponding plot can be found in Fig. 1. The relative error for S^{vib} is estimated at $\pm 0.7\%$ (Dachs & Bertoldi 2005).

These preliminary results yield a positive excess entropy with a maximum of $S^{\text{ex}} \approx 2 \text{ J mol}^{-1} \text{ K}^{-1}$. Further samples are being prepared for calorimetric analysis to close the current gap at $X_{\text{Or}} = [0.1, 0.3]$. As soon as the missing calorimetric data is available a Margules mixing model will be fitted to the data in order to obtain S^{vib} and S^{ex} as a function of X_{Or} .

Table 1. Vibrational entropy S^{vib}
at $T = 298.15 \text{ K}$

| X_{Or} | S^{vib} |
|-----------------|--|
| [] | [$\text{J mol}^{-1} \text{ K}^{-1}$] |
| 0.06 | 207.0 |
| 0.33 | 211.2 |
| 0.40 | 211.4 |
| 0.50 | 212.2 |
| 0.56 | 212.4 |
| 0.60 | 211.9 |
| 0.68 | 212.7 |
| 0.83 | 212.9 |
| 0.93 | 212.9 |
| 1.00 | 213.1 |

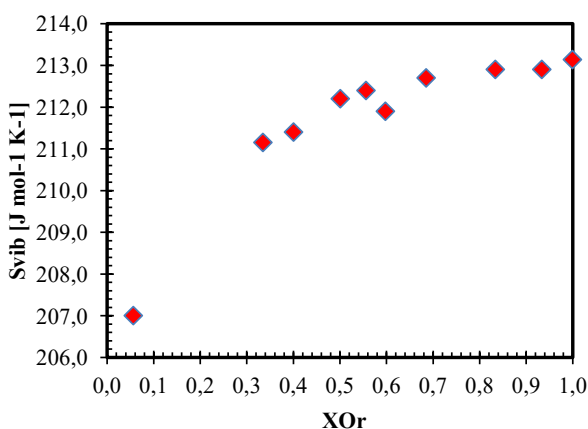


Figure 1. Vibrational entropy S^{vib} at $T = 298.15 \text{ K}$

Dachs E, Bertoldi C (2005): Precision and accuracy of the heat-pulse calorimetric technique: low-temperature heat capacities of milligram-sized synthetic mineral samples. – Eur J Mineral 17, 251-261

Impurities in quartz from Amazon river sands

D. Jaeger¹, T. Ludwig², S. Andó³, E. Garzanti³, A.O. Sawakuchi⁴, C. Chiessi⁴,
M. Strasser¹, R. Stalder¹

¹*University of Innsbruck*

²*Heidelberg University*

³*University of Milano*

⁴*University of São Paulo*

e-mail: roland.stalder@uibk.ac.at

Incorporation of impurities in quartz is primarily controlled by (1) the availability of the respective impurity in the chemical system and (2) the crystallisation condition. Even if the concentration of some of the impurities (such as OH species) may later be affected by metamorphic overprint, the total impurity inventory of each individual grain reflects its geological history. As the impurities are rather stable throughout sedimentary processes, quartz from siliciclastic sediments may thus serve as archive for the crystallisation conditions of the rocks in the source area. As hydrous defects are usually charge balanced by trace metals, concentrations in the most important charge balancing elements (Al, Li, B) may be reflected in the IR spectra, unless the sample lost OH by diffusion during metamorphic dehydration.

In this study quartz from several sediment samples from the lower Amazon and from three major tributaries of the Amazonian river system were analysed by FTIR spectroscopy and secondary ion mass spectrometry (SIMS) in order to characterise individual grains with respect to hydrous defects and trace metal contents.

Differences between the four samples are subtle but discernable. Trace element contents relevant for hydrous defects (Al, Li, B) are in general lower in quartz from the rivers draining the old continental shields (Xingu and Rio Negro) compared to quartz from the lower Amazon River; grains from Solimões, partly drained from the Andean orogeny, exhibit in general the highest trace element concentrations. The trace element contents are partly reflected in the OH signatures of quartz: samples from Solimões and lower Amazon exhibit a larger fraction of OH-rich grains, and the Li- and Al-specific absorption bands is less evolved in grains from Xingu and Rio Negro.

Taking into account trace element contents and OH signatures in quartz, quartz grains from the lower Amazon sample represent a mixture with significant contributions from Andean and shield sources. Conversely, heavy-mineral analysis indicates the Solimões River as the dominant source of sediment. This apparent discrepancy is reconciled considering that Andean detritus has a much higher heavy-mineral concentration than detritus recycled from siliciclastic rocks exposed in the Andean foothills, siliciclastic covers of the Brazilian-Guiana Shield, and quartz-rich sediments incised all across the retroarc basin and Amazonian lowlands.

Amphibole megacrysts with cavities reveal rapid crystal growth at mantle depth during the 1951 eruption of Fogo (Cape Verdes)

W.-A. Kahl¹, A. Klügel²

¹*MAPEX Center of Materials and Processing, Universität Bremen, 28359 Bremen, Germany*

²*Faculty of Geosciences, Universität Bremen, 28359 Bremen, Germany*

e-mail: wakahl@uni-bremen.de, akluegel@uni-bremen.de

The late basaltic deposits of the 1951 Fogo eruption contain peridotite xenoliths, ultramafic cumulate xenoliths, and euhedral kaersutite megacrysts up to 12 cm in size. The megacrysts contain abundant of cavities that locally contain vesicular basaltic glass with small clinopyroxene phenocrysts, with compositions more primitive than the host magma. Some of these cavities remind of hopper textures. Micro-CT analyses reveal that the cavities are only in part interconnected and in some cases form funnel-like openings to the crystal surface. In addition to some spinel and clinopyroxene inclusions, the kaersutite contain numerous pyrrhotite rods aligned perpendicular to the crystal surface, and some pyrrhotite blebs. We interpret these structures to result from rapid crystal growth in a volatile-rich silicate melt with abundant droplets of exsolved sulfide melt. Barometric data indicate that this rapid growth occurred in the uppermost mantle. Possible causes for the rapid growth event include magma mixing or sudden H₂O loss to raise the liquidus.

Interstitial diamonds reveal dry exhumation of UHP metamorphic rocks - insights from 3-D spatially resolved X-ray microtomography data

W.-A. Kahl¹ , H.-P. Schertl²

¹MAPEX Center of Materials and Processing, Universität Bremen, 28359 Bremen, Germany,

²Institute of Geology, Mineralogy and Geophysics, Ruhr-University Bochum, 44780 Bochum, Germany

e-mail of communicating author: wakahl@uni-bremen.de

The Kokchetav Massif of northern Kazakhstan is part of one of the largest suture zones in Central Asia and contains slices of HP and UHP metamorphic rocks. The Kumdy Kol area is the first recorded locality of diamondiferous UHP rocks (Sobolev & Shatsky 1990) that were formed due to subduction processes at mantle depths. The diamond grains in these rocks are exceptionally large for such an environment reaching 200 µm. In a calcsilicate rock studied they form inclusions within Grt or Cpx, or occur as interstitial grains along Grt-Cpx boundaries. Such diamonds were reported to have formed by C-O-H fluids, but is it possible to identify potential fluid pathways? Our true spatially resolved tomography data of a piece of rock indicate, that the location of diamonds is related to a network of deformational microcracks. Local hydrothermal alteration in parts accompanied by Hbl-formation refers to a late event. Our data corroborate a diamond formation by fluids and an early dry exhumation history after peak metamorphic conditions were reached.

Sobolev NV, Shatsky VS (1990): - Nature 343, 742–746

3D electron and powder X-ray diffraction: the best of both worlds to study the crystal structure of γ -Na₂Ca₆Si₄O₁₅

V. Kahlenberg¹, H. Krüger¹, J. Vinke¹, S. Ito², C.J. Schürmann³

¹*Institute of Mineralogy and Petrography, University of Innsbruck, Innrain 52, 6020 Innsbruck, Austria*

²*Rigaku Corporation, 3-9-12 Matsubaru-cho, Akishima, Tokyo 196-8666, Japan*

³*Rigaku Europe SE, Hugenottenallee 167, 63263 Neu Isenburg, Germany*

e-mail: volker.kahlenberg@uibk.ac.at

Phase assemblages of mixtures containing Na₂CO₃, CaCO₃, and SiO₂ in the molar ratio 1:3:2 have been studied at elevated temperatures. Synthesis experiments have been performed at 1000, 1100 and 1200 °C within a DTA-TGA apparatus. Mass losses during heating and annealing periods of the high-temperature treatment have been studied *in-situ* using thermogravimetry. For the run at 1200 °C, the solid-state reactions resulted in almost phase pure polycrystalline material of a previously unknown high-temperature polymorph of Na₂Ca₆Si₄O₁₅, whose formation was triggered by significant Na₂O losses at the reaction temperature. The new so-called γ -phase has been structurally characterized by a combination of 3D single-crystal electron and powder X-ray diffraction.

Basic crystallographic data at ambient conditions are as follows: monoclinic symmetry, space group *C*2, $a = 17.2066(1)$ Å, $b = 5.47863(3)$ Å, $c = 7.32583(4)$ Å, $\beta = 91.435(4)^\circ$, $V = 690.38(1)$ Å³, $Z = 2$. Structure solution was accomplished by electron diffraction, whereas the subsequent refinement calculations were based on the Rietveld method using high-resolution data from a laboratory powder diffractometer. Similarly to the two already known Na₂Ca₆Si₄O₁₅ modifications, the crystal structure of the γ -phase contains both [Si₂O₇] dimers and insular [SiO₄] moieties. Tetrahedra and [CaO₆] octahedra form a three-dimensional framework whose topological characteristics have been studied. The remaining Ca and Na cations are located on five symmetrically independent positions in the cavities of the network.

There are sufficiently strong arguments that previously described “triclinic Na₂Ca₃Si₂O₈” is actually misinterpreted γ -Na₂Ca₆Si₄O₁₅ and that a sodium calcium silicate with a molar ratio of Na₂O:CaO:SiO₂ = 1:3:2 probably does not exist. Our investigation is an excellent example that 3D electron diffraction has transformed from an exotic technique for crystal-structure determination into an indispensable method for problems where small sizes of the crystallites is an issue.

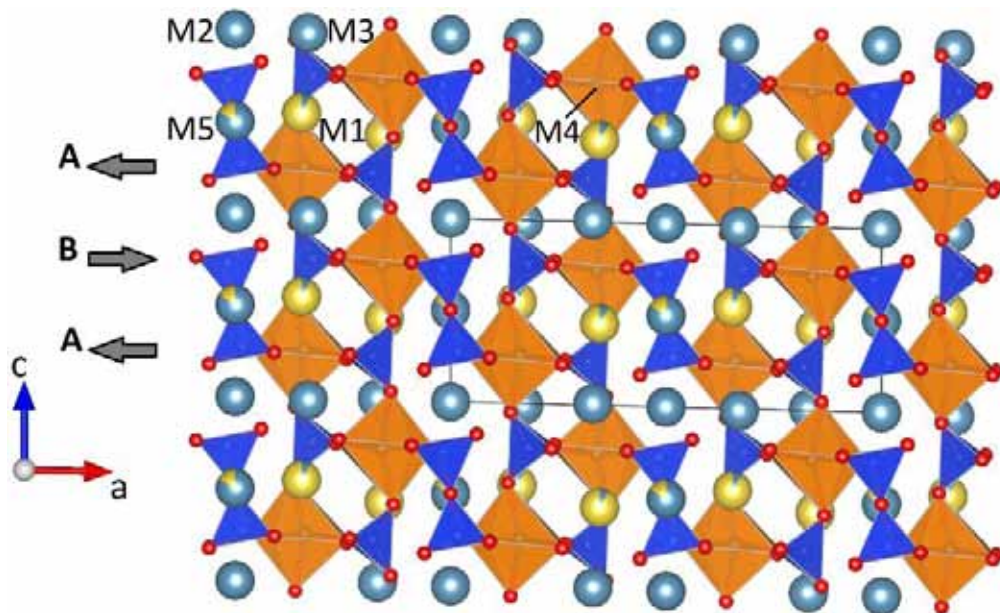


Figure 1. Projection of the whole crystal structure of $\gamma\text{-Na}_2\text{Ca}_6\text{Si}_4\text{O}_{15}$ (monoclinic) along $[0\bar{1}0]$. $[\text{SiO}_4]$ tetrahedra and calcium dominated $[\text{M}_4\text{O}_6]$ octahedra are shown in dark blue and orange, respectively. Small red spheres represent oxygen atoms. Interstitial Ca and Na atoms are given in light blue and yellow. Bi-colored spheres indicate mixed Ca-Na positions. The alternating ...ABA... stacking sequence of adjacent layers building up the network as well as the relative shift vectors are indicated.

Investigation of Martian and other meteorites using Raman spectroscopy

M. Kaliwoda^{1,2}, F. Joseph^{1,2}, V. Helmbrecht², J. Zuncke^{1,2}, A. Nömer², L. Eckle²,
I. Drozdovsky³

¹*Mineralogical State Collection Munich (SNSB)*

²*Department of earth and environmental sciences, LMU, Ludwig-Maximilians University*

³*European Astronaut Centre (EAC) - European Space Agency (Linder Höhe, D-51147 Cologne, Germany
e-mail: kaliwoda@snsb.de*

Our solar system consists of a wide range of different objects. Planet Mars is one of them, and its proximity to Earth makes it an important place to study. Investigations are currently related to rover missions; human missions are planned, and, in addition, the study of meteorites provides us with a lot of new data. Martian meteorites deliver us a sample in a "nutshell" that can tell us about (1) the composition of the Martian surface, (2) the chemical composition of minerals, (3) rock temperatures and pressures during formation, (4) and possible melting processes.

In the Mineralogical state collection Munich (MSM) there are several Martian but also other meteorites, i.e. from the Moon, Vesta or other extraterrestrial bodies for investigation with Raman-Spectroscopy, SEM and electron microprobe. In the following context, we want to present two Martian meteorites NWA13366 and NWA7032. Our first investigations belong to NWA13366, this meteorite is composed of olivine with 55 vol.-% and pyroxene with 35 vol.-%. Olivine is generally Mg-rich and pyroxenes have an enstatitic composition. Another present phase is maskelynite with 5 vol.-% next to older feldspar grains. Maskelynite is a plagioclase glass that possibly formed during a high-pressure impact. Minor amounts of ilmenite, chromite, hematite, iron sulfide (possibly troilite), calcite, and calcium phosphate (possibly merrillite) also occur in the NWA 13366, the meteorite belongs furthermore to the shergottite group of Martian meteorites. NWA 13366 has a bimodal texture of poikilitic and non-poikilitic areas. Poikilitic domains consist of mm-sized anhedral magnesian low-Ca pyroxene crystals (oikocrysts) and smaller interlocked subhedral to euhedral Mg-rich olivine crystals (chadacrysts). Cr-rich chromite is also present. Olivine grains show chemical zoning from Fe-rich rims to Mg-rich cores in poikilitic domains. Pyroxene in poikilitic areas might be zoned as well. Non-poikilitic domains contain smaller olivine and pyroxene grains, that are chemically more evolved with higher Fe- and Ca-contents. Calcium carbonate (calcite) is present in fracture zones. It could originate from primary Martian aqueous or hydrothermal alteration or due to secondary alteration on Earth. The meteorite shows many features indicative of high shock stages. The chemical differences and the bimodal texture in the shergottite indicate a complex crystallization history of the meteorite. NWA7032 belongs also to the Martian group of meteorites and shows gabbroitic compositions. The rock is at the moment under investigation, more details will be shown later on. The detailed investigation of meteorites helps us to understand the composition of the Martian surface and besides this gives us important data for the in-house Raman database (MSM-MRD), which also takes part in the Raman database of the ESA [1].

Drozdovskiy I, Ligeza G, Jahoda P, Franke M, Lennert P, Vodnik P, Payler SJ, Kaliwoda M, Pozzobon R, Massironi M, Turchi L, Bessone L, Sauro F (2020): The PANGAEA Mineralogical Database. - Journal D i Brief S2352-3409(20), 30879-9, <https://doi.org/10.1016/j.dib.2020.105985>

Crystal-chemical effects of high-temperature treatment on Mg-dominant tourmalines

P. Kardošová¹, P. Bačík^{1,2}, J. Fridrichová¹, O. Rybníková¹, M. Miglierini³, T. Mikuš⁴

¹Comenius University in Bratislava, Faculty of Natural Sciences,

Department of Mineralogy, Petrology and Economic Geology, Bratislava, Slovak Republic

²Earth Science Institute of the Slovak Academy of Science, Bratislava, Slovak Republic

³Slovak University of Technology, Faculty of Electrical Engineering and Information Technology

Institute of Nuclear and Physical Engineering, Bratislava, Slovak Republic

⁴Earth Science Institute of the Slovak Academy of Science, Bratislava, Slovak Republic

e-mail: kardošova6@uniba.sk

We present a detailed study of oxidation-induced deprotonation and its influence on tourmaline breakdown. The crystal-chemical effects of high-temperature treatment on Mg-dominant tourmalines, the oxidation of Fe^{3+} associated with the deprotonation of OH^- groups and its subsequent effect on the breakdown of tourmaline. Tourmaline samples were studied using a wide range of analytical methods. The chemical composition of all samples is Mg dominant, but with variable X_{Mg} [$\text{Mg}/(\text{Mg}+\text{Fe})$]: TSCH – schorlitic dravite from Tanzania with X_{Mg} of 0.5-0.8; CHD – Mg-dominant dravite from China with $X_{\text{Mg}} > 0.9$; TUV – Cr-bearing uvite from Tanzania with $X_{\text{Mg}} > 0.98$). Tourmaline samples were heat-treated in air at atmospheric pressure at temperatures from 700 to 1000 °C to obtain information on the effect of oxidation on the deprotonation of OH^- groups.

The majority of Fe was oxidized after heating at 800 °C which was observed in the Mössbauer spectrum of TSCH and optical spectrum of CHD. This CHD sample had insufficient Fe content for Mössbauer spectroscopy but changes in the optical spectrum indicated partial Fe oxidation – an increase in band intensity at 750 nm and the shift of the absorption edge to the green region due to electron interactions between Fe^{2+} and Fe^{3+} ions. The influence of the possible cation oxidation on the OH^- groups bonded at the edges of YO_6 octahedra was determined by IR spectroscopy. The TSCH sample shows a significant decrease in absorbance of OH^- bands which indicates deprotonation induced by Fe oxidation, the absorbance decrease in the CHD spectra is less pronounced, and TUV does not show any decrease in absorbance suggesting no oxidation could take place due to a very low Fe, Mn, and V content. This influenced the appearance of samples after the structural breakdown: TSCH heated at 1000 °C changed appearance and cracked but there were no volumetric changes; CHD and TUV samples expanded. This suggests that before the structural breakdown, TSCH released water gradually due to Fe oxidation but CHD and TUV samples kept a majority of water in the structure due to the low content of Fe and released at one moment causing the expansion of samples.

However, the CHD and TUV samples retained most of the water in the structure due to the low Fe content that could oxidize, so the OH^- groups were not significantly deprotonated. Deprotonation occurred in one sudden moment as the structure broke down, with the released water escaping rapidly in the form of steam in all directions, causing the samples to expand. The contents of chromophores in the samples were too low to colour the resulting products in the new forms.

Meta-igneous rocks from the Kaintaleck Metamorphic Complex as indicators of a Variscan Ocean within the Eastern Alps

K. Karner-Rühl¹, C.A. Hauzenberger¹, E. Skrzypek¹, H. Fritz¹

¹University of Graz, Universitaetsplatz 2, 8010 Graz, Austria
e-mail: kevin.karner-ruehl@edu.uni-graz.at

The Kaintaleck Metamorphic Complex is part of the Eastern Greywacke Zone, Eastern Alps. The Eastern Greywacke Zone is subdivided into three Alpine nappes, with the Veisch nappe being overlaid by the Silbersberg and Noric nappe. The Silbersberg nappe contains intercalated crystalline fragments of Variscan age, the Kaintaleck Metamorphic Complex. It is represented by a mafic suite, comprising amphibolite, garnet-amphibolite, greenschist and serpentinite, and a felsic suite, that consists mostly of gneiss and mica schist, some of them garnet-bearing. Petrological, geochemical and geochronological investigations were carried out to provide new insights into the metamorphic and tectonic evolution of the Kaintaleck Metamorphic Complex. Geochemical results indicate, that the mafic suite originates from tholeiitic basalts. Amphibolites from the locality of Frauenberg show an enrichment in LREE indicative for either an E-MORB or OIB affinity. Garnet-amphibolites, amphibolites, and greenschists from the localities of Prieselbauer, Oberdorf, Unteraich, Kalwang, Arzbach and Schlöglmühl show flat REE patterns with only a slight depletion in HREE and resemble T-MORB. Samples from the localities of Stübminggraben and Utschgraben are depleted in LREE, typical for N-MORB affinity. U-Pb zircon dating of a garnet-amphibolite sample from the locality of Prieselbauer yields an Early Devonian age of 414.2 ± 5.6 Ma, interpreted as the age of protolith formation. Garnets from these garnet-amphibolites show distinct plagioclase-epidote-rich symplectitic coronae, indicating decompression from former high-pressure metamorphic conditions. The evolution of the Kaintaleck Metamorphic Complex might be related to the opening and closure of the short-lived Balkan-Carpathian Ocean. The onset of rifting might be due to slab roll-back and back-arc spreading during Late Ordovician and Early Silurian. During the Late Devonian and Early Carboniferous, the Balkan-Carpathian Ocean was subducted. The mafic suite of the Kaintaleck Metamorphic Complex, comprising the oceanic crust of the Balkan-Carpathian Ocean, was dragged into the subduction channel and underwent HP metamorphism with conditions of $\sim 550^\circ\text{C}$ and $\sim 1.7\text{--}2.2$ GPa. Subsequent exhumation resulted in a near isothermal decompression. Further relics of Devonian age are exposed in the North-Gemeric Klatov and Rakovec Complexes in the Western Carpathians (Putiš et al. 2009). Neubauer et al. (2022) propose, that the Klatov and Rakovec Complexes are small remnants of the Balkan-Carpathian Ophiolite, dated with an age of 405.0 ± 2.6 Ma by Zakariadze et al. (2012). Similarities in their age, the affinity to MORBs, the presence of serpentinite and the general conception, that the Klatov Complex might be a continuation of the Kaintaleck Metamorphic Complex within the Western Carpathians, might relate the mafic suite of the Kaintaleck Metamorphic Complex to the Balkan-Carpathian Ocean.

- Putiš M, Ivan P, Kohút M, Spišiak J, Siman P, Radvanec M, Uher P, Sergeev S, Larionov A, Méres Š, Demko R, Ondrejka M (2009): Meta-igneous rocks of the West-Carpathian basement, Slovakia: indicators of Early Paleozoic extension and shortening events. - *Bull Soc Géol Fr* 180, 461–471
- Neubauer F, Liu Y, Dong Y, Chang R, Genser J, Yuan S (2022): Pre-Alpine tectonic evolution of the Eastern Alps: From Prototethys to Paleotethys. - *Earth-Science Reviews* 226, doi:10.1016/j.earscirev.2022.103923
- Zakariadze G, Karamata S, Korikovskiy S, Ariskin A, Adamia S, Chkhotua T, Sergeev S, Solov'eva N (2012): The Early–Middle Palaeozoic Oceanic events along the Southern European Margin : The Deli Jovan Ophiolite Massif (NE Serbia) and Palaeo-oceanic Zones of the Great Caucasus. - *Turkish J Earth Sci* 21, 635–668, doi:10.3906/yer-1011-2

- Putiš M, Ivan P, Kohút M, Spišiak J, Siman P, Radvanec M, Uher P, Sergeev S, Larionov A, Méres Š, Demko R, Ondrejka M (2009): Meta-igneous rocks of the West-Carpathian basement, Slovakia: indicators of Early Paleozoic extension and shortening events. - *Bull Soc Géol Fr* 180, 461–471
- Neubauer F, Liu Y, Dong Y, Chang R, Genser J, Yuan S (2022): Pre-Alpine tectonic evolution of the Eastern Alps: From Prototethys to Paleotethys. - *Earth-Science Reviews* 226, doi:10.1016/j.earscirev.2022.103923
- Zakariadze G, Karamata S, Korikovskiy S, Ariskin A, Adamia S, Chkhotua T, Sergeev S, Solov'eva N (2012): The Early–Middle Palaeozoic Oceanic events along the Southern European Margin : The Deli Jovan Ophiolite Massif (NE Serbia) and Palaeo-oceanic Zones of the Great Caucasus. - *Turkish J Earth Sci* 21, 635–668, doi:10.3906/yer-1011-2

The anatectic genesis of lithium pegmatite from the Austroalpine Unit Pegmatite Province

T. Knoll¹, B. Huet², R. Schuster¹, H. Mali³

¹ Division of Geophysical and Applied Geological Services, Geosphere Austria,
Neulinggasse 38, 1030 Vienna, Austria

² Division of Basic Geological Services, Geosphere Austria, Neulinggasse 38, 1030 Vienna, Austria

³ Department of Applied Geosciences and Geophysics, Montanuniversität Leoben
Peter-Tunnerstraße 5, 8700 Leoben, Austria
e-mail: tanja.knoll@geosphere.at

Whether rare element pegmatites are always related to fractional crystallization of melts derived from large fertile granite bodies or they can also form directly from limited portions of enriched anatectic melt is since long a debated topic (e.g. Stewart 1978; Cerný 1991). We here present the results of a recent case study that documents continuous evolution from anatectic melt generated in staurolite-bearing micaschist to albite-spodumene pegmatite (Knoll et al., 2023). The investigated Austroalpine Unit Pegmatite Province (AUPP, Eastern Alps) formed in the Adria crust during Permian lithospheric extension (Figure 1a, Schuster & Stüwe 2008) and all levels of the Permian crust are now accessible in a Cretaceous nappe stack (Froitzheim et al. 2008).

It can be shown that the Permian pegmatites of the AUPP are neither spatially nor genetically related to large fertile granite bodies. Geochronological data proofs that emplacement of pegmatite and leucogranite is broadly contemporaneous with high temperature-low pressure metamorphism of the country rocks in a time range between 247 and 288 Ma (Knoll et al. 2023; and references therein). Permian albite-spodumene pegmatites are restricted to certain lithostratigraphic complexes (e.g. Rappold Complex, Strieden Complex or Silvretta Complex; Schuster et al. 2001; Knoll et al. 2018). Pegmatite-bearing units mainly consist of aluminosilicate-bearing partly migmatitic micaschist and paragneiss as well as staurolite-bearing micaschist. Field observations give clear evidence of a genetic link between simple pegmatite, leucogranite, evolved pegmatite and albite-spodumene pegmatite, on the one hand, and the subsolidus or suprasolidus metasediment hosting them on the other hand. These relationships are supported by geochemical investigations of major and trace elements in all mentioned rock types and the minerals they contain.

The Li source rock is found to be an Al-rich metapelite, richer in Li (70-270 ppm) than the average upper continental crust. The primary Li-carrier is staurolite with up to 3000 ppm Li. The pegmatite and leucogranite are derived from anatectic melts that formed at 0.6-0.8 GPa and 650-750 °C, corresponding to 18-26 km depth. During melt formation staurolite was consumed by sillimanite forming reactions. Subsequently, the melts were enriched in Li during their ascent to higher crustal levels by fractional crystallization of quartz and feldspar. While simple pegmatite and inhomogeneous leucogranite formed in lower and intermediate levels, evolved and albite-spodumene pegmatite crystallised at high levels at 0.3-0.4 GPa and 500-570 °C, corresponding to about 12 km depth.

On the basis of this data we developed a geochemical model showing that Li can be transferred from a metasediment into an anatectic melt if Li-bearing staurolite is stable or metastable at the onset of melting (Figure 1b). Such a melt can initially contain between 200

and 1000 ppm Li and be further enriched by fractional crystallization, with up to 5000-10000 ppm Li allowing crystallization of spodumene (Figure 1c). Estimated fractionation degrees vary between 81 and 99 %, depending on the protolith composition, the melting scenario and the partitioning coefficients. Li-Al-rich metasediments are therefore a significant source of Li when they first melt. This anatectic model provides an alternative explanation for the formation of Li-rich pegmatite if no fertile parent granite can be identified.

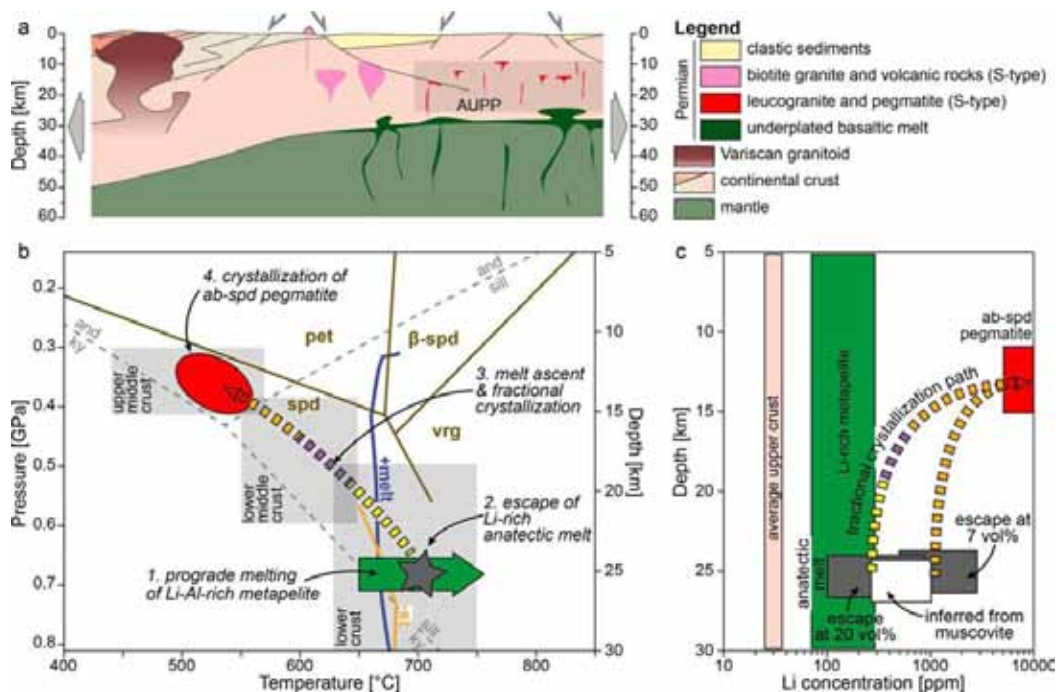


Figure 1. a. Position of the Austroalpine Unit Pegmatite Province (AUPP) within the Adria continental crust during Permian lithospheric extension. b. The main processes of the genetic model placed on a pressure–temperature diagram: 1. Prograde melting of Li-Al-rich metapelite in the lower crust. 2. Escape of Li-rich anatectic melt from the migmatite of the lower crust. 3. Ascent of the melt through the lower middle crust and progressive fractional crystallization. 4. Crystallization of residual melt as albite-spodumene pegmatite in the upper middle crust. c. Postulated evolution of Li concentration in anatectic melt during ascent (see also Knoll et al. 2023).

- Cerný P (1991): Rare-element granitic pegmatites. Part I: Anatomy and internal evolution of pegmatite deposits. - *Geosci Canad* 18, 49–67
- Froitzheim N, Plasienska D, Schuster R (2008): In: McCann, T. (Ed.), *The Geology of Central Europe, 2. Mesozoic and Cenozoic*. - *J Geol Soc* 1141–1232
- Knoll T, Schuster R, Huet B, Mali H, Onuk P, Horschinegg M, Ertl A, Giester G (2018): Spodumene Pegmatite and Related Leucogranite from the Austroalpine Unit (Eastern Alps, Central Europe): Field Relations, Petrography, Geochemistry, and Geochronology. - *Canad Mineral* 56, 489–528
- Knoll T, Huet B, Schuster R, Mali H, Ntaflou T, Hauzenberger C (2023): Lithium pegmatite of anatectic origin-A case study from the Austroalpine Unit Pegmatite Province (Eastern European Alps): geological data and geochemical model. - *Ore Geol Rev* 154, 105298
- Schuster R, Scharbert S, Abart R, Frank W (2001): Permo-Triassic extension and related HT/LP metamorphism in the Austroalpine-Southalpine realm. - *Mitt Ges Geol Bergbaustud Österr* 45, 111–141
- Schuster R, Stüwe K (2008): Permian metamorphic event in the Alps. - *Geology* 36, 603–606
- Stewart D B (1978): Petrogenesis of lithium-rich pegmatites. - *Amer Mineral* 63, 970–980

The crystal structure of a new natural Na-(Sr,Ba,Ca,K)-Fe-tungstophosphate, a derivative of the betpakdalite-group topology from Le Mazet, Échassières, Allier, France

U. Kolitsch^{1,2}

¹Mineralogisch-Petrographische Abteilung, Naturhistorisches Museum, Burgring 7, A-1010 Wien, Austria

²Institut für Mineralogie und Kristallographie, Universität Wien, Josef-Holaubek-Platz 2, A-1090 Wien, Austria
e-mail: uwe.kolitsch@nhm.at

A new tungstophosphate mineral was found on dumps of the Le Mazet wolframite-bearing quartz vein of the Les Montmins mining district (Échassières, Allier, France). It was not yet found at the nearby, very mineral-rich Ste Barbe vein. The new mineral forms very small, bright yellow to orange-yellow, pseudo-octahedral crystals, indistinct corroded tabular crystals and anhedral grains. The mineral, which shows a vitreous lustre, sits in small voids of a dark pink-grey, fine-grained quartz matrix. The colour of the mineral is somewhat reminiscent of that cyrilovite which also occurs at the locality.

The complex crystal structure was solved from single-crystal intensity data (MoK α ; 293 K). The space group is $R\bar{3}m$ (no. 166), with $a = 10.874(2)$, $c = 28.243(6)$ Å, $V = 2892.1(1)$ Å³; $R(F) = 2.1\%$. The asymmetric unit contains one Na site with refined occupancy Na_{0.54(3)}, one (Sr,Ba,Ca,K) site, two Fe sites, one (P,As) site (refined P:As ratio = 0.719(19):0.281), one W site and nine O sites, four of which represent H₂O molecules. The latter are all partially occupied. The new mineral has the following simplified (and presently tentative) formula: [Na_{0.27}(Sr_{0.46}Ba_{0.31}Ca_{0.17}K_{0.08})(H₂O,OH)_{9.02}][W₃(P,As)Fe³⁺₂O₁₆]. The (P,As)O₄ tetrahedron is, via its basal corners, connected to three Fe(2)O₆ octahedra. The remaining apex is shared with a cluster of three edge-sharing, strongly distorted WO₆ "octahedra". This cluster is connected via an Fe(1)O₆ octahedron to symmetrically equivalent clusters. Channels and voids in the resulting 3D framework extend along [100] and [110] and are filled with (Sr,Ba,Ca,K)O_{12-x} polyhedra and partially occupied NaO₆ octahedra.

The atomic arrangement is a derivative of that of the members of the betpakdalite group, a group of monoclinic heteropolymolybdates with a pseudo-hexagonal symmetry of their framework topology (Kampf et al. 2012). A comparison with betpakdalite-CaMg, [Ca₂(H₂O)₁₇Mg(H₂O)₆][Mo₈As₂Fe³⁺₃O₃₆(OH)], shows that the two corner-sharing Mo(3)O₆ octahedra, which link adjacent units, are replaced in the new mineral with a single Fe(1)O₆ octahedron. The Ca site is replaced with a (Sr,Ba,Ca,K) site, while the Mg site is a Na site in the new mineral.

Further SEM-EDS analyses and additional single-crystal determinations of unit-cell parameters of other samples show that some samples are As-free, and suggest that some may be As-dominant (i.e., a tungstoarsenate). The atomic ratio Sr:Ba:Ca:K is variable, but Sr is always clearly dominant. The Na content is also variable.

Heinz Förch and the late Hans Schmid are thanked for providing samples for study.

Kampf AR, Mills SJ, Rumsey MS, Dini M, Birch WD, Spratt J, Pluth JJ, Steele IM, Jenkins RA, Pinch WW (2012): The heteropolymolybdate family: structural relations, nomenclature scheme and new species. - Mineral Mag 76, 1175-1207

Crystal structure of anthropogenic $\text{Ca}_2(\text{OH})(\text{AsO}_4) \cdot 2\text{H}_2\text{O}$ found in the Clara mine, Black Forest, Germany

U. Kolitsch^{1,2}

¹Mineralogisch-Petrographische Abteilung, Naturhistorisches Museum, Burgring 7, 1010 Wien, Austria

²Institut für Mineralogie und Kristallographie, Universität Wien, Josef-Holaubek-Platz 2, 1090 Wien, Austria
e-mail: uwe.kolitsch@nhm.at

The arsenate compound $\text{Ca}_2(\text{OH})(\text{AsO}_4) \cdot 2\text{H}_2\text{O}$, known from studies of the system Ca-As-O-H and reported to be stable in the pH range 11-12 (Bothe & Brown 1999, 2002), had a previously unknown unit cell (unindexed powder diffraction pattern ICDD-PDF 18-289) and crystal structure. Its formula was given in the various literature as $4\text{CaO} \cdot \text{As}_2\text{O}_5 \cdot 5\text{H}_2\text{O}$, $\text{Ca}_3(\text{AsO}_4)_2 \cdot \text{Ca}(\text{OH})_2 \cdot 4\text{H}_2\text{O}$, or $\text{Ca}_4(\text{OH})_2(\text{AsO}_4)_2 \cdot 4\text{H}_2\text{O}$.

The anthropogenic occurrence of $\text{Ca}_2(\text{OH})(\text{AsO}_4) \cdot 2\text{H}_2\text{O}$ in the famous Clara baryte and fluorite mine, Black Forest, Germany, was reported by Blaß & Graf (1995), based on X-ray powder diffraction data. This occurrence is due to the use of concrete underground; several other Ca arsenates (both crystalline and amorphous) are known to occur in such assemblages (named „Beton-Paragenese“ among collectors). $\text{Ca}_2(\text{OH})(\text{AsO}_4) \cdot 2\text{H}_2\text{O}$ was also detected by the present author in 2017 on two samples from the Clara mine. The first sample shows white sprays of colourless, lath-shaped, glassy, transparent crystals up to ~0.3 mm in length. The second sample, erroneously labelled „Calcit, Svabit“, shows pale bluish, blocky, transparent to translucent crystals (up to ~0.5 mm) arranged to form sprays and rounded aggregates. SEM-EDS analyses of carbon-coated fragments showed, apart from Ca, As and O, very minor Si in the first sample, and traces to very minor amounts of Na, Cu, Si and Cl in the second sample.

The crystal structure of $\text{Ca}_2(\text{OH})(\text{AsO}_4) \cdot 2\text{H}_2\text{O}$ was solved from single-crystal intensity data (MoK α ; 293 K). The space group is $P2_1/c$ (no. 14), with $a = 6.178(1)$, $b = 15.688(3)$, $c = 6.876(1)$ Å, $\beta = 99.67(3)^\circ$, $V = 656.96(19)$ Å³; $R(F) = 2.1\%$. The asymmetric unit contains two Ca sites, one As site containing minor Si [refined As:Si ratio = 0.911(2):0.089], seven O sites, one of which represents an OH group and two of which represent water molecules, and five H sites (all detected and refined). The structure is built from an (As,Si)O₄ tetrahedron ($\langle \text{As-O} \rangle = 1.684$ Å) linked to a distorted [6]CaO₆ polyhedron and a [7]CaO₇ polyhedron. The Ca-O polyhedra share edges with themselves and corners with three of the O ligands of the As atom to form a heteropolyhedral layer parallel to {010}. Hydrogen bonds connect these layers; the “free” O ligand of the As site, O2, is acceptor of three H-bonds of medium strength (2.660 - 2.703 Å).

Heinz Förch and Richard Bayerl are thanked for providing samples for study.

Blaß G, Graf HW (1995): Namibit, ein Neufund aus dem Schwarzwald. - Mineralien-Welt 6, 20-22

Bothe JV, Brown PW (1999): The stabilities of calcium arsenates at 23±1 °C. - J Hazard Mat 69, 197-207

Bothe JV, Brown PW (2002): CaO-As₂O₅-H₂O system at 23° ± 1 °C. - J Amer Ceram Soc 85, 221-224

A potentially new mineral $\text{Ca}_2\text{Mg}_2\text{Fe}_{14}\text{O}_{25}$ from Hatrurim Basin, Israel

B. Krüger¹, I. Galuskina², M. Tribus¹, G. Cametti³, Ye. Vapnik⁴, E. Galuskin²

¹Institute of Mineralogy and Petrography, University of Innsbruck, Innsbruck, Austria,

²Faculty of Natural Sciences, Institute of Earth Sciences, University of Silesia, Poland

³Institute of Geological Science, University of Bern, Bern, Switzerland

⁴Department of Geological and Environmental Sciences,
Ben-Gurion University of the Negev Beer-Sheva, Israel

e-mail: biljana.krueger@uibk.ac.at

A potentially new mineral $\text{Ca}_2\text{Mg}_2\text{Fe}_{14}\text{O}_{25}$ was discovered in ferrite-rich veins of gehlenite-bearing hornfelses, found near the east slope of Mount Ye'elim in the Hatrurim Basin, Israel (Vapnik et al., 2007; Galuskina et al., 2017). Xenomorphic aggregates of this natural ferrite are observed in association with hematite, magnesioferrite, franklinite, fluorapatite, and minerals of the khesinite-devilliersite series. The empirical formula, established by microprobe analysis is $\text{Ca}_2(\text{Mg}_{0.61}\text{Cu}_{0.48}\text{Zn}_{0.41}\text{Ca}_{0.32}\text{Ni}_{0.13}\text{Mn}^{2+}_{0.03}\text{Fe}^{2+}_{0.02})\Sigma_2(\text{Fe}^{3+}_{13.78}\text{Al}_{0.22})\Sigma_{14}\text{O}_{25}$.

The dimensions of the unit cell are $a = 5.932$ (1) and $c = 31.302(7)$ Å. The space group $P\bar{3}c1$ of natural $\text{Ca}_2\text{Mg}_2\text{Fe}_{14}\text{O}_{25}$ correspond to that of the synthetic β -CFF phase $\text{Ca}_{2.5}\text{Fe}_{15.5}\text{O}_{25}$ reported by Arakcheeva & Karpinskii (1983). Its crystalline structure is built by an alternating stacking of spinel blocks and F blocks along the c axis (Fig. 1). The spinel block contains two kagome-type layers with $(\text{Fe,Mg})\text{O}_6$ octahedra connected by mixed layers made of $(\text{Fe,Mg})\text{O}_6$ octahedra and FeO_4 tetrahedra. In block F, two layers with mixed polyhedra $(\text{Fe,Mg})\text{O}_6$, FeO_4 , and CaO_7 are connected by a central layer built by trigonal FeO_5 bipyramids.

There are a large number of minerals, in which the triple spinel module intercalates with additional modules, like M-type ferrites (e.g., $\text{BaFe}_{12}\text{O}_{19}$). However, structurally $\text{Ca}_2\text{Mg}_2\text{Fe}_{14}\text{O}_{25}$ is closely related to Y-ferrites, such as $\text{Ba}_2\text{Zn}_2\text{Fe}_{12}\text{O}_{22}$, whose natural analogues are still not found. So far, four polytypes of the CFF phase (α , β , γ , and δ) are known, exhibiting different numbers of spinel and F-blocks along the c axis (Arakcheeva & Karpinskii 1989).

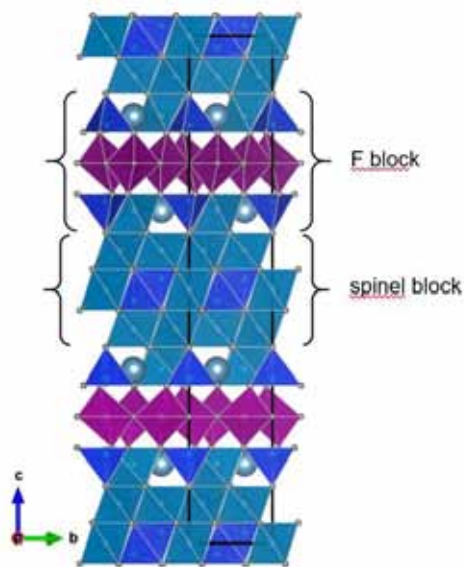


Figure 1. Structure of $\text{Ca}_2\text{Mg}_2\text{Fe}_{16}\text{O}_{25}$. $(\text{Fe,Mg})\text{O}_6$ in cyan, FeO_5 in magenta, FeO_4 in blue colour, and Ca as spheres

Arakcheeva AV, Karpinskii OG (1983): Crystal structure of hexagonal ferrite $\text{Ca}_{2.95}\text{Fe}_{14.85}\text{O}_{25}$. - Dokl Akad Nauk SSSR 273, 1127

Arakcheeva AV, Karpinskii OG (1983): Crystal chemical concept of formation of high-ferrous ferrites. - Kristallografiya 35, 1160-1166

Galuskina I, Vapnik Y, Lazic B, Armbruster T, Murashko M and Galuskin E (2014) Harmunite, CaFe_2O_4 – a new mineral from the Jabel Harmun, West Bank, Palestinian Autonomy, Israel. - Amer Mineral 99, 965-975

Vapnik, Y, Sharygin, VV., Sokol, EV and Shagam R (2007): Paralavas in a combustion metamorphic complex: Hatrurim Basin, Israel. - Rev Eng Geol 18, 1-21

Incommensurate structure and phase transition of cymrite

H. Krüger¹, K. Skrzyńska², R. Juroszek²

¹Institute of Mineralogy and Petrography, University of Innsbruck, Innsbruck, Austria

²Institute of Earth Sciences, University of Silesia, Sosnowiec, Poland

e-mail: Hannes.Krueger@uibk.ac.at

Cymrite, from a hydrothermally altered pyrometamorphic rock of the Hatrurim Complex, found on the east slopes of Mt. Yeelim (Israel), has been investigated using high-temperature single-crystal X-ray diffraction. The empirical formula, as established by electron microprobe analysis, is $\text{Ba}_{0.97}\text{Na}_{0.01}(\text{Al}_{2.00}\text{Si}_{2.01})\text{O}_8 \cdot 1.48 \text{H}_2\text{O}$.

The diffraction pattern of cymrite exhibits a pseudo-hexagonal lattice ($a = 5.3$ and $c = 7.67 \text{ \AA}$), with additional satellite reflections in the $\mathbf{a}^*\mathbf{b}^*$ -plane ($\mathbf{q} \approx 0.125\mathbf{a}^*$, Figure 1), however, the true symmetry is lower. Some crystals show obvious differences in the intensities of the satellites along the three twin-related directions. A more suitable interpretation of the diffraction pattern is obtained using a (pseudo-orthorhombic) C-centred monoclinic lattice ($a = 5.34$, $b = 9.24$, $c = 7.69 \text{ \AA}$). The satellite reflection can be indexed with $\mathbf{q} = 0.31\mathbf{b}^*$. A temperature-dependent series of diffraction experiments revealed that the \mathbf{q} -vector does not change significantly up to 160°C . Between 160 and 250°C , it decreases linearly from $0.31\mathbf{b}^*$ to $0.26\mathbf{b}^*$. Above 250°C , no significant changes are observed until the satellites disappear between 400 and 450°C and a transformation to a hexagonal structure takes place. At 450°C , cymrite adopts space group $P6/mmm$.

Earlier studies on cymrite from the Baikal region (Drits 1975) and Alaska (Bolotina 2010) report fourfold superstructures ($4 \times b$, with respect to the given monoclinic lattice). The observed temperature-dependent change of the \mathbf{q} -vector proves that cymrite from Hatrurim exhibits an incommensurately modulated structure. Possibly, this is related to the water content. *Acknowledgements:* KS acknowledges support from Federal Ministry of Education, Science and Research (BMBWF) OeAD – Austria's Agency for Education and Internationalisation (project-No MPC-2022-03371).

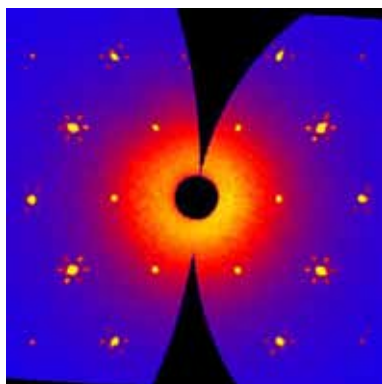


Figure 1. $hk0$ -layer (pseudo hexagonal setting) of the diffraction pattern of cymrite from Israel, exhibiting three pairs of satellite reflections for each Bragg spot as a result of twinning.

Drits VA, Kashaev, AA, Sokolova GV (1975): Crystal structure of cymrite. – *Sov Phys Crystallogr* 20, 171-175
Bolotina NB, Rastsvetaeva RK, Kashaev AA (2010): Refinement of the twinned structure of cymrite from the Ruby Creek Deposit (Alaska). – *Crystallogr Rep* 55, 569-574

Tracing high-pressure metamorphism: The spatial evaluation of the Eoalpine metamorphic gradient in the Texel unit (S-Tyrol, Italy)

J. Lanziner-Oberrauch¹, P. Tropper¹, K. Fassmer², H. Pomella², G. Hoinkes³

¹*Institute of Mineralogy and Petrography, University of Innsbruck, Austria*

²*Institute of Geology, University of Innsbruck, Austria*

³*Institute of Earth Sciences, University of Graz, Austria*

e-mail: peter.tropper@uibk.ac.at

In the Austroalpine basement west of the Penninic Tauern Window there are four different units that can be attributed to the Upper Austroalpine, but can be distinguished on the basis of their different lithologies and metamorphic histories. These are 1) the Ötztal-Bundschuh nappe system, which includes the Ötztal unit, 2) the Koralpe-Wölz high pressure nappe system including the Schneeberg and Texel units, 3) the Silvretta-Seckau nappe system with the Ortler-Campo unit, and 4) the Drauzug-Gurktal nappe system, which includes the Matsch unit, the Tonale nappe, and the Meran-Mauls nappe stack.

The Texel unit consists of a metasedimentary sequence with intercalating orthogneisses, amphibolites, and eclogites. Previously, the so-called Laas unit was considered both as part of the Texel unit and as an independent unit. However, because of intense Permo-Triassic metamorphism, for which there is as yet no evidence in the rest of the Texel unit, it should be considered as a separate unit called the Lodner unit (Hoinkes et al. 2021). In their present position in the alpine nappe stack, these two units lie in the above of the Ortler-Campo unit and below the Schneeberg and Ötztal units. Based on the Eoalpine age of the eclogites, the Texel unit is considered to be part of the Koralpe-Wölz nappe system and thus an intracontinental subduction-related high-pressure area related to the Neotethys closure. Overall, the Texel unit has been significantly overprinted by Variscan and Eoalpine metamorphism. Only the so-called Lodner unit shows a Permo-Triassic overprint. The Texel unit reached eclogite-facies during subduction. P-T conditions reached 1.2 to 2.2 GPa and 540 to 620 °C or 680 to 730 °C and 2.7 to 2.9 GPa, depending on the author. The age of the pressure maximum of Eoalpine metamorphism in the Texel unit is 85 ± 5 Ma. The eclogites occur only locally in the Texel unit and the question arose whether this "high-pressure memory" is also detectable in the mica schists and paragneisses.

For this purpose 24 metapelite samples (garnet + biotite + plagioclase + muscovite + quartz \pm kyanite) were investigated geothermobarometrically (Thermocalc v.3.33, mode 1 and mode 2). It was found that the P-T data can be divided into three groups: P = 0.6-0.8 GPa, P = 0.8-1.2 GPa, and P = 1.2-1.6 GPa, and T = 570-600 °C, T = 600-700 °C, and T > 700 °C. Most pressures were in the range 0.8-1.2 GPa, but some samples taken in the vicinity the eclogites still show elevated P values of 1.2-1.6 GPa. Mineral chemically, a pressure-affected earlier stage of Eoalpine metamorphism can also be detected in the elevated Si contents (3.2-3.3 apfu) of muscovite cores. Regionally, a "central zone" with the highest pressure values in the Texel unit can currently be identified. This correlates spatially with the area in the Texel unit where the eclogites occur. Towards the edge of the Texel unit the pressures decrease again.

Hoinkes G, Krainer K, Tropper P (2021): Ötztaler Alpen, Stubai Alpen und Texelgruppe. - Sammlung geologischer Führer, Band 112, Gebrüder Bornträger

Bismoclite BiOCl from the Jean Baptiste mine, Lavrion area, Greece

I. Liebhart¹, B. Rieck¹, M. Zeug^{1,2}, G. Giester¹

¹Department of Mineralogy and Crystallography, University of Vienna, Josef-Holaubek-Platz 2, 1090 Vienna

²Landesamt für Geologie und Bergwesen, An der Fliederwegskaserne 13, 06130 Halle (Saale), Germany

e-mail: gerald.giester@univie.ac.at

Bismoclite was first discovered and described from a museum specimen No 4465 in the McGregor Museum, Kimberly. The sample is from Jakkalswater, South Africa (Mountain, 1935). Chemical analysis resulted in Bi₂O₃ 89.41, Cl 13.67, less O=Cl₂ 3.08, sum 100 wt. % (Mountain, 1935). In the same year, Bannister & Hey (1935) synthesised the compound BiOCl and named it bismoclite. The crystal structure was solved on synthetic samples in space group *P4/nmm*, with unit cell data $a = 3.887(5)$, $c = 7.354(5)$ Å and refined to $R = 9.17\%$ (Keramidas et al. 1993). Furthermore, a sample from a Bi-Cu-Au deposit, Argentina was studied by infrared analysis, thermal analysis using DTA and TGA, chemical analysis using inductively coupled plasma mass spectrometry (ICP-MS) and an instrumental neutron activation analysis (INAA), microscopy analysis using scanning electron microscopy (SEM), and by pXRD (Testa et al. 2016).

Recently, rare bismoclite was discovered at the 2nd level of the Jean Baptiste Mine in the central part of the Agios Konstantinos area, Lavrion mining district, Attica, Greece. Natural bismoclite was investigated for the first time by single-crystal X-ray diffraction, confirming space group *P4/nmm* with unit cell parameters $a = 3.887(2)$, $c = 7.357(5)$ Å, $Z = 2$, $V = 111.16(14)$ Å³ and refined to final values $R1 = 0.0134$ and $wR2 = 0.0363$. Examined by Raman spectroscopy, the spectrum shows the most intense Raman band at 144 cm⁻¹, smaller bands were observed at 198 and 396 cm⁻¹.



Figure 1. White, in thin sections colourless bismoclite surrounded by ore minerals. FOV 2.9 mm. Foto: B. Rieck

Bannister FA, Hey MH (1935): The crystal-structure of the bismuth oxyhalides. - Mineral Mag 24, 49–58

Keramidas KG, Voutsas GP, Rentzeperis PI (1993): The crystalstructure of BiOCl. - Z Kristallogr 205, 35–40

Mountain ED (1935): Two new bismuth minerals from South Africa. - Mineral Mag 24, 59–64

Testa FJ, Cooke DR, Zhang L, Mas GR (2016): Bismoclite (BiOCl) in the San Francisco de los Andes Bi–Cu–Au Deposit, Argentina. First occurrence of a bismuth oxychloride in a magmatic–hydrothermal breccia pipe and its usefulness as an indicator phase in mineral exploration. - Minerals 6, 62

In-situ powder diffraction study on the formation and reaction pathways of potassium calcium silicates

H. Liu, V. Kahlenberg, C. Hejny, H. Krüger

*University of Innsbruck, Institute of Mineralogy and Petrography, Innrain 52, 6020 Innsbruck, Austria
e-mail: hang.liu@uibk.ac.at*

The K_2O - CaO - SiO_2 system is critically influential in several industrial sectors involving glasses, ceramics, pyrometallurgical processes, energy production, and biomass power. It is of particular interest due to the presence of potassium calcium silicates in the ashes from biomass combustion, modified electric arc furnace slag as well as fertilizers produced from the residues of oil-shale industry or from steelmaking slags. Understanding their high-temperature behaviour can i) contribute to avoid negative effects in the production process due to slagging, fouling or sintering and ii) facilitate the reutilization of residual materials.

In recent years, numerous potassium calcium silicates have been successively identified. $\text{K}_2\text{Ca}_2\text{Si}_2\text{O}_7$ and $\text{K}_2\text{Ca}_6\text{Si}_4\text{O}_{15}$, notable for their comparatively high melting points, are key contributors to slagging within the system (Santoso et al. 2020). They have been reported to remain in the solid state at temperatures reaching up to 1200 °C. $\text{K}_2\text{Ca}_3\text{Si}_3\text{O}_{10}$, located adjacent to $\text{K}_2\text{Ca}_2\text{Si}_2\text{O}_7$ within the phase diagram, has been reported to occur under ambient pressure at temperatures of 900 °C, but does not prevail as a primary phase (Schmidmair et al. 2015). While the crystal structures of these potassium calcium silicates have been deciphered, no information is available concerning the question how the complex solid-state reactions in this system proceed and if intermediate / metastable phases are involved.

In the present study, the reaction pathways during the formation of the aforementioned three compounds from silica and carbonate educts were reconstructed through a combination of in-situ powder X-ray diffraction, DTA/TG, and isothermal annealing experiments. Our current observations suggest that K_2CO_3 absorbs water and CO_2 from the air to form KHCO_3 at room temperature and reverts through a dehydration process when heated to around 120 °C. Potassium carbonate in the educts tends to combine with CaCO_3 to form $\text{K}_2\text{Ca}(\text{CO}_3)_2$ before the formation of the silicates, and undergoes a polymorphic transition from Bütschliite to Fairchildite at ~500 °C. Upon complete decarbonation (~730-800 °C), in all starting mixtures corresponding to the target compositions $\text{K}_2\text{Ca}_2\text{Si}_2\text{O}_7$ (E₁₂₂), $\text{K}_2\text{Ca}_6\text{Si}_4\text{O}_{15}$ (E₁₆₄), and $\text{K}_2\text{Ca}_3\text{Si}_3\text{O}_{10}$ (E₁₃₃) the same two crystalline silicate phases could be identified equivocally: $\text{K}_2\text{Ca}_2\text{Si}_2\text{O}_7$ and Ca_2SiO_4 . $\text{K}_2\text{Ca}_6\text{Si}_4\text{O}_{15}$ begins to form at ~890 °C, originating from the combination of Ca_2SiO_4 and probably potassium silicate. The temperature range between 920 and 1070 °C can be considered the dominant range for $\text{K}_2\text{Ca}_2\text{Si}_2\text{O}_7$, where the previously formed $\text{K}_2\text{Ca}_6\text{Si}_4\text{O}_{15}$ further reacts with potassium silicate to form $\text{K}_2\text{Ca}_2\text{Si}_2\text{O}_7$, and Ca_2SiO_4 undergoes complete resorption. Starting at 1070 °C, $\text{K}_2\text{Ca}_6\text{Si}_4\text{O}_{15}$ is the main phase. However, after further heating to 1150 °C, $\text{K}_2\text{Ca}_6\text{Si}_4\text{O}_{15}$ almost fully reacts into Ca_2SiO_4 which exhibits a notable potassium solubility. Above ~1150 °C, no crystalline phases were present for mixture E₁₃₃. In particular, $\text{K}_2\text{Ca}_3\text{Si}_3\text{O}_{10}$ is not observable in any stage of the heating process of the three educts.

Schmidmair D, Kahlenberg V, Perfler L, Tribus M, Hildebrandt J, Többsen DM (2015)1: On the ambient pressure polymorph of $\text{K}_2\text{Ca}_3\text{Si}_3\text{O}_{10}$ - An unusual mixed-anion silicate and its structural and spectroscopic characterization. - J Solid State Chem 228, 90-98

Santoso I, Taskinen P, Jokilaakso A, Paek M-K, Lindberg D (2020): Phase equilibria and liquid phase behavior of the K_2O - CaO - SiO_2 system for entrained flow biomass gasification. - Fuel 265, 116894

Thermal expansion of SiO₂ polymorphs keatite, RUB-11 and silica-sodalite

B. Marler¹, I. Grosskreuz¹

¹Department. of Geology, Minerology, and Geophysics, Ruhr University Bochum, Germany
e-mail: bernd.marler@rub.de

With very few exceptions, dense silica polymorphs like α -quartz or β -cristobalite exhibit a positive volume thermal expansion while microporous silica polymorphs (= guest free silica zeolites) like siliceous faujasite or siliceous chabasite show negative expansion (Lightfoot et al. 2001).

Here, we present the analysis of the thermal expansion coefficients of three silica polymorphs, which have, so far, not been investigated.

Keatite (tetragonal, $\rho = 2.50 \text{ g cm}^{-3}$) is a rare, metastable SiO₂ polymorph possessing a dense silica framework, synthetic keatite is known since 1954 (Keat et al. 1954) and has more recently been discovered as a mineral (Hill et al. 2013).

The all-silica form of sodalite (cubic above 412 K, $\rho = 1.67 \text{ g cm}^{-3}$) has the same microporous framework comprising cage-like voids (Werthmann et al. 2000) as the sodalite mineral, Na₈Cl₂[Si₆Al₆O₂₄].

RUB-11 (monoclinic, $\rho = 2.11 \text{ g cm}^{-3}$) can be regarded as an Interlayer Expanded Zeolite of the natural layer silicate magadiite, Na₂[Si₁₄O₂₈(OH)₂] · 8H₂O, however, with additional SiO₄ tetrahedra interconnecting the silicate layers instead of intercalated sodium and water. RUB-11 possesses a silica framework with channel-like pores (Grosskreuz et al. 2023).

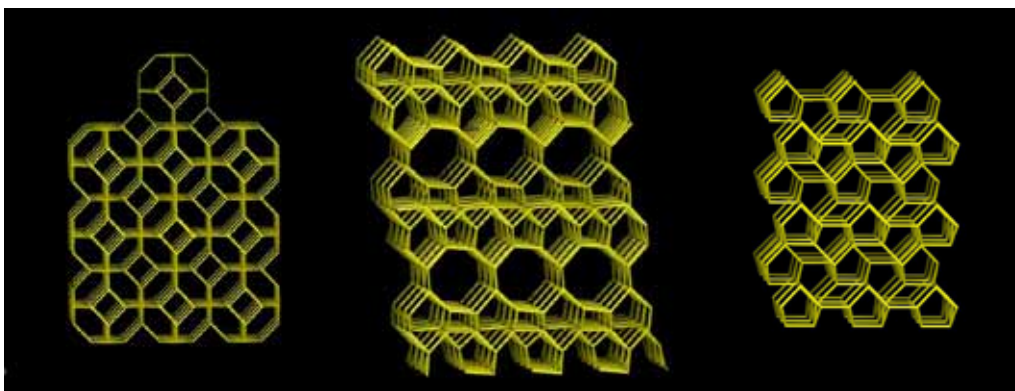


Figure 1. The framework structures of cubic silica sodalite (left), RUB-11 (middle), and keatite (right).

Experimental data: Keatite was synthesized heating a silicate gel prepared from Si(OC₂H₅)₄, LiNO₃, Cr(NO₃)₃ and water at 830 K. Trioxane-silica-sodalite and RUB-11 were hydrothermally synthesized from reaction mixtures of SiO₂/Trioxane/H₂O and SiO₂/ethylenediamine/H₂O/Xe, respectively. Trioxane-silica-sodalite was subsequently heated to remove all organic material from the cage-like pores producing pure silica-sodalite.

Powder XRD data (CuK α ₁) of all samples, kept in glass capillaries, were collected in Debye-Scherrer geometry. Silicon or quartz powder served as an internal standard. The samples were heated in steps of 50 K (silica-sodalite), 100 K (RUB-11) and 110 K (keatite) up to 729, 898 or 713K. Rietveld refinements revealed the lattice parameters and unit cell volumes.

The guest-free silica sodalite is trigonal at room temperature and transforms into a cubic symmetry at 412 K (Werthmann et al. 2000). The cubic silica sodalite exhibits isotropic (negative) expansion while RUB-11 and keatite show a pronounced anisotropic behaviour with negative and positive expansion in different directions. Linear expansion coefficients are Silica-sodalite (454 – 729 K): $\alpha[100] = -3.7 \cdot 10^{-6}$
RUB-11 (298 – 898 K): $\alpha[100] = -10.2 \cdot 10^{-6}$, $\alpha[010] = +10.1 \cdot 10^{-6}$, $\alpha[001] = -2.1 \cdot 10^{-6}$
Keatite (293 – 713 K): $\alpha[100] = -6.1 \cdot 10^{-6}$, $\alpha[001] = +15.0 \cdot 10^{-6}$
Corresponding expansion coefficients of the volumes $\alpha(V)$ are:
cubic silica sodalite = $-11.2 \cdot 10^{-6}$; RUB-11 = $-6.4 \cdot 10^{-6}$ and keatite = $+2.9 \cdot 10^{-6}$

When listing microporous and dense silica polymorphs with densities ranging from 1.3 to 2.9 gcm⁻¹ it appears that materials with intermediate densities (about 2.0 gcm⁻¹) have particular small (positive or negative) expansion coefficients (see Table 1). Considering this fact, it seems not impossible to discover or specifically synthesize a silica polymorph with nearly zero expansion. Since SiO₂ polymorphs are chemically, mechanically and thermally very stable when exposed to most chemicals, pressure and/or high temperature such a material might be useful for many purposes.

Table 1. Selection of SiO₂ polymorphs of intermediate density

| SiO ₂ polymorph | Density [gcm ⁻¹] | Volume thermal expansion coefficient [ppm/K], (temperature range) | Reference |
|-----------------------------|------------------------------|---|--------------------|
| MFI-type zeolite | 18.4 | -7.6 (373-673 K) | Bhange et al. 2007 |
| RWR-type zeolite | 19.2 | +3.7 (298-773 K) | Koike et al. 2023 |
| High density zeolite RUB-11 | 21.1 | -6.4 (298-898 K) | This study |
| High density zeolite RUB-5 | 22.0 | -7.5 (293-743 K) | Marler et al. 2020 |
| Silica glass | 22.0 | +0.5 (273-873 K) | Heraeus 2023 |
| High density zeolite RWZ-1 | 22.1 | -3.9 (298-773 K) | Koike et al. 2023 |

Bhange DS, Ramaswamy V (2007): High temperature thermal expansion behavior of silicalite-1 molecular sieve: in situ HTXRD study. - Micropor Mesopor Mater 103, 235-242
Grosskreuz I, Krysiak Y, Gies H, Mugnaioli E, Marler B (2023): Synthesis and real structure of RUB-11, a novel high-density silica zeolite based on magadiite layers. - Submitted.
Heareus: Properties of fused silica (accessed April 27th 2023) - https://www.heraeus.com/en/hca/fused_silica_quartz_knowledge_base_1/properties_1/properties_hca.html#tabs-608478-5
Hill TR, Konish H, Huifang X (2013): Natural occurrence of keatite precipitates in UHP clinopyroxene from the Kokchetav Massif: A TEM investigation. - Am Mineral 98, 187-196
Koike M, Grosskreuz I, Asakura Y, Miyawaki R, Gies H, Wada H, Shimojima A, Marler B, Kuroda K. (2023): Bridging the gap between zeolites and dense silica polymorphs: Formation of all-silica zeolite with high framework density from natural layered silicate magadiite. - Submitted to Angew Chem
Keat PP (1954): A new crystalline silica. - Science 120, 328-330
Lightfoot P, Woodcock DA, Maple MJ, Villaescusa LA, Wright PA (2001): The widespread occurrence of negative thermal expansion in Zeolites. - J Mater Chem 11, 212-216
Marler B, Krysiak Y, Kolb U, Grafweg C, Gies H (2020): Two new members of the Silica-X family of materials: RUB-5, a silica zeolite with a very high framework density and RUB-6, a hydrous layer silicate, Micropor. - Mesopor Mater 296, 109981
Werthmann U, Marler B, Gies H (2000): Gastmolekülfreier Silica-Sodalith: Eine neue SiO₂-Modifikation, Z Kristallogr Supplement Issue, 17, 188

Corundum-rich rocks in the Tauern Window, Austria

F. Melcher¹, M. Feichter¹, H. Mali¹, H. Grill², B. Huet³

¹*Department of Applied Geosciences and Geophysics, Montanuniversität Leoben, Austria,*

²*Birkenweg, Neumarkt, Austria*

³*Geosphere Austria, Vienna, Austria*

e-mail: F.Melcher@unileoben.ac.at

In the search for the origin of a 60 kg block of a dark grey corundum-rich rock that was found in the river bed of the Obersulzbach Valley near Hopffeldboden, Venediger Alps (Salzburg, Austria; Melcher et al. 2022), boulders of similar material were discovered underneath a cliff in the region named Bettlerscharte. In this area, Variscan granite gneisses of the Central Gneiss Supersuite are intercalated with metavolcanics (amphibolite, chlorite schist) and metasedimentary rocks (micaschist, graphitic phyllite, quartzite) attributed to the Habach Group. Corundum-bearing rocks with or without sulphide mineralization are associated with a diverse suite of metasedimentary and metavolcanic rocks that outcrop in the cliff northwest of the Bettlerscharte. Rocks comprise white, partly kyanite-bearing quartzite, garnet-bearing chloritoid-chlorite-muscovite schist, amphibolite, and epidote schist with massive bands of magnetite. The quartzites show strong foliation and disseminated sulphide mineralization comprising mainly pyrite, but in places also abundant molybdenite. The assemblage resembles the one described as type locality of the Habach Formation (Steyrer 1983).

Similar to the specimen found in the Obersulzbach valley investigated earlier (Melcher et al. 2022), microscopic examination of the corundum-bearing rocks reveals abundant magnetite, ilmenohematite, and variable pyrite in a very fine-grained non-foliated matrix, in which rare white mica flakes and aggregates are visible. The fine matrix consists mainly of anhedral corundum of 30-50 µm grain size intergrown with green-blue pleochroic Fe-rich chloritoid (#Mg = 15-27) and less abundant light green chlorite with #Mg ranging from 40-60. White mica aggregates consist of intergrown margarite and paragonite and are often surrounded by large chloritoid crystals. Apatite is present throughout the rock, although grain size and abundance vary. Accessory phases include diaspore, epidote/allanite, zircon, and monazite. Oxide minerals mainly consist of magnetite and ilmenohematite. Uraninite and Nb-rich rutile (4-6 wt% Nb₂O₅) are subordinate. Sulphides postdate the oxide-silicate assemblage and mainly consist of pyrite and chalcopyrite, with rare molybdenite. The corundum-rich assemblage is associated with rocks carrying relict garnet replaced by chloritoid, chlorite and white mica. These rocks also carry abundant magnetite, ilmenohematite and pyrite.

Chemical analysis of corundum-rich rocks by wavelength-dispersive X-ray fluorescence spectroscopy on fused discs reveals high contents of Al₂O₃ (36-55 wt%) and Fe₂O₃ (22-35 wt%), low SiO₂ (3.8-22 wt.%), CaO (0.7-2.6 wt.%), MgO (0.7-2.1 wt.%), K₂O (<1.8 wt.%) and Na₂O (<1.2 wt.%). Sulphur contents in some samples reach up to 10 wt.%. TiO₂ (2.2-4.2 wt.%) and P₂O₅ (0.7-1.2 wt.%) are severely enriched compared to typical crustal rocks. Among the trace elements, high contents of Zr (356-848 ppm), V (321-559 ppm), Nb (39-89 ppm), Cu (156-1550 ppm) and Ga (49-106 ppm) are noteworthy, along with low Cr, Ni, Y and REE.

Chemical composition and mineralogy both strongly argue in favour of a bauxitic origin of the samples, resembling Si-depleted, Fe-rich bauxite. Compared to other metabauxites, the P content is extraordinarily high. Apart from S, Fe, Cu and P, levels of minor and trace elements are within the ranges expected for bauxite. Trace element concentrations, especially low Ni-Cr contents favour an origin from acidic precursor rocks.

The association with both, rocks typical of the Habach Formation (amphibolite) and quartzitic metasediments is regarded as an indication for a situation where pre-Permian rocks have been weathered producing local bauxitic rocks associated with less Si-depleted, clay-rich material. These paleosoils have been covered by impure sandstone, probably in the Lower Triassic. Weathering horizons in similar stratigraphic and tectonic positions have been described from other areas within the Tauern Window (Barrientos & Selverstone 1987; Franz et al. 2021).

Preliminary metamorphic P-T conditions have been determined for the metabauxite using pseudosections calculated with the Theriak-Domino software package (de Capitani & Petrakakis 2010). The targeted sample is the one investigated in Melcher et al. (2022). The observed oxide-silicate assemblage with corundum, chloritoid, chlorite, margarite, paragonite, rutile, hematite, ilmenite and magnetite points to peak conditions at 500 ± 30 °C and 8.5 ± 1.5 kbar. In this range, the model predicts stability of corundum, chloritoid, chlorite, margarite, paragonite and rutile together with a complex topology between the fields containing one or two of the three Fe-Ti oxides hematite, ilmenite and magnetite. This explains the observed complex reaction features between those.

- Barrientos X, Selverstone J (1987): Metamorphosed soils as stratigraphic indicators in deformed terranes: An example from the Eastern Alps. – *Geology* 15, 841-844
- de Capitani C, Petrakakis K (2010): The computation of equilibrium assemblage diagrams with Theriak/Domino software. – *Amer Mineral* 95, 1006-1016
- Franz G, Kutzschbach M, Berryman EJ, Meixner A, Loges A, Schultze D. (2021): Geochemistry and paleogeographic implications of Permo-Triassic metasedimentary cover from the Tauern Window (Eastern Alps). – *Eur J Mineral* 33, 401-423
- Melcher F, Feichter M, Mali H, Grill H (2022): Ein ungewöhnliches Korundgestein im Tauernfenster: Metabauxite in der Habach-Gruppe? – *Mitt Österr Mineral Ges* 168, 89-99
- Steyrer HP (1983): Die Habachformation der Typlokalität zwischen äußerem Habachtal und Untersulzbachtal (Pinzgau/Salzburg). – *Mitt Österr Geol Ges* 76, 69-100

On preventing Sn-loss in experimental studies

J. A.-S. Michaud¹, F. Holtz¹, T. Fusswinkel²

¹*Institute of Mineralogy, Leibniz University, Callinstrasse 3, 30167 Hannover, Germany*

²*Institute of Applied Mineralogy and Economic Geology, RWTH Aachen University
Willnerstraße 2, 52062 Aachen, Germany*

e-mail: j.michaud@mineralogie.uni-hannover.de

Tin (Sn) transport and concentration are essentially controlled by a combination of melt- and fluid-driven processes and its cycle within the crust strongly depends on its partitioning. Given the complexity of natural systems, it is rather hard to evaluate the effect of individual parameters (e.g., pressure (P), temperature (T), proportion and composition of involved phases or redox conditions) on Sn behaviour.

As an alternative, natural processes can be simulated experimentally under a range of conditions relevant to natural systems. However, in experiments conducted at elevated P-T, samples containers are made of noble-metal capsules (e.g., Au, Pt, Au-Pd) and Sn alloys with all these materials especially under reducing conditions and when an aqueous phase is present. This often results in capsule failure and/or to problems for the accurate determination of Sn partitioning between phases due to partial Sn loss during the experiment. Several experimental studies have focused on Sn behaviour (e.g., Keppler & Wyllie 1991; Schmidt et al. 2020; Michaud et al. 2021; Pichavant 2022) but to our knowledge none of the methods proposed so far were completely satisfactory when it comes to preventing Sn loss and determining partition coefficients accurately and reproducibly.

Inspired from Lerchbaumer & Audétat (2012) and Derrey et al. (2017), we propose a new capsule setup (Fig.1) which has been tested on the example of Sn partitioning experiments

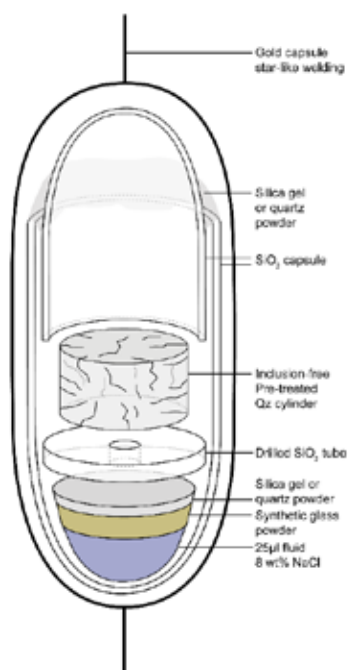


Fig.1: Capsule setup designed to prevent Sn-loss during HT-HP experiments.

between a strongly peraluminous melt and an aqueous phase. In order to avoid interactions with the noble-metal capsule and minimise Sn loss, 15 mg of glass powder containing *ca.* 600 ppm Sn, 25µl of 8wt% NaCl fluid and a pre-cracked quartz cylinder are inserted in an inner silica capsule consisting of two fitting tubes. Silica gel or quartz powder is added to insure sealing of the silica tubes during heating.

Several experiments were run at 800°C, 150 MPa, under boiling conditions (i.e., phase separation resulting in coexisting brine and vapour-rich fluid inclusions), for 24 and 48h and under oxidising (QFM+3; fO_2 is 3 log units higher than fO_2 buffered by Quartz-Fayalite-Magnetite buffer) and reducing conditions (QFM -0.5).

Boiling assemblages were found in all samples, with brine and vapour-rich inclusions entrapped in quartz cylinders having generally a size in the range of 10 to >25 µm. Under reducing conditions, quenched glasses contain numerous albite crystals and few cassiterites. Under oxidising conditions, the glass is rather homogeneous and cassiterite has only been found within what was formerly a silica drilled tube separating the quartz cylinder from the rest (see Fig. 1).

Tin concentrations were measured in quenched glasses and brine and vapour-rich inclusions with electron microprobe and LA-ICP-MS. Under oxidising conditions, Sn concentrations are rather homogeneous in the quenched glass (i.e., ~ 200-250 ppm) and a bit more scattered in brine inclusions (i.e., 100-640 ppm; median 347 ppm) but all lower than the Sn concentration in the starting glass. Under reducing conditions, Sn concentrations in glass are more scattered in the 24h run (i.e., median 2631 ± 1464 ppm) than in the 48h one (i.e., median 1752 ± 699 ppm). This heterogeneity is probably related to the high crystallinity observed in these glasses. Concentrations in brine inclusions are rather clustered for both duration (i.e., median 107 ± 38 ppm and 84 ± 50 ppm for the 24 and 48h runs, respectively). Concentrations in vapour-rich inclusions could only be measured in the 48h run and are very low (i.e., median 0.6 ± 6 ppm).

Overall, Sn shows a contrasted behaviour depending on redox conditions, being preferentially partitioned to the fluid under oxidising and to the melt under reducing conditions. This result is supported by the presence of cassiterite crystallizing from the fluid at oxidizing conditions and of cassiterite crystallizing from the melt at reducing conditions. Our dataset and mass balance calculations indicate that the use of a silica capsule inserted in noble metal capsules is rather successful in preventing important Sn-loss during experiments.

- Derrey IT, Albretch M, Dupliy E, Botcharnikov RE, Horn I, Junge M, Weyer S, Holtz F (2017): Experimental tests on achieving equilibrium in synthetic fluid inclusions: Results for scheelite, molybdenite, and gold solubility at 800 °C and 200 Mpa. - *Amer Miner* 102, 275-283
- Keppler H, Wyllie PJ (1991): Partitioning of Cu, Sn, Mo, W, U and Th between melt and aqueous fluid in the systems haplogranite-H₂O-HCl and haplogranite-H₂O-HF. - *Contr Miner Petrol* 109, 139-150
- Lerchbaumer L, Audétat A (2012): The quartz capsule - a new method to avoid alloying problems with noble-metal capsules in hydrothermal experiments. - *Eur J Miner* 24, 683-693
- Michaud JA-S, Pichavant M, Villaros A (2021): Rare elements enrichment in crustal peraluminous magmas: insights from partial melting experiments. - *Contr Miner Petrol* 176, 96
- Pichavant M (2022): Experimental crystallisation of the Beauvoir granites as a model for the evolution of Variscan rare metal magmas. - *J Petrol* 63, 1-28
- Schmidt C, Romer R, Wohlgemuth-Ueberwasser CC, Appelt O (2020): Partitioning of Sn and W between granitic melt and aqueous fluid. - *Ore Geol Rev* 117, 103263

LA-ICPMS U-Pb dating of garnet from the Adula nappe, Central Alps

L.J. Millonig¹, J. Pleuger², T. John², A. Gerdes¹

¹*FIERCE, Goethe University Frankfurt am Main*

²*Freie Universität Berlin*

e-mail: l.millonig@em.uni-frankfurt.de

The Adula nappe is located in the Lepontine Alps, Switzerland and Italy, and comprises crustal gneisses, metasediments and mica schists, as well as mafic and ultramafic units including eclogites, amphibolites and peridotites. Rocks from the Adula nappe show a gradual increase in pressure and temperature from north to south and record a high-pressure (HP) event followed low-pressure (LP)/high-temperature (HT) conditions, with the intensity of the overprint also increasing to the south. HP metamorphism and subsequent LP-HT overprint are considered to result from a single P–T evolution. However, geochronological data from the Adula nappe yielded partially inconsistent results and the timing and extent of HP metamorphism in the Adula nappe remains somewhat ambiguous. While eclogites from the southern part of the nappe yielded ages between 42 and 34 Ma (garnet Lu–Hf and Sm–Nd; zircon U–Pb), eclogites in the northeastern part of the nappe yielded only Palaeozoic ages of ~330–340 Ma (U–Pb zircon) and ~324 Ma (Lu–Hf garnet) for the HP stage. Eclogites from the central part of the Adula nappe gave both Alpine (~37–39 Ma) and Variscan (336 Ma) garnet Lu–Hf ages and zircon U–Pb ages (~31–33 and ~370 Ma). P–T conditions recorded by the Adula nappe are attributed to Variscan-Alpine polymetamorphism and a polyphase Alpine deformation history, which obscured the mineral equilibria developed during each high-grade metamorphic event. Polymetamorphism of the Adula nappe is reflected in compositionally and chronologically distinct garnet domains and generations. However, published ages from polymetamorphic garnet from the Adula nappe represent approximate maximum or minimum ages, because the mixing of different garnet age domains during hand picking cannot be ruled out when using conventional dating techniques. We therefore applied in-situ garnet U–Pb dating by LA-ICP-MS to spatially resolve different garnet growth zones, as revealed by major and trace element mapping.

Our preliminary results indicate that Variscan metamorphism in the northeastern Adula nappe also occurred at ~370 Ma, whereas lithologies from the central and southern Adula nappe yielded garnet U–Pb dates of ~40–35 Ma. Moreover, some samples from the central Adula nappe yielded single well-defined Alpine garnet growth ages, whereas others indicate ill-defined pre-Alpine garnet growth events. Such samples will be further investigated in greater detail to resolve the two growth events.

In-situ monitoring of ATP hydrolysis as a function of p-T-Mg²⁺: new insights into metabolic kinetics

C. Moeller¹, C. Schmidt², D. Testemale³, F. Guyot⁴, M. Kokh^{1,5}, M. Wilke¹

¹Institut für Geowissenschaften, Universität Potsdam, Germany

²Helmholtz-Zentrum Potsdam, Deutsches GeoForschungsZentrum GFZ, Germany

³Univ. Grenoble Alpes, CNRS, Institut Néel, Grenoble, France.

⁴IMPMC Muséum National d'Histoire Naturelle, Paris, France

⁵Institut für Mineralogie, Westfälische-Wilhelms-Universität, Münster, Germany

e-mail: chmoeller@uni-potsdam.de

The thriving exploration of geologically extreme environments has led to the discovery of new habitats of extremophiles. Fascinating biological communities were discovered at hot springs, in deep oceanic sediments, and hydrothermal vents. Biological-geological interaction enables life up to 120 °C and 300 MPa. Experimental studies, albeit controversial, expanded this T-P-range (Sharma et al. 2002, Takai et al. 2008). Stability of vital molecules like ATP can serve as proxies to determine physicochemical boundary conditions for life (Bains et al. 2015)

The exergonic enzymatic hydrolysis of adenosine triphosphate (ATP) to adenosine diphosphate (ADP) is a key reaction in all metabolic systems. It is counteracted by the abiotic hydrolysis of ATP; therefore, the rate constant and the related half-life can be used as a proxy for bioavailability. The abiotic hydrolysis is kinetically enhanced at elevated temperatures and low pH values (Leibrock et al. 1995; Moeller et al. 2022). The dependence on pressure of the rate constant of the hydrolysis can be best described by a power law and shows only a vanishingly low effect up to 500 MPa. Addition of Mg²⁺ and Ca²⁺ decelerate the hydrolysis; in contrast to Cu (II) and Co (III) complexes, which lead to an acceleration (Buisson and Sigel 1974, Suzuki et al. 1978).

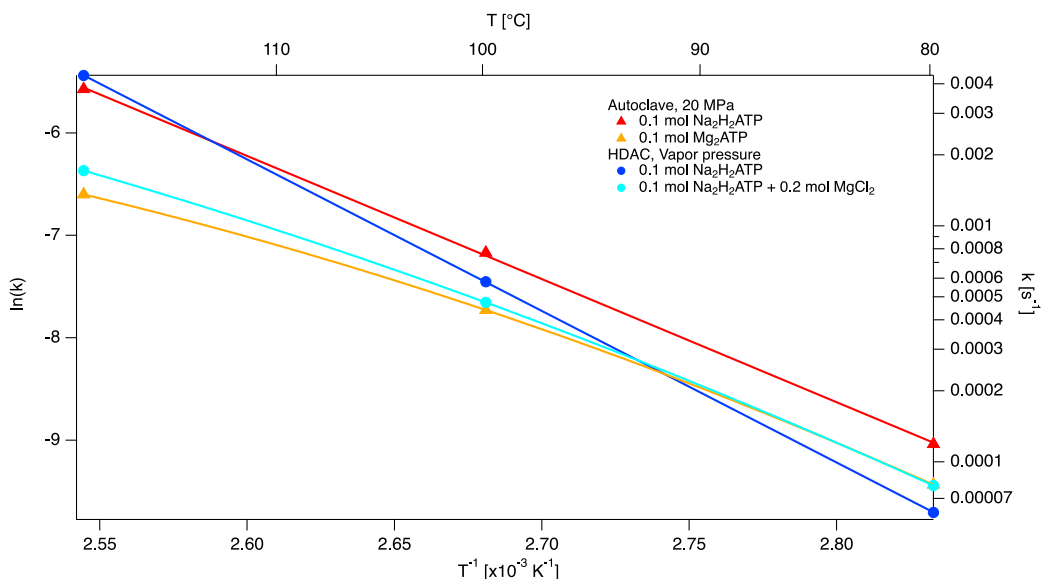


Figure 1: Arrhenius graph of the hydrolysis rate constants of ATP.

In biological systems, ATP is commonly found in a complexed form with Mg^{2+} . Earlier, experimental studies were performed on monovalent analogs of ATP like $\text{Na}_2\text{H}_2\text{ATP}$ as commercial Mg_2ATP salts are rare and expensive. Effects of Mg^{2+} were simulated by addition of magnesium salts (e.g., in Leibrock et al. 1995). A novel in-situ protocol based on the combination of optical high-pressure cells and Raman spectrometry allowed us to determine the hydrolysis rate constants on small sample volumes without any artifacts due to quenching. The investigated temperature range was from 80 – 120 °C for sample solutions of $\text{Na}_2\text{H}_2\text{ATP} + \text{MgCl}_2$ and of Mg_2ATP . Our preliminary results verify a decrease of the hydrolysis rate constant by 30% at 80 °C. In contrast to studies on $\text{Na}_2\text{H}_2\text{ATP}$ systems, our initial data suggest a significant deviation from the Arrhenius relation in the investigated T-interval (Fig. 1). This very new insight on the kinetic stability of Mg_2ATP suggests that the reaction mechanism changes at high temperature in the presence of magnesium. In terms of bioavailability, Mg^{2+} almost doubles the half-life of ATP at 120 °C which is 20% higher than previously assumed.

- Sharma A, Scot JH, Cody GD, Fogel ML (2002): Microbial Activity at Gigapascal Pressures. - *Science* 295, 5539, 1514-1516
- Takai K, Nakamura K, Toki T, Horikoshi K (2008): Cell proliferation at 122°C and isotopically heavy CH_4 production by a hyperthermophilic methanogen under high-pressure cultivation. - *PNAS* 10949-10954
- Bains W, Xiao Y, Yu C (2015): Prediction of the maximum temperature for life based on the stability of metabolites to decomposition in water. - *Life* 5, 1054-1100
- Leibrock E, Bayer P, Lüdemann HD (1995): Nonenzymatic hydrolysis of adenosinetriphosphate (ATP) at high temperatures and high pressures. - *Biophys Chem* 54, 175-180
- Moelle C, Schmidt C, Guyot F, Wilke M (2022): Hydrolysis rate constants of ATP determined in situ at. - *Biophys Chem* 290
- Buisson DH, Sigel H (1974): Significance of binary and ternary copper(II) complexes for the promotion and protection of adenosine 5'-di- and triphosphate toward hydrolysis. – *Biochim Biophys Acta (BBA) - General Subjects* 343, 45-63
- Suzuki S, Higashiyama T, Nakahara A (1978): Nonenzymatic hydrolysis reactions of adenosine 5'-triphosphate and its related compounds—III: Catalytic aspects of some cobalt(III) complexes in ATP-hydrolysis. - *Bioinorg Chem* 8, 277-289

Determination of the electronic polarizabilities of bromine in bromates, perbromates, and bromides

S. Nezamabadi¹, P. Fuzon², F. Kraus², R.D. Shannon³, I. Spieß¹, R.X. Fischer¹

¹ FB 5 Geowissenschaften, Universität Bremen, Klagenfurter Straße, D-28359 Bremen, Germany

² FB Chemie, Philipps-Universität Marburg, Hans-Meerwein-Str. 4, D-35032 Marburg, Germany

³ Geological Sciences/ CIRES, University of Colorado, Boulder, Colorado 80309, USA

e-mail: rfischer@uni-bremen.de

Empirical electronic polarizabilities of Br^{5+} , Br^{7+} , and Br^- were determined to predict refractive indices of bromates, perbromates, and bromides, respectively, at $\lambda = 589.3$ nm. Polarizabilities of the bromine ions were derived from the total electronic polarizabilities of compounds containing Br calculated from the mean refractive indices using the Anderson-Eggleton relationship (Anderson, 1975; Eggleton, 1991; Shannon and Fischer, 2016). Refractive indices (RI) of bromates and bromides are taken from literature data and from measurements on potassium bromate (KBrO_3) and potassium bromide (KBr), respectively. Because of the lack of literature data on perbromates, we have done RI measurements on sodium perbromate monohydrate ($\text{NaBrO}_4 \cdot \text{H}_2\text{O}$).

Structure analyses were performed using single-crystal X-ray diffraction data of KBrO_3 , KBr , and $\text{NaBrO}_4 \cdot \text{H}_2\text{O}$. Refractive indices were determined using the immersion method with a micro-refractometer spindle stage at $\lambda = 589.3$ nm as described by Medenbach (1985), yielding $n_e = 1.538$ and $n_o = 1.677$ ($\langle n \rangle = 1.6307$) for optically uniaxial KBrO_3 (Figure 1), and $n_x = 1.470$, $n_y = 1.491$, $n_z = 1.492$ ($\langle n \rangle = 1.4843$) for an optically biaxial $\text{NaBrO}_4 \cdot \text{H}_2\text{O}$ crystal (Figure 2).



Figure 1: (a) KBrO_3 crystal mounted on the spindle stage of the polarization microscope. (b) orientation of the crystal to determine $n_e = 1.538$. (c) orientation of the crystal to determine $n_o = 1.677$. Due to the equality of the refractive indices of the sample and the immersion oil, the sample is not visible in (b) and (c).

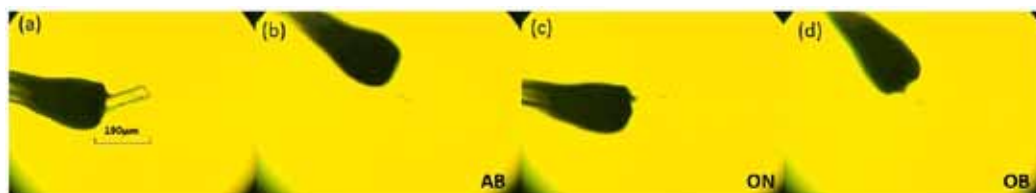


Figure 2: (a) $\text{NaBrO}_4 \cdot \text{H}_2\text{O}$ crystal mounted on the spindle stage of the polarization microscope. (b) orientation of the crystal to determine $n_x = 1.470$. (c) orientation of the crystal to determine $n_y = 1.677$. (d) orientation of the crystal to determine $n_z = 1.492$. Since the refractive index of the sample matches that of the oil, the sample is not visible in (b), (c), and (d).

Analyzing 18 compounds with established refractive indices containing Br^{5+} , along with data from this study, the polarizability of $^{[3]}\text{Br}^{5+}$ was determined by calculating the difference between the total polarizabilities of the respective compounds and the sum of polarizabilities of their ions omitting Br with values for the ions taken from Shannon and Fischer (2016). The individual electronic polarizability of $^{[3]}\text{Br}^{5+}$ was found to be $2.20 \pm 0.34 [\text{\AA}^3]$.

The determination of the refractive indices of $\text{NaBrO}_4 \cdot \text{H}_2\text{O}$ with four-coordinated Br^{7+} yielded an electronic polarizability value of $1.086 [\text{\AA}^3]$ for Br^{7+} . Using this value now enables the prediction of refractive indices of perbromates with polarizability values from Shannon & Fischer (2016) as listed in Table 1.

Table 1: Predicted mean refractive indices of compounds containing tetrahedrally coordinated Br^{7+} . Crystal data are from the ICSD database. V_m is the molar volume of the compound, α_{tot} is the total electronic polarizability of the compound and $\langle n \rangle$ is the mean refractive index.

| Compound | Space group | $V_m [\text{\AA}^3]$ | $\alpha_{\text{tot}} [\text{\AA}^3]$ | $\langle n \rangle (\pm 0.025)$ |
|---|-----------------|----------------------|--------------------------------------|---------------------------------|
| KBrO_4 | $P n m a$ | 98.98 | 8.949 | 1.541 |
| CsBrO_4 | $I 4_1/a m d$ | 122.5475 | 10.680 | 1.522 |
| $\text{NH}_4(\text{BrO}_4)$ | $P n m a$ | 107.73 | 9.785 | 1.544 |
| $\text{LiBrO}_4 \cdot \text{H}_2\text{O}$ | $C 1 2/c 1$ | 100.4775 | 9.349 | 1.557 |
| $\text{LiBrO}_4 \cdot 3\text{H}_2\text{O}$ | $P 6_3 m c$ | 147.565 | 12.630 | 1.513 |
| $\text{Ba}(\text{BrO}_4)_2 \cdot 3\text{H}_2\text{O}$ | $P 6_3/m$ | 237.185 | 22.955 | 1.580 |
| $\text{Ca}(\text{BrO}_4)_2 \cdot 4\text{H}_2\text{O}$ | $P \bar{1}$ | 266.25 | 23.190 | 1.522 |
| $\text{Co}(\text{BrO}_4)_2 \cdot 6\text{H}_2\text{O}$ | $P \bar{3} m 1$ | 305.34 | 26.543 | 1.521 |
| $\text{Ni}(\text{BrO}_4)_2 \cdot 6\text{H}_2\text{O}$ | $P \bar{3}$ | 291.18 | 26.467 | 1.544 |

For the anion Br^- the two parameters α^0 and N_0 were determined describing the anion polarizability α^- of Br^- according to $\alpha^- = \alpha^0 \cdot 10^{-N_0/V}$ with $V = V_{\text{an}}^{1.2}$ where V_{an} is the anion volume (see Shannon & Fischer, 2016).

- Anderson OL (1975): Optical properties of rock-forming minerals derived from atomic properties. - Fortschr Miner 52, 611–629
- Eggletton RA (1991): Gladstone-Dale constants for the major elements in silicates: Coordination number, polarizability, and the Lorentz-Lorentz relation. - Canad Miner 29, 525–532
- Medenbach O (1985): A new microrefractometer spindle-stage and its application. - Fortschr Miner 63, 111-133
- Shannon RD, Fischer RX (2016): Empirical electronic polarizabilities of ions for the prediction and interpretation of refractive indices: oxides and oxysalts. - Amer Mineral 101, 2288–2300

Micro-CT analyses from a prehistoric work and settlement site in Kundl, Tyrol

L. Oettel¹, P. Tropper¹, G. Degenhart²

¹University of Innsbruck, Institute of Mineralogy and Petrography

²Core facility μ CT at the Medical University Innsbruck

e-mail: lena.oettel@uibk.ac.at

Prehistoric mining and production sites for copper are known from the Eastern Alps, reaching back to the beginning of the Early Iron Age, but the further processing of the copper products (bronze foundries etc.) could so far only be localized indirectly.

A key site for the production step between mining and metal processing, which has hardly been investigated so far, is offered by the Late Bronze and Iron Age workshop area of Kundl in the Tyrolean Lower Inn Valley, which was used over a long period of time, from the late 11th century BC, with an interruption in the 8th/7th century, until the 1st century BC. In Kundl (district of Kufstein), the largest archaeological excavation in North Tyrol to date was carried out in 2018 and 2019, during which nearly 31,000 finds were recovered. The excavation area of around 11,000 m² in the area of the Wimpissinger gravel pit is located directly next to the Iron Age burial ground of the Fritzens-Sanzeno culture discovered in the 1970s.

During the more recent excavations, Late Bronze Age as well as Iron Age use horizons were discovered, which were separated from each other by meter-thick gravel layers, resulting in an excellent preservation of the finds and features (Staudt et al. 2021).



Figure 1. Oven battery with roasting bed (picture: Talpa GnbR, 2019)

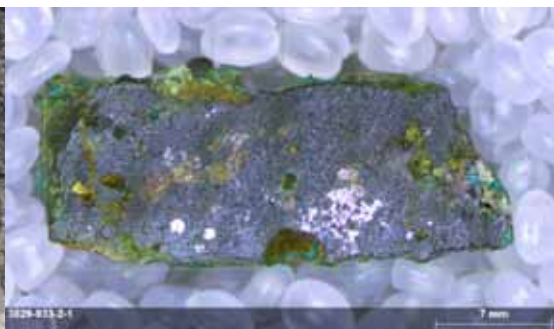


Figure 2. Heterogenous slag from early bronze age horizon (picture: L. Oettel, 2021)

Due to the temporal diversity of the slag finds (Bronze Age to Iron Age), the Kundl site is an ideal pilot project for slag investigations using microcomputed tomography, as this allows to visualize the improvement of the production process of copper to be traced as a function of time. Early as well as Middle and Late Bronze Age slag finds were excavated from various horizons. Furthermore, within the horizons there are samples of all slag categories (heterogeneous slag, plate slag, slag sand and furnace slag), which have preserved the different working steps.

Staudt M, Bader M, Eß LM, Lueger D, Oettel LS, Tropper P, Trebsche P (2021): Eine Werksiedlung aus der Bronze- und Eisenzeit bei Kundl (Nordtirol). - Vorbericht über die Ausgrabungen 2018–2019 in der Schottergrube Wimpissinger. In: Archaeol Austr 105, 249–282

NanoExtrem-NanoExtrem2: Nano-focus end-station for experiments at ID27 at ESRF

**L. Pennacchioni¹, M. Mezouar², C. L. Sahle², W. Morgenroth¹, S. Jahn³, M. Herrmann³,
M. Schulze³, A. Pakhomova², B. Wehinger², G. Garbarino², S. Bauchau², K. Martel², F. Gerbon²,
D. Andraut⁴, M. Wilke¹**

¹*University Potsdam, Potsdam, Germany*

²*European Synchrotron Facility, ESRF, Grenoble, France*

³*University of Cologne, Cologne, Germany*

⁴*Université Clermont Auvergne, Clermont-Ferrand, France*

e-mail: lea.pennacchioni@uni-potsdam.de

Research groups from the Universities of Potsdam and Cologne contributed to the construction and improvement of an end station for nano-focused X-ray diffraction (XRD), fluorescence (XRF), and imaging (XRI) at the ID27 high-pressure beamline at the ESRF, Grenoble, in a BMBF project 'Nanoextrem'. A second BMBF project, 'Nanoextrem2', was funded to expand the experimental possibilities with the addition of a high-resolution X-ray emission (XES) spectrometer and pulsed laser heating to the beamline.

An end station for in situ XRD, XRF, XRI and XES at extreme conditions will allow to investigate samples in the field of high-pressure materials and solid state physics in an unprecedented manner.

The end station allows for different focusing schemes by Kirkpatrick-Baez (KB) mirror systems (covering an energy range of 15 to 60 keV) arranged to serve either a nano focus setup, a laser-heating setup, a micro focus arrangement for spatial flexibility and heavy load setups. A Soler slit system was developed and implemented to reduce the Compton scattering of complex sample environments.

Highlights of the setup that have been already characterized : (i) the focusing of the nano-beam (available in the energy range between 15 and 25 keV) to 300×300 nm; (ii) the gain of a factor 70 in flux obtained using a submicron-focused pink beam compared to the monochromatized microbeam (FWHM for pink and monochromatic beam is $0.8 \mu\text{m} \times 0.8 \mu\text{m}$ at $0.3738 \text{ \AA} / 33.17 \text{ keV}$).

As an example, preliminary results on high-pressure XRD experiments on hydrous and anhydrous SiO₂ glasses up to 40 GPa will be presented, as well as performance parameters. In particular, pressure induced structural changes in the SiO₂-H₂O system will be discussed and the first results of a laser-heating experiment up to 4000 K to study the structures of the respective melts will be shown.

Coherent lamellar intergrowth from exsolution of alkali feldspar

E. Petrishcheva, D. Heuser, R. Abart

Department of Lithospheric Research, University of Vienna
e-mail: elena.petrishcheva@univie.ac.at

We investigate coherent lamellar intergrowth resulting from exsolution in alkali feldspar. This structure forms when an initially homogeneous alkali feldspar of intermediate composition enters the miscibility gap during cooling below about 550°C and separates into lamellae of more Na-rich and lamellae of more K-rich composition. As the lattice parameters of alkali feldspar are strongly compositional dependent, formation of these lamellae induces strains and stresses within the structure. In coherent intergrowth the elastic and chemical strains interact in such a way that coherent boundaries are maintained between the lamellae.

The presence of elastic deformation affects the system's free energy and consequently influences its equilibrium phase relations such as binodal points and the miscibility gap. In earlier papers, due to the problem of having fewer equations than unknown variables, certain simplifying assumptions were made regarding the strains. In particular, the strains lying in the plane parallel to the lamellar interfaces were assumed to be zero, which we deem unphysical. Instead, we take advantage of the principle that the system tends towards the state with the minimum energy among all possible equilibrium states.

To determine the elastic stresses and strains and their impact on the system's free energy, we calculate and minimize the overall elastic energy of the lamellar structure. The elastic energy acts against the separation of Na-rich and K-rich lamellae, leading to binodal points deviating from the expectations based solely on chemical equilibrium in an unstrained state. By accounting for the elastic energy, we obtain both the corrected binodal points and the miscibility gap as represented by the so-called *coherent solvus*, which now is not unique and depends on the composition of the homogeneous precursor feldspar.

The main mathematical challenge lies in the fact that calculation of the elastic energy requires knowledge of the binodal points, the latter in turn, are determined by the total free energy of the system. To overcome this challenge, we employ a method of successive approximations. Observed lamellar orientations agree well with our calculations. These results represent a significant improvement and generalization of earlier work by Robin (1974).

Robin PYF (1974): Stress and strain in cryptoperthite lamellae and coherent solvus of alkali feldspars. - Amer Mineral 59, 1299-1318

Micro-CT and micro-XRF investigations of an Early Bronze-Age smelting crucible fragment

M. Piccolruaz¹, P. Tropper¹, G. Degenhart²

¹University of Innsbruck, Institute of Mineralogy and Petrography, 6020 Innsbruck, Austria

²Medical University of Innsbruck, Institute of Radiology, 6020 Innsbruck, Austria

e-mail: peter.tropper@uibk.ac.at

In this investigation, a fragment of an early Bronze Age smelting crucible fragment with an adherent slag crust was examined. Together with ore fragments, raw copper and copper objects this fragment documents the evidence of small-scale smelting activity at the early Bronze Age site Buchberg near Wiesing in the Inn valley.

The sample was analyzed by electron microprobe analysis as well as micro-XRF. Mineralogically and chemically three different areas can be distinguished. The first area (Bereich A) away from the slag crust is unmelted and consists mainly of clay minerals and different temper components (orthogneiss, quartz, plagioclase, K-feldspar, muscovite). The second area (Bereich B) closer to the slag crust shows melting and thus consists mainly of a glass matrix with occasional inclusions of covellite (CuS). The third area (Bereich C) represents the slag crust and contains clinopyroxenes in a glass matrix, and also small amounts of acanthite (Ag₂S). Furthermore, abundant Cu-Sb-Fe-Zn-O phases (possibly the alteration phase theisite, Cu₅Zn₅(AsO₄,SbO₄)₂(OH)₁₄) and chalcosine (Cu₂S) occur. The glass in area C contains high concentrations of phosphorus, arsenic and antimony and the SiO₂ content decreases strongly in the glass from area B to area C.

The crucible fragment was scanned using a micro-CT, which resulted in a three-dimensional image illustrating the distribution of high-density phases in the crucible fragment and the slag crust. Quantitative evaluation of the CT results of the slag crust yielded in very little pore space of 3 vol.%, whereas the amount of the high-density phases (Cu-Sb-Fe-Zn-O phases) is 43 vol.% and thus is clearly concentrated in the slag crust.

Finally, the results show that the ores used for copper smelting in the Early Bronze Age were As-rich tetraedrites deriving most likely either from the Devonian Schwaz Dolomite or the carbonates of the Schwaz Triassic (the occurrence of acanthite points towards it). The high phosphorous contents in the slag can either be interpreted as resulting from firing plant materials (wood) or the possible addition of bone apatite to the smelting process.

Blue- and green-spotted "K2 gneiss" from the Goldberggruppe, Austria

J. Portenkirchner¹, E. Libowitzky²

¹Department of Lithospheric Research, University of Vienna

²Department of Mineralogy and Crystallography, University of Vienna

e-mail: eugen.libowitzky@univie.ac.at

"K2 gneiss" or "K2 granite" is a grey to white (meta)granite with cm-sized round blue (and sometimes green) spots stained by fine-grained azurite (and sometimes malachite). Due to its attractive appearance it has been carved to various stone artefacts and traded world-wide. Although this rock-type has been known exclusively from the slopes of the K2 in the Himalaya Mountains (hence the name), a second occurrence has been found in the Goldberggruppe in Austria some two years ago.

This special gneiss (Fig. 1) from the N wall of Hoher Sonnblick, Rauris Valley, Salzburg, has never been described in previous literature, although the mapping of the area has been done in great detail (Exner 1962, 1964). Extended field trips during the past years were not successful to confirm "K2 gneiss" in the neighboring areas SW - NW of Hoher Sonnblick peak. Only a special rock with similar appearance has been known from the "Weiße Wand" at Stanzwurten, Möll Valley, Carinthia, some 6 km SSW of Hoher Sonnblick. However, this rock shows a matrix of barite, calcite and quartz with blue and green spots of azurite and malachite.

Besides of normal petrographic investigations with the polarizing microscope (i.e. quartz, feldspar, muscovite, calcite), the blue and green spots were probed with micro-Raman spectroscopy. By comparison with reference spectra from the RRUFF data base (Downs 2006) azurite (Fig. 2) and malachite were unambiguously identified in all samples.

While the barite rocks from "Weiße Wand" contain also tiny chalcopyrite and tennantite grains as obvious primary source of copper, "K2 gneiss" from Hoher Sonnblick lacks any primary copper sulfides; only tiny striated cubes of pyrite have been observed (note the relics of tiny brown spots of limonite in the center of Fig.1).

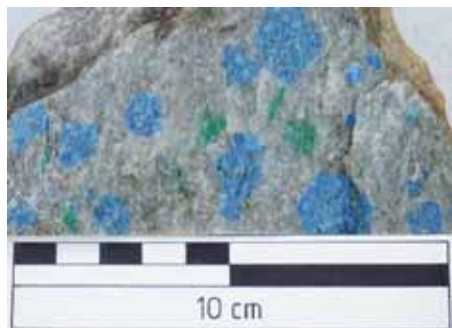


Figure 1. "K2 gneiss" from the Goldberggruppe with spots of azurite (blue) and malachite (green)

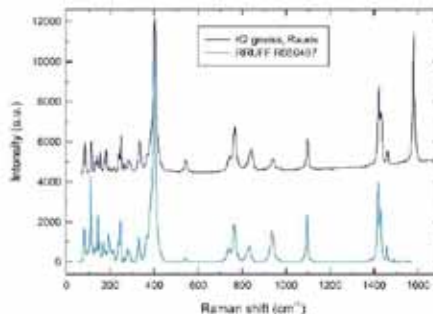


Figure 2. Micro-Raman spectra of azurite from "K2 gneiss" compared to an azurite reference from the RRUFF data base (Downs 2006).

Downs RT (2006): The RRUFF Project: an integrated study of the chemistry, crystallography, Raman and infrared spectroscopy of minerals. – Progr Abstr 19th General Meeting IMA, Kobe, Japan, O03-13

EXNER C (1962): Geologische Karte der Sonnblickgruppe, 1:50000. – Verlag der Geologischen Bundesanstalt, Wien

EXNER C (1964): Erläuterungen zur Geologischen Karte der Sonnblickgruppe, 1:50000. – Verlag der Geologischen Bundesanstalt, Wien

Expanding the magmatic and metamorphic geochronological record of the Isua supracrustal belt

A. Ramírez-Salazar^{1,2}, D. Sorger³, T. Müller³, S. Piazzolo¹

¹ School of Earth and Environment, University of Leeds, Leeds

² Instituto de Geología, Universidad Nacional Autónoma de México, Ciudad Universitaria 04510, Mexico City, Mexico

³ Geoscience Centre, University of Göttingen, Goldschmidtstraße 1, Göttingen, Germany
e-mail: r.s.anthonyy@gmail.com

The emplacement history of the protoliths of the Isua supracrustal belt (ISB), southwestern Greenland, goes back to the Eoarchean and is often interpreted to preserve one of the oldest metamorphic records on Earth. Thus, in many studies the metamorphic characteristics of this belt are used to advance our understanding of Archean tectonics. However, the age of its main tectonometamorphic event(s) remains debated with main arguments derived from cross-cutting relationships while direct dating of metamorphic minerals is sparse. Recent microstructural and quantitative P-T analyses (Ramírez-Salazar et al., 2021; Zuo et al., 2021) showed that the ISB experienced a syn-tectonic amphibolite facies event at 550–600 °C and 0.5–0.7 GPa (M₁), followed by a relatively static (lower) amphibolite facies episode at <540 °C and <0.5 GPa (M₂), both later overprinted by greenschist facies fluid-related metamorphism (M₃). In order to constrain the timing of different tectonometamorphic, as well as magmatic, events of the ISB, we combine microstructural and P-T analyses with several geochronometers (Sm-Nd and Lu-Hf in garnet, and U-Pb in rutile and titanite). Our results expand the history of the ISB and reveal new events occurring in its associated rock formation.

Local metamorphism at 650–675 °C and 0.4–0.6 GPa associated with the emplacement of a tonalite-trondhjemite-granodiorite (TTG) body occurring at ≈3,660 Ma is recorded in hornblende enclaves adjacent to the ISB. Additional information on the magmatic history is provided by an intrusive, garnet-bearing granitoid showing potentially igneous garnet crystallization at ≈3,550 Ma. Sm-Nd and Lu-Hf dates derived from metamorphic garnets within ISB supracrustal rocks show no evidence of a regional, major tectonometamorphic event (M₁) prior to ≈3,400 Ma. Instead, the analysis of syn-tectonic garnets suggests that M₁ most likely occurred at ≈2700 Ma. Moreover, new U-Pb data of post-tectonic titanite suggest that static post-tectonic metamorphism (M₂) occurred during the Neoarchean (≈2,700–2,600 Ma), whereas late retrogression event(s) are most likely Paleoproterozoic (<2,200 Ma) in age.

Our findings highlight that the observed main regional ISB metamorphism and concomitant deformation did not occur in the Eoarchean. While results of this study cannot fully discriminate between different geodynamic interpretations, our results suggest that the main tectonometamorphic event forming the current structures of the ISB are not related to pre 3,400 Ma Early Earth, but rather to late Archean geodynamics.

Ramírez-Salazar A, Müller T, Piazzolo S, Webb AAG, Hauzenberger C, Zuo J, Haproff P, Harvey J, Wong TK, Charlton C (2021): Tectonics of the Isua Supracrustal Belt 1: P-T-X-d constraints of a poly-metamorphic terrane. - *Tectonics* 40, doi:10.1029/2020TC006516

Zuo J, Webb AAG, Piazzolo S, Wang Q, Müller T, Ramírez-Salazar A, Haproff PJ (2021): Tectonics of the Isua Supracrustal Belt 2: Microstructures reveal distributed strain in the absence of major fault structures: *Tectonics* 40, doi:10.1029/2020TC006514

Diabases are petrologists best friends: quantitative *P-T* constraints on the Eoalpine metamorphic gradient in the Ötztal Complex using diabase dikes

G. Raso¹, P. Tropper¹, D. Rammlmair²

¹University of Innsbruck, Institute of Mineralogy and Petrography, A-6020 Innsbruck, Austria

²Institute of Mineralogy, Leibniz University, Hannover, Germany

e-mail: peter.tropper@uibk.ac.at

The Ötztal Complex (ÖC) is a large crystalline complex in the western part of the Austroalpine units. The ÖC consists of quartzofelspathic and metapelitic metasediments with various intercalations of orthogneisses, amphibolites and rare metacarbonates. The oldest metamorphic event is Ordovician in age (460 – 490 Ma), leading to the formation of orthogneisses and scattered occurrences of migmatites. The Variscan metamorphic overprint ranges from 390 – 295 Ma and the first stage of the Variscan event was a high-pressure metamorphism around 373 – 359 Ma, leading to the formation of eclogites in the central part of the ÖC. The conditions of the eclogite-facies metamorphism were estimated to be 650 – 750 °C and 20 – 28 kbar. The dominant Variscan amphibolite-facies metamorphism occurred around 330 – 350 Ma with estimated *P-T* conditions of 570 – 640 °C and 5.8 – 7.5 kbar for the northwestern part of the ÖC. Subsequently after Variscan amphibolite-facies metamorphism diabase dikes intruded into the polymetamorphic basement. The youngest metamorphic event in this Austroalpine basement occurred during the Cretaceous Eo-Alpine orogeny (100 – 73 Ma). The intensity of the Eo-Alpine overprint varies within the ÖC and increases from NW (lower greenschist-facies) to SE (epidote-amphibolite facies) and reaches 550 - 600°C and ≥11 kbar in the Schneeberg Complex. Unfortunately, so far, no quantitative data concerning the *P-T* conditions of the Eoalpine metamorphic overprint in the NW of the ÖC exist. This is where the post-Variscan diabase dikes come in.

The importance of these diabase dikes lies in the fact that field- and textural investigations revealed a post-Variscan emplacement since these dikes only show Eoalpine metamorphism and deformation. The mineral assemblage of these dikes is amphibole + plagioclase + epidote + biotite + muscovite + titanite + quartz +/- garnet. Changes in plagioclase and amphibole chemistry are concordant with a prograde metamorphic evolution. Plagioclase changes from almost pure albite ($X_{An} < 0.1$) to intermediate plagioclase with $X_{An} = 0.3-0.4$. Amphiboles show a strong increase in Al^6 and Al^4 as well as Na^B and Na^A from NW to SE. This is qualitatively indicative of increasing *P-T* conditions. The *P-T* calculations were done using the programs Thermocalc v.3.21 and v.3.33 and mode-2 calculations (only using linearly independent reactions and statistical evaluation). The increase in *T* is from 400°C in the NW to almost 600 °C in the SE at the Timmelsjoch. Similarly *P* increases from 6-7 kbar in the NW to almost 12 kbar in the SE using Thermocalc v.3.33. Calculations using Thermocalc v.3.21 yielded slightly different *P-T* conditions from 300 °C and 3 kbar in the NW to 600 °C and 9 kbar in the SW. These differences are due to the use of different activity models for amphibole solid solutions, which has a profound impact on the calculations. Nonetheless these data represent the first quantitative *P-T* estimates for the Eoalpine metamorphic gradient north above the chloritoid isograd.

Metamorphism induced strength inversion at high-pressure conditions

A. Rogowitz^{1,2}, S. Schorn¹, B. Huef³, L. Menegon⁴, B. Grasemann²

¹*Institute of Earth Sciences, University of Graz, Austria*

²*Department of Geology, University of Vienna, Austria*

³*GeoSphere Austria, Vienna, Austria*

⁴*Njord Centre, University of Oslo, Norway*

e-mail: anna.rogowitz@uni-graz.at

We present structural, microstructural and petrographical data from an eclogite-facies shear zone of the Hohl locality (Koralpe, Eastern Alps, Austria). The shear zone spans over about 6 meter in thickness and shows a pronounced foliation (average: 047/63) characterized by alternating layers of proto- to ultramylonitic eclogite with different mineralogical content. Two stretching lineations have been identified: (1) a penetrative NW-SE striking mineral lineation (average: 122/27) defined by the shape and orientation of prismatic minerals and (2) a N-S striking stretching lineation (average: 354/20) which occurrence is limited to ultramylonitic layers. The latter appears to cross-cut the NW-SE striking lineation and is therefore considered as younger. The shear zone bears rocks with two distinct eclogite facies mineral assemblages of which one is dominated by clinozoisite, amphibole and garnet. This lithology occurs as foliated sigmoidal lenses hosted by typical eclogite containing omphacite, garnet, clinozoisite, amphibole, quartz, kyanite and rutile.

Both lithologies derived from NMORB gabbro which intruded during Permian rifting. Whole rock geochemical data shows that the lenses are enriched in Al and depleted in Mg and Fe when compared to the eclogite matrix. Protolith assemblage calculations suggest that lenses have originally been plagioclase-rich cumulates within a clinopyroxene-plagioclase gabbro matrix. Considering experimentally derived flow-laws on clinopyroxene-plagioclase aggregates (Dimanov & Dresen, 2005) indicates that lenses were less competent than the gabbro. However, the sigmoidal shape of lenses surrounded by ultramylonitic eclogite suggests that the lenses were stronger during shear zone development.

Microstructural investigations reveal an ultramylonitic fabric dominated by fine-grained (~50 µm) euhedral clinopyroxene within the host eclogite. Triple- and quadro-junctions, open grain boundaries and a lack of intracrystalline strain suggest that eclogite dominantly deformed by fluid supported grain boundary sliding. On the other hand, the microstructure of lenses is dominated by coarse-grained elongated clinozoisite (~300 µm) and amphibole aggregates (~2 mm). Amphibole aggregates are sigmoidal and characterized by a coarse-grained highly strained clast and strain free slightly elongated crystals in strain shadows. These observations indicate that lenses deformed by combined dislocation and dissolution-reprecipitation creep.

Our data shows how mineral replacement resulted in a strength inversion whereas the lenses, initially weaker than their host, are stronger than the surrounding eclogite after metamorphism at eclogite-facies conditions (720 ± 20 °C, 21 ± 3 kbar). The switch in strength caused stress concentration at the lithological contacts and subsequent strain localization in the weaker eclogitic mineral assemblage. Activation of fluid assisted grain boundary sliding in eclogite ultramylonites is assumed to have further weakened the eclogite, causing drastic strain partitioning. Later N-S-directed deformation subsequently solely localized within the weaker ultramylonitic eclogite.

Hydrothermal pyritization of nano-magnetite and the record of biominerals in ancient sulfide systems

E.A. Runge^{1,2}, T.H. Chiu³, M. Mansor³, A. Kappler^{3,4}, J.-P. Duda^{1,2}

¹*Geobiology, Geoscience Center, University of Goettingen, Germany,*

²*Sedimentology & Organic Geochemistry, University of Tuebingen, Germany*

³*Geomicrobiology, University of Tuebingen, Germany*

⁴*Cluster of Excellence EXC 2124, Controlling Microbes to Fight Infection, University of Tuebingen, Germany*
e-mail: eric.runge@uni-tuebingen.de

The microbial formation of magnetite nanoparticles in hydrothermal environments can be driven by enzymatically controlled reactions or occur as a by-product of microbial Fe cycling. The resulting biogenic magnetite has characteristic traits that distinguish it from its abiotic counterpart, which makes it a potential biosignature. Furthermore, the precipitates may preserve chemical and isotopic information that provide valuable insights into conditions during their formation; hence, they might be used as environmental proxies. However, sulfidic diagenesis driven by hydrothermal fluids and microbial S cycling may cause the rapid transformation of microbial magnetite to Fe sulfide minerals, potentially altering or erasing biosignatures and proxies encoded in the primary precipitates. Thus, understanding the mechanisms, and characterizing the products of such sulfidation reactions is crucial for reading the record of biominerals in ancient hydrothermal sulfide deposits. Here, we present sulfidation experiments with synthetic and biogenic magnetite at physical and chemical conditions relevant to microbial niches in hydrothermal environments (<121 °C, excess S/Fe). By integrating multiple analytical techniques (e.g., scanning electron microscopy, sequential Fe extraction, Raman spectroscopy), we demonstrate a potential taphonomic bias against biogenic magnetite in hydrothermal environments and a strong influence of diagenetic fluid-mineral interactions on magnetite preservation. We further suggest that a portion of Fe sulfide minerals in hydrothermal deposits may be secondary products of magnetite sulfidation, highlighting the importance of understanding their diagenetic history for (bio)geochemical analyses. Our approach will aid the identification of biominerals and their transformation products in ancient rocks and pave the way for a more robust reconstruction of microbial evolution and environmental change through geological time.

Partial melting of hornblende–epidote eclogite at the pressure maximum (eclogite type-locality, Eastern Alps, Austria)

S. Schorn¹, A. Rogowitz^{1,2}, C. Hauzenberger¹

¹*Institute of Earth Sciences, NAWI Graz Geocenter, University of Graz, Universitätsplatz 2, 8010 Graz, Austria*

²*Department of Geology, University of Vienna, Josef Hlaubek-Platz 2, 1090 Vienna, Austria
e-mail: simon.schorn@uni-graz.at*

Pristine hornblende–epidote eclogite from within the eclogite type-locality (Hohl, Koralpe) of the Eastern Alps in Austria preserves cm-thick, concordant leucocratic segregations of coarse-grained euhedral hornblende–epidote–quartz and fine-grained disseminated garnet–omphacite–rutile. Petrographic- and mineral chemical data and phase diagram modelling are interpreted in terms of limited melting at or close to the well-established pressure maximum (21 ± 3 kbar and $680\text{--}740$ °C) followed by melt crystallization near these conditions. Plagioclase \pm amphibole/ clinopyroxene films formed at sub-eclogite facies conditions from final melt vestiges. Natural variability in rock composition and bulk oxidation state leads to variable mineral modes and calculated high-pressure solidus temperatures for compositional endmembers sampled at Hohl. Oxidized conditions ($X\text{Fe}^{3+} \sim 0.5$) favour hydrous but refractory amphibole–epidote-rich assemblages with a fluid-present solidus temperature of ~ 740 °C at 20 kbar, whereas more reduced rocks ($X\text{Fe}^{3+} \sim 0.2$) are fertile ‘true’ eclogites (>70 vol. % garnet + omphacite) that commence melting at ~ 720 °C. The interlayering of such eclogites constitutes a fluid source–sink couple at appropriate (pressure–)temperature conditions, favouring fluid transfer from neighbouring dehydrating layers to melt-bearing ones down gradients in chemical potential of H_2O ($\mu\text{H}_2\text{O}$). Moderate degrees of fluid-fluxed melting (<10 %) would not alter the peak assemblage provided the resulting melts are removed from the source rock. We suggest that eclogites with a comparable composition and metamorphic history are however unlikely to produce voluminous melts, thus not significantly contributing to adakite magmatism and crustal differentiation in collisional settings.

Chemical composition and crystal structure of oxy-dravite from the Beluga occurrence, Nunavut Territory, Canada

L. Skrápková¹, J. Cempírek¹

¹*Departement of Geological Sciences, Faculty of Science, Masaryk University, Kotlářská 2, 602 00 Brno
e-mail: lenka.skrapkova@gmail.com*

A new occurrence of oxy-dravite was found in a composition near its ideal end-member at the Beluga occurrence, Nunavut territory, Canada. Oxy-dravite belongs to the sodic group of the tourmaline supergroup with dominant ^WO, and commonly forms a solid solution with foitite, schorl, and oxy-schorl. Since its original description (Bosi & Skogby 2013) from the quartz-muscovite schist from Osarara (Narok district, Kenya), the mineral has been found at several localities worldwide, typically in metamorphic environments, and typically in solid solution with other species (Čopjaková et al. 2012; Cempírek et al. 2013; Pieczka et al. 2018).

The contribution provides new information about the occurrence, chemical composition, physical and structural properties of the oxy-dravite with a near-endmember composition from the Beluga occurrence. These data improve characterization of physical properties of oxy-dravite, allow examination of oxy-dravite solid solutions with respect to other species, improve the interpretation of Al–Mg disorder among the Y- and Z-sites, and discuss its petrogenetic importance.

The Beluga property is located in the southern part of Baffin Island, Nunavut territory, Canada. The locality is known largely due to the occurrence of sapphire-bearing calc-silicate pods. These pods are hosted in a shelf sequence of clastic rocks and carbonates along with garnet-bearing metasediments of the Lake Harbour Group, Trans-Hudson orogeny (St-Onge et al. 2007).

The tourmaline sample has a relatively homogenous composition, with only minor change from the crystal core to its rims. The X-site is predominantly occupied by Na (up to 0.91 apfu), its Ca content is low (max. 0.12 apfu) and vacancies are minimal. The octahedral Y-site is dominated by Al and Mg (2.77–2.81 apfu), Fe content is low (max. 0.18 apfu); Li content measured using LA-ICP-MS is negligible. The octahedral Z-site is similarly to Y-site also occupied by Al with minor Mg. The T-site is dominated by Si (up to 5.95 apfu), substituted by inconsiderable amount of Al. The V- and W-sites are characterised by high OH (2.92–3.00 apfu) and O contents (0.80–0.95 apfu), with minor F (0.12–0.17 apfu) only.

The crystal structure of the oxy-dravite sample was refined from single-crystal X-ray diffraction data. The refinements were performed using the SHELXTL crystallographic software package (Sheldrick 2008, 2015) of Bruker AXS. Scattering factors for neutral atoms were employed for the cations and ionic factors for O²⁻ were used for oxygen (Hovestreydt 1983). The structure of dravite after Foit and Rosenberg (1979) was introduced as an initial model for refinement that was processed (by refining occupancy of Na at X-site, and Mg Fe vs. Al at the Y and Z sites) to a final R index of ~ 1.45 % for an anisotropic displacement model. The H3-atom site was located in residual electron density maps whereas the H1 site was impossible to locate. The H3-site isotropic displacement parameter was constrained to be equal to 1.2 times of that of the O3-site. The distance of the H3 from the donor oxygen atom was not constrained, and the structure refinement provided O3–H3 = 0.949 Å. The mean bond-lengths of the individual sites are: <X–O> ~ 2.673 Å, <Y–O> ~ 1.999 Å, <Z–O> ~ 1.928 Å, <T–O> ~ 1.621 Å, and <B–O> ~ 1.375 Å.

The Beluga oxy-dravite has trigonal symmetry, space group $R3m$ with $a = 15.9121(2)$ Å, $c = 7.1788(10)$ Å, $V = 1574.12(5)$ Å³ and $Z = 3$. The crystal structure was refined to $R1 = 1.45$ using 1613 unique reflections. The oxy-dravite is optically uniaxial negative, with $\omega = 1.6453(5)$ and $\varepsilon = 1.6074(18)$ and strongly pleochroic – light yellowish-brown colour in the omega direction and colourless in the epsilon direction; its calculated density is 3.069 g.cm^{-3} with a compatibility index 0.016 (superior category).

The Beluga oxy-dravite, ideally $\text{Na}(\text{Al}_2\text{Mg})(\text{Al}_5\text{Mg})(\text{Si}_6\text{O}_{18})(\text{BO}_3)_3(\text{OH})_3(\text{O})$, has similarly to the holotype (Bosi & Skogby 2013) disorder between Y- and Z-site. However, the final form of Mg-disorder between the octahedral sites heads towards $(\text{Mg}_2\text{Al})(\text{Al}_6)$ rather than $(\text{Al}_2\text{Mg})(\text{Al}_5\text{Mg})$. This is the evidence that the oxy-dravite structure has more stable configurations and it is not necessary to divide Mg in ratio of 1:1 between the octahedral sites.

In comparison with other Mg-dominant end-members (oxy-dravite, dravite, fluor-dravite, uvite a Mg-foitite a Mg-lucchesiite), the Beluga oxy-dravite has lower density and comparable to lower values of refractive indexes ω and ε . Similarly, the Beluga oxy-dravite has lower unit cell volume and calculated density, the only exception is magnesiofoitite with the lowest values.

The main petrogenetic environments of oxy-dravites are aluminous metapelites and metapsammites, low-Ca ultramafics and (Cr,V)-rich metasediments (Pieczka et al. 2018). The oxy-dravite holotype was described by Bosi & Skogby (2013) from a quartz-muscovite schist in the Osarara locality. Čopjaková et al. (2012) found oxy-dravite in tourmalinites associated with mica-schist of the Krkonoše-Jizera Crystalline Massif, whereas Pieczka et al. (2018) reported a further occurrence of oxy-dravite from a quartz vein cutting granitic gneisses of the Kowary Unit. Oxy-dravite was also described by Ertl et al. (2003) from a primitive pegmatite vein cutting a gneiss of the Gföhl Unit. Oxy-dravite was also formed in amphibolite (Şek et al. 2022) or in the metaevaporite layers within dolomitic marbles (Krmíček et al. 2021). The Beluga oxy-dravite occurs in calc-silicate pods in association with dolomitic marbles (Belley et al. 2017); the necessary conditions for its crystallization (besides high B_2O_3 content) are increased content of Al and Na, and low content of F in the Mg-rich system.

- Belley PM, Dzikowski TJ, Fagan A, Cempírek J, Groat LA, Mortensen JK, Fayek M, Giuliani G, Fallick AE, Gertzbein P (2017): Origin of scapolite-hosted sapphire (corundum) near Kimmirut, Baffin Island, Nunavut, Canada. - *Can Mineral* 55, 669
- Bosi F, Skogby H (2013): Oxy-dravite, $\text{Na}(\text{Al}_2\text{Mg})(\text{Al}_5\text{Mg})(\text{Si}_6\text{O}_{18})(\text{BO}_3)_3(\text{OH})_3\text{O}$, a new mineral species of the tourmaline supergroup. - *Am Min* 98, 1442-1448
- Cempírek J, Houzar S, Novák M, Groat LA, Selway JB, Šrein V (2013): Crystal structure and compositional evolution of vanadium-rich oxy dravite from graphite quartzite at Bítoványky, Czech Republic. - *J Geosci* 58, 149-162
- Čopjaková R, Škoda R, Vašinová-Galiová M (2012): „Oxy-dravit“ z turmalinitů krkonoško-jizerského krystalinika. - *Bulletin Min-Pet Odd NM Praha* 20, 37
- Ertl A, Hughes JM, Brandstätter F, Dyar MD, Prasad PSR (2003): Disordered Mg-bearing olenite from a granitic pegmatite at Goslar, Austria: A chemical, structural, and infrared spectroscopic study. - *Can Mineral* 41, 1363-1370
- Foit FF, Rosenberg PE (1979): The structure of vanadium-bearing tourmaline and its implications regarding tourmaline solid solutions. - *Am Min* 64, 788-798
- Hovestreydt E (1983). On the atomic scattering factor for O^{2-} . - *Acta Crystallogr* A39, 268-269
- Krmíček L, Novák M, Trumbull RB, Cempírek J, Houzar S (2021): Boron isotopic variations in tourmaline from metacarbonates and associated calc-silicate rocks from the Bohemian Massif: Constraints on boron recycling in the Variscan orogen. - *Geosci Front* 12, 219-230
- Pieczka A, Ertl A, Sek MP, Twardak D, Zelek S, Szeleg E, Giester G (2018): Oxy-dravite from Wolowa Góra Mountain, Karkonosze massif, SW Poland: Crystallochemical and structural studies. - *Mineral Mag* 82, 913-928

Monazite fission-track dating of a heavy mineral sand, NE Sri Lanka

E. Skrzypek¹, S. Jones², B. Kohn², L. Chung², A. Gleadow²

¹*Institute of Earth Sciences, University of Graz*

²*School of Geography, Earth and Atmospheric Sciences, The University of Melbourne*

e-mail: etienne.skrzypek@uni-graz.at

Monazite fission-track (MFT) analysis appears to have potential for ultra-low temperature thermochronology. Recent experiments suggest that the nominal MFT closure temperature is ~25-45 °C (Jones et al., 2021). However, monazite commonly shows a wide range of compositions, so that it is crucial to assess the influence of compositional variations on fission-track systematics. For that, a MFT study of monazite grains from a heavy mineral beach sand (Polmuddai, NE Sri Lanka) was undertaken.

Electron microprobe analyses of 84 grains show significant variations in SiO₂ (0.12 - 2.63 wt.%), CaO (0.13 - 2.03 wt.%), ThO₂ (1.30 - 13.38 wt.%), UO₂ (0.07 - 1.28 wt.%) or Ce₂O₃ (23.94 - 34.31.03 wt.%). The analyses show that actinides were incorporated in monazite through the cheralite and/or huttonite substitutions. Eighty grains statistically define a main age population with a weighted mean Th-U-total Pb age of 502 ± 5 Ma (MSWD=1.3), while four other grains show older dates (ca. 1600 - 1900 Ma).

Spontaneous fission tracks were revealed by etching polished monazite mounts in a H₂O:HCl (1:1 by volume) solution at 90 °C. Due to the variability of monazite compositions, step-etching at five-minute intervals was performed to avoid under-/over-etching and limit surface damage. The majority of grains were well-etched after 10 - 15 minutes, whereas a few required up to 60 minutes. Fission tracks were manually counted using both reflected- and transmitted-light images.

The different monazite grains or domains yield individual MFT dates ranging from 3.90 to 0.25 Ma. It is recommended to use electron microprobe analyses to approximate the density of monazite domains, as it can noticeably influence the MFT age calculation. Only Si appears to show a fair correlation with MFT date, suggesting that higher Si content (SiO₂ = 1.5-2.0 wt.%) slows down FT annealing. This finding is supported by a tendency for Si-rich monazite grains to show longer confined track lengths (> 9 µm) than Si-poor ones (< 9 µm). A remaining question for further investigation is whether FT formation and annealing could also have an impact on U-Th dating of monazite, especially on radiogenic Pb loss.

Jones S, Gleadow A Kohn B (2021): Thermal annealing of implanted ²⁵²Cf fission tracks in monazite: *Geochronology* 3, 89–102

Formation of reaction textures in aluminous paragneisses during near-isothermal exhumation

D. Sorger^{1,2}, C.A. Hauzenberger², F. Finger³, M. Linner⁴, E. Skrzypek², S. Schorn²

¹*Geoscience Center, Georg-August-University Göttingen, Goldschmidtstraße 1, Göttingen 37077, Germany*

²*NAWI Graz Geocenter, University of Graz, Universitätsplatz 2, Graz 8010, Austria*

³*Department of Geography and Geology, University of Salzburg, Hellbrunnerstraße 34, Salzburg 5020, Austria*

⁴*Department of Hard Rock Geology, Geological Survey of Austria, Neulinggasse 38, Vienna, 1030, Austria*
e-mail: dominik.sorger@uni-goettingen.de

Two different types of aluminous paragneiss found in the Loosdorf complex in NE Austria, were studied to investigate the post-peak history of the Gföhl unit in the southern Bohemian Massif. Both paragneiss types contain coarse-grained granulite assemblages and retrograde reaction textures. The peak metamorphic conditions, estimated using phase equilibrium modelling, indicate that the Loosdorf complex experienced metamorphism at 0.9–1.1 GPa and 780–820 °C. The dominant mineral assemblage during this peak metamorphism includes garnet-biotite-sillimanite-plagioclase-K-feldspar-quartz-granitic melt \pm kyanite \pm ilmenite \pm rutile.

The first type of paragneiss, called Ysper paragneiss, exhibits cordierite moats around garnet and cordierite-spinel or cordierite-quartz symplectites at former garnet-sillimanite interfaces. These textures suggest a post-peak near-isothermal decompression path reaching around 0.4 GPa. The second type, Pielach paragneiss, shows only intermittent cordierite coronae around garnet porphyroblasts and lacks symplectites. The presence of cordierite suggests near-isothermal decompression to 0.4–0.5 GPa and 750–800 °C. This relatively high-temperature decompression path is attributed to the simultaneous exhumation of a large high-pressure-ultrahigh-temperature (HP-UHT) granulite body.

The timing of regional metamorphism in the granulites and the southern Bohemian Massif is well constrained and peaked around 340 Ma. Monazite from the Loosdorf paragneiss samples yield a slightly younger age of approximately 335 Ma. Although these ages overlap within the error, they are interpreted as reflecting near-isothermal decompression and exhumation, which led to the formation of the observed reaction textures.

Tl-retention by jarosite-group minerals in technosoils from the central part of the Allchar deposit, North Macedonia

**F. Stadler¹, T. Đorđević^{2,1}, A. Vaněk³, M. Mihaljevič⁴, T. Serafimovski⁵, G. Tasev⁵,
I. Boev⁵, B. Boev⁵**

¹*Institut für Mineralogie und Kristallographie, Universität Wien, Josef-Holaubek-Platz 2, 1090 Wien, Austria*

²*University Service Centre for TEM, Technische Universität Wien,*

Wiedner Hauptstraße 8-10, 1040 Vienna, Austria

³*Department of Soil Science and Soil Protection, Faculty of Agrobiological Sciences, Czech University of Life Sciences Prague, Kamýcká 129, 165 00, Prague 6, Czech Republic*

⁴*Institute of Geochemistry, Mineralogy and Mineral Resources, Faculty of Science, Charles University, Albertov 6, 128 43, Prague 2, Czech Republic*

⁵*Faculty of Natural Sciences, University "Goce Delčev"-Štip, Goce Delčev 89, 2000 Štip, North Macedonia
e-mail: stadlerfiona63@gmail.com*

Areas naturally enriched in thallium (Tl) represent a severe threat to surrounding ecosystems as the bioavailability of this highly toxic heavy metal strongly depends on its retention by the weathering-induced formation of secondary Tl-minerals. Estimations on the remediation potential of such areas therefore require a detailed mineralogical characterization of included Tl-bearing secondary minerals. This study focusses on the Allchar Sb-As-Tl-Au deposit in the southern part of North Macedonia, as its mineralogical composition is a rarity in the world. It contains remarkable concentrations of Tl, estimated to be around 1,000 tons of metal. In this study, stockpile material from abandoned, surface-exposed mining wastes and surrounding soils of the Sb-rich central part of the Allchar deposit was examined for the presence of secondary Tl-minerals. A combination of optical microscopy, powder X-ray diffraction (PXRD) and scanning electron microscopy with energy dispersive spectroscopy (SEM-EDS) was performed to determine the speciation of Tl in heavily weathered technosoils. The chemical composition of the soils measured by inductively coupled plasma mass spectrometry (ICP-MS) showed Tl-concentrations in the range of 480 to 4600 ppm. The main constituents of the examined samples could be identified as quartz, gypsum, sheet silicates, iron oxides and iron oxyhydroxides, followed by the presence of heavily weathered pyrite, marcasite and realgar, as well as traces of arsenopyrite and stibnite. Further weathering products comprise arsenates such as scorodite, alumopharmacosiderite, arseniosiderite, Ca-antimonates of the roméite-group, tripuhyite and sulfates of the jarosite group. Minor contents of Ce-monazite, apatite, zircon, rutile, baryte, sphalerite and native gold could also be encountered. This paragenesis is suggesting acidic weathering conditions with pH-values ranging from 2-3. During weathering, dissolved Tl was mainly incorporated in an incomplete solid-solution between jarosite and dorallcharite with Tl concentrations up to 2.2 at%, which consequently represent the main host minerals of Tl. However, Tl could also be encountered in iron oxyhydroxides (up to 0.5 at%) and sheet silicates (up to 0.2 at%). Based on our results, Tl-jarosites are important secondary host phases for Tl in the central part of Allchar. Yet, the instability of jarosite at near-neutral pH conditions also characterizes it as a possible source of soluble Tl. Consequently, it is essential to further examine the role of jarosite-group minerals in Tl-retention under various environmental conditions.

This work was supported by the Austrian Science Fund (FWF) [grant number P 36828-N to T. Đorđević].

The "Schaudepot" for minerals and rocks of the Krahuletz-Gesellschaft in Eggenburg, Lower Austria

F. F. Steininger¹, A. Rauscher²

¹*Neue Gasse 7, 3730 Eggenburg, Austria*

²*Hofwiesenstrasse 46, 3511 Furth-Aigen, Austria*

e-mail: Fritz.Steininger@senckenberg.de

The Krahuletz-Gesellschaft in Eggenburg, Lower Austria, operates a local but internationally much noticed museum. The three-story main building in the city centre hosts the permanent exhibition accompanied by special presentations mostly with a regional focus which change regularly. The entire area in the north-western part of Lower Austria is noticeable rich in prehistoric and early history besides folklore. But not only remains from the early settlers can be found here. The region belongs to the Bohemian Massif with its very complex geological setting. The exhibits in the museum belonging to Earth's history range from mineralogy to geology and palaeontology. The collection is that large and the number of display items is still growing. Hence two further buildings were provided by the city of Eggenburg. They serve as depots for the extensive scientific collections:

Depot 1 is a former cinema (named "Lichtspielhaus") hosting the extensive paleontological collections. They focus on the many regional geological units (e.g., from the Carboniferous of Zöbing and the Lower Miocene of Eggenburg). Also prehistoric and early historical objects that cannot be shown in the main building are stored here. Worthy to note is the large library compiling Earth science topics besides descriptions of the flora and fauna of the area. It hosts a large collection of offprints, scientific journals, and geological maps. This depot is named in honour of the long-serving governor of Lower Austria "Dr. Erwin Pröll Study Collection".

Depot 2 is a two-storey building used earlier as the production site by a furniture factory, it is known as the "MöFa". It is, besides other objects, dedicated to Geosciences. It combines an exhibition of minerals, rocks, and some fossils from the area in showcases besides the storage of samples for scientific investigations in the future. As the area is heavily forested, outcrops are short-lived. Minerals and rocks originating from sites that will not be accessible without great effort in future (e.g., road constructions, building pits, progress in quarry mining) are preserved. These samples are maintained in the depot's racks. From these two purposes result the name "Schaudepot" that means "look and store".

On the ground floor of the building there is the new two-track exhibition and storage area for minerals and rocks. It includes five rooms with a total area of 183 m². In the entire collection are only mineral specimens and rock samples from the Austrian part of the Bohemian Massif - Waldviertel, the Dunkelsteiner Wald (located south of the Danube between Melk and Krems), and the Mühlviertel (located to the west and belongs already to Upper Austria). The samples were donated by finds and private donations from collectors of this area. So far, there are in total about 7,700 mineral specimens and about 1,500 rock samples stored. The exhibition area comprise five rooms that are briefly characterized here.

Showroom 1 (23 m², 5 showcases) exhibits minerals and rock from some quarries: Among them is Amstall (about 20 km west of Krems), a graphit deposit well known for reddish corundum or xenotime. It is the type locality for Amstallite (a rare Ca-Al-silicate). The Eibenstein quarry (close to the border to the Slovakia) is located in the "Bunte Serie"

(metamorphic rocks including biotite- and hornblende gneisses, amphibolites, calcsilicate rocks, marbles) and exhibits rarely pegmatite veins. The Loya quarry (a few steps north from the Danube and close to Ybbs-Persenbeug) is well known for wollastonite and thulite (a pink variety of zoisite). Pegmatite veins are located in the entire Waldviertel including the Southern Dunkelsteiner Wald and in the Western Mühlviertel. Famous mineral samples found in these pegmatites are smoky quartz (var. morion from Brunn near Fratres), opal (from Waldkirchen), or quartz (cutted samples from Langau).

Also some fossils from the Eggenburg area (Loibersdorf, Eggenburgian, Lower Miocene) are shown here; remarkable is a giant “Herzmuschel“ (Larvicardium kübecki).

Showroom 2 (10 m²) is dedicated to the large variety of rocks occurring in the Waldviertel. The rocks are stored on shelves and might be touched. Slices of Chalcedony and Garnet Pyroxenites are illuminated from the reverse; also these samples are from the Waldviertel.

The Collection & showroom 3 (Fig. 1) is the largest room and captures nearly half of the entire area (80 m², 16 cabinets). To enable an easy access, samples are stored according to location in an alphabetical order (from Aggsbach-village to Zissersdorf). In one cabinet samples from the southern Lower Austria and the Mühlviertel are stored. Others contain a systematic collection of silicates from the Waldviertel, private collections were handed over in a grateful manner. In some show cases minerals of the Waldviertel are arranged according to their tectonic units. Series of quartz crystals (from Äpfelgschwendt, Loiwein, and Felling), pegmatite minerals (from Wanzenau, Horn, and the Königsalm), opals (from Waldkirchen) are on display.

Despite the large exhibition area, also the window niches are used to store large samples and a hardness scale according to Mohs and Rosiwal. Also a rock cleft is rebuilt.



Fig. 1 View to the main storage (room 3).

The relatively small display **Showroom 4** (10 m²) is dedicated exclusively to the Amethysts from the Waldviertel. Most of them are from Maissau, a small village about 10 km south of Eggenburg. A long time ago farmers when tilling the fields and mineral collectors became aware of Amethyst specimens often with an astonishing bright violet colour and sometimes large in size. The outcrop was excavated by the Krahuletz-Society in 1986 and 1988. The amethyst bearing quartz vein was rich in wonderful samples up to a size of some 0.2 m. Crystals (partly multiple zoned and exhibiting distinct varieties) are shown besides cut slices and polished specimens. Furthermore, finds from other localities in the Waldviertel are on display, among them are samples from Eggenburg, Grafenberg, Maigen, or Kautzen. Spectacular are amethyst sections in transmitted light. Two tubular showcases exhibit polished amethysts from Maissau and Eggenburg, respectively.



Fig. 2: The storage of minerals and rocks (room 5)

The collection **showroom 5 (Fig. 2)** (60 m²) hosts mineral and rock samples from the Waldviertel that came from former scientific investigations or result from new finds during constructions of roads or other buildings. They are exclusively reserved for scientific investigations in future. The samples stored here reflect the variety of minerals and rocks that can be found in the entire area. The rocksamples range from plutonites to sediments and metamorphites. Cuttings and mineral samples are stored in a systematic order in pull-out cabinets and drawer units. Furthermore, a working area for microscopic investigations, a stone cutting device and a storage of reference literature can be found here.

Opening hours: every 1st Saturday a month (10 am to 4 pm). Information: www.krahuletzmuseum.at. Contact: A. Rauscher (+43 66473571480). Steininger (Fritz.Steininger@senckenberg)

Rauscher A, Steininger F (2023): Kurzführer durch das Schaudépot für Mineralien und Gesteine der Krahuletz-Gesellschaft – 3730 Eggenburg, Museumsgasse 6. – Pub. Krahuletz-Ges. 2023/1: 29 S., 26 Abb., Raumplan, Verkehrsspinne.- Eggenburg (Krahuletz-Gesellschaft)

Crystal chemistry and structural transformations in Fe²⁺-bearing talc studied by Raman spectroscopy

L. Stoeck¹, S. Aspiotis^{1,2}, B. Mihailova¹

¹Department of Earth Sciences, University of Hamburg, Grindelallee 48, Hamburg, 20146, Germany

²Centre for the Study of Manuscript Cultures (CSMC), Cluster of Excellence 'Understanding Written Artefacts', University of Hamburg, Warburgstrasse 28, Hamburg, 20354, Germany
e-mail: lennard.stoeck@studium.uni-hamburg.de

High temperature behaviour of Fe²⁺-bearing hydrous silicates have recently gained much attention, because they are important reservoirs of water and can contribute into volatile cycling as well as into redox processes in the vicinity of subduction zones (Spandler et al. 2007; Bernardini et al. 2023), especially after the discovery of thermally induced reversible Fe²⁺ ↔ Fe³⁺ oxidation in Fe²⁺-bearing double-chain silicates, resulting in the activation of delocalized e⁻ and H⁺ with anisotropic mobility (Mihailova et al. 2021; Rösche et al. 2022). Therefore, Fe-bearing hydrous silicates with a strong anisotropic structure, such as amphiboles, can be an important factor to explain the occurrence of anisotropic conductivity anomalies in the lithosphere.

Talc (Mg₃Si₄O₁₀(OH)₂) is another rock-forming mineral with a highly anisotropic structure and significant implications in several fields, including petrology, geophysics and environmental science (Spandler et al. 2007). Besides talc is among the most important industrial minerals, because of its properties, such as chemical inertness, affinity for organic chemicals and hydrophobicity. These characteristics allow its use in several applications including paper coating, paint, cosmetics and polymer industries, for which the knowledge of the stability field of talc is critical (Ulian et al. 2014). So far temperature-induced changes in the structure and properties of talc have mostly been analyzed via X-ray diffraction, Fourier-transform infrared spectroscopy and thermogravimetry-differential scanning calorimetry (Liu et al. 2014).

In this contribution, we present (i) a new approach to quantify minor amounts of elements such as Fe and Mn in the octahedral sheets of talc using Raman spectroscopy (ii) results analyzing the temperature-induced changes in talc to gain further insight into the oxidation processes at high temperatures and structural transformations on an atomic level scale.

We analyzed a Fe²⁺-bearing sample from Zillertal in Austria, whose exact chemical formula (Mg_{2.93}Fe²⁺_{0.08}Ni_{0.01}Si_{4.04}OH_{1.81}O_{0.19}) was determined by electron microprobe analysis (Aspiotis et al., 2023). Spectra have been collected in two different sample orientations within the temperature range 150K-1400K in ranges from 15-1215cm⁻¹ and 3370-3770cm⁻¹.

We show that the Mg²⁺ (and Fe²⁺+ Mn²⁺) contents can be quantified by fractional intensities of the OH-stretching peaks assigned to various M1M2M2 local configurations as well as by the wavenumber of the MO₆-vibrational mode near 360 cm⁻¹ (Aspiotis et al., 2023). Heating/cooling experiments demonstrate that the Raman peak at 3660cm⁻¹ associated with the OH-Fe²⁺MgMg stretching mode vanishes at 1250K but recovers when cooling down to room temperature. This clearly indicates the occurrence of reversible oxidation mechanisms at least at 1250K, and the existence of delocalized charge carriers (e⁻ and H⁺). Upon further heating up to 1400K talc undergoes a structural breakdown, decomposing into clinoenstatite

(Wesołowski, 1984). Therefore, we prove the existence of the “oxo-state” for talc between 1250K and 1400K, where Fe^{2+} is oxidized into Fe^{3+} , without a structural breakdown.

The trends for Fe^{2+} -bearing talc will be compared to pure-Mg talc, which is currently being analyzed by in situ-temperature Raman spectroscopy.

Acknowledgements: The research for this study was funded by the Deutsche Forschungsgemeinschaft (DFG, German Research Foundation) under Germany’s Excellence Strategy – EXC 2176 ‘Understanding Written Artefacts: Material, Interaction and Transmission in Manuscript Cultures’, project no. 390893796. The research was conducted within the scope of the Centre for the Study of Manuscript Cultures (CSMC) at Universität Hamburg. We thank Stefanie Heidrich and Peter Stutz, Universität Hamburg, to help with WD-EMPA measurements and sample preparation. We are very grateful to the Mineralogical Museum, Hamburg for kindly providing the talc crystals.

- Aspöth S et al. (2023) Raman spectroscopy for crystallochemical analysis of Mg-rich layered silicates: serpentine and talc. - to be submitted to J Raman Spectr
- Bernardini S, Della Ventura G, Schlüter J, Mihailova B (2023): Thermally-activated electron hopping in Fe-rich amphiboles: Implications for the high-conductivity anomalies in subduction zones. - *Geochem* 83, 125942
- Liu X, Liu X, Hu Y (2014): Investigation of the thermal decomposition of talc.- *Clays Clay Miner* 62, 137-144
- Mihailova B, Della Ventura G, Waesermann N, Xu W, Schlüter J, Galdenzi F, Marcelli A, Redhammer GJ, Boiocchi M, Oberti R (2021): Atomistic insight into lithospheric conductivity revealed by phonon–electron excitations in hydrous iron-bearing silicates. - *Commun Mater* 2, 57
- Rösche C, Waesermann N, Petrova M, Malcherek T, Schlüter J, Mihailov B (2022): Oxidation processes and thermal stability of actinolite. - *Phys Chem Miner* 49, 47.
- Spandler C, Hermann J, Faure K, Mavrogenes JA, Arculus RL (2008): The importance of talc and chlorite “hybrid” rocks for volatile recycling through subduction zones; evidence from the high-pressure subduction mélange of New Caledonia. - *Contr Mineral Petrol* 155, 181-198
- Ulani G, Tosoni S, Valdrè CG (2014): The compressional behaviour and the mechanical properties of talc $[\text{Mg}_3\text{Si}_4\text{O}_{10}(\text{OH})_2]$: a density functional theory investigation. - *Phys Chem Miner* 41, 639-650
- Wesołowski M (1984): Thermal decomposition of talc: a review. - *Thermochim Acta* 78, 395-421

Micromorphology meets micro-XRF: A case study from the Iron Age site of Haselbach (Lower Austria)

F. Stuffer¹, S. Cereda², P. Tropper¹, P. Trebsche²

¹University of Innsbruck, Institute of Mineralogy and Petrography, 6020 Innsbruck, Austria

²University of Innsbruck, Institute of Archaeologies, 6020 Innsbruck, Austria

e-mail: peter.tropper@uibk.ac.at

In the context of this investigation a chemical characterization of archaeological sediments from Haselbach (Lower Austria) was carried out on six uncovered thin sections by means of micro-XRF analysis. The elemental mapping was carried out with a Bruker M4 Tornado. The analysed thin sections were collected at the boundary between the loess substrate and the fill (cultural layer) of different structures: five come from pit houses and one from a pit. Samples were first examined with a polarization microscope and, subsequently, “objects” of interest were selected to clarify their chemical composition.

The results of the micro-XRF analysis show the exact spatial distribution of the detected elements in thin section: aluminum (Al_2O_3), silicon (SiO_2), magnesium (MgO), calcium (CaO), iron (FeO), phosphorus (P_2O_5), potassium (K_2O), titanium (TiO_2), sulfur (SO_3), and manganese (MnO). False colour maps were also produced to enhance the relative concentration of the aforementioned elements. Furthermore, the objects found in the thin sections could be quickly identified, by combining their morphological characteristics with their elemental composition. They consist of: bone and pottery fragments, aggregates of trampled debris, charcoal, faecal remains, ashes and different types of pedofeatures.

Thanks to the elemental analysis it was also possible to determine that, in all six thin sections, the in-situ loess is mainly composed of the elements Al, Fe, K, Mn, Si, and Ti, while the fill deposits show increasing contents of the elements Ca, P and S. Both microscopic and chemical results show that organic matter occurs in the cultural layer, indicating the influence of humans and animals in the formation of these deposits. The loessy substrate, on the other hand, has remained largely untouched by human and animal activity. Specific archaeological questions, such as the actual use of the pit houses and the pit, could not be answered on the basis of these results alone. Further analyses (i.e., micromorphological and archaeological) are thus required for a comprehensive understanding of these built features.

In-situ $^{40}\text{Ar}/^{39}\text{Ar}$ dating of phenocrysts in the phonolite from Late Quaternary East Eifel Olbrück volcano

M. Sudo¹, U. Altenberger¹, C. Günter¹

*¹University of Potsdam, Institute of Geosciences, Potsdam, Germany
e-mail: msudo@geo.uni-potsdam.de*

Since 2002, University of Potsdam has started the $^{40}\text{Ar}/^{39}\text{Ar}$ dating laboratory with a CO_2 continuous laser and a pulsed Nd-YAG UV laser, then the in-situ $^{40}\text{Ar}/^{39}\text{Ar}$ dating has been applied to metamorphic rocks with 400-10 Ma ages. However, it was not well known to what extent in-situ $^{40}\text{Ar}/^{39}\text{Ar}$ dating was available to younger samples. In order to investigate the applicability of $^{40}\text{Ar}/^{39}\text{Ar}$ dating to very young samples, we used phonolite from Olbrück volcano, a late Quaternary monogenetic volcano group in the East Eifel, where Lippolt et al. (1990) had reported the presence of excess ^{40}Ar in nosean or hauyne in the phonolites. Sudo et al. (2014) reported for Ar isotopic ratio measurements on natural samples and also preliminary dating results of the first $^{40}\text{Ar}/^{39}\text{Ar}$ dating including assumptions, because the analyses were done more than one year after the neutron irradiation. Since then, three more neutron irradiations and $^{40}\text{Ar}/^{39}\text{Ar}$ dating have been done so far, then those results of the $^{40}\text{Ar}/^{39}\text{Ar}$ dating have been accumulated and are reported here.

For the samples for Ar isotope analyses, thick rock sections with a thickness of about 0.5 mm and a long diameter of up to 12 mm were prepared, then their surfaces were examined in detail by SEM-EDS. Then they are irradiated with fast neutrons for 4 h at the CLICIT facility of the OSTR nuclear reactor at the University of Oregon, USA. In-situ spot analysis of the sample surfaces was then carried out at the University of Potsdam using a UV pulse laser at a wavelength of 266 nm to determine the Ar isotope ratios. In most cases, one spot did not yield enough gas for targets of sanidine, leucite, nosean or groundmass parts, and in the case of nosean, up to 5-6 spots of 200 microns diameter laser irradiation was conducted for a single measurement.

The results of the dating by weighted averaged when they agree within error, as follows; sanidine: 0.42 ± 0.29 Ma ($N = 3$, error 1sigma), leucite: 0.08 ± 0.16 Ma ($N = 3$), groundmass 0.71 ± 0.17 Ma ($N = 2$). These ages agree with the Ar/Ar age of 0.41 ± 0.01 Ma by Lippolt within 2 sigma error from sanidine and leucite. In contrast, the nosean, in which the excess ^{40}Ar has been reported, yielded two results, done in two separate irradiations, as 3.14 ± 0.45 Ma ($N = 8$), 31.06 ± 4.1 Ma ($N = 5$) and one outlier 154.5 ± 11.2 Ma. The nosean ages by Lippolt et al. (1990) were 11.2-12.2 Ma, suggesting that the excess ^{40}Ar in nosean is heterogeneously distributed. Sudo et al. (2014) reported the existence of melt inclusions in the nosean and the concentration of Cl in them. This time the correlation was also observed between the excess ^{40}Ar and Cl-derived ^{38}Ar in nosean.

Lippolt HJ, Troesch M, Hess JC (1990): Excess argon and dating of Quaternary Eifel volcanism, IV. Common argon with high and lower-than atmospheric $^{40}\text{Ar}/^{36}\text{Ar}$ ratios in phonolitic rocks, East Eifel, F.R.G. - Earth Planet Sci Lett 101, 19-33

Sudo M, Altenberger U, Günter C (2014): In-situ Ar isotope, $^{40}\text{Ar}/^{39}\text{Ar}$ analysis and mineral chemistry of nosean in the phonolite from Olbrück volcano, East Eifel volcanic field, Germany: Implication for the source of excess ^{40}Ar . – Geophysical Research Abstracts, EGU General Assembly 2014

Don't drink that stuff: mineralogical constraints on the Ni-anomaly in waters from rock glaciers in the Ötztal Complex

P. Tropper¹, K. Krainer², G. Winkler³, G. Bertolotti², V. Schmit²

¹University of Innsbruck, Institute of Mineralogy and Petrography, 6020 Innsbruck, Austria

²University of Innsbruck, Institute of Geology, 6020 Innsbruck, Austria

³University of Graz, Institute of Earth Sciences, 8010 Graz, Austria

e-mail: peter.tropper@uibk.ac.at

The hydrology of intact rock glaciers is complex and mainly controlled by climatic factors (weather), bedrock composition, size, composition and internal structure. Rock glaciers may serve as aquifers, storing and releasing water over different timescales and thus are of increasing interest as reservoirs for drinking water supply. However, still little is known on the quality (chemistry) of water released from permafrost springs.

Increasing concentrations of ions and heavy metals were detected in two high Alpine lakes, which are impacted by meltwater from rock glaciers. During the last years, abnormally high Ni concentrations (and high concentrations of other elements such as Cu, Co Zn) high above the upper limit for drinking water were recorded from a number of springs released from intact rock glaciers and permafrost-related springs in the Ötztal Alps. High concentrations of Ni, Co, Zn, Mn, Fe and Al were recently recorded from permafrost ice of a core drilled on rock glacier Lazaun. It has previously been shown that creeks and high alpine lakes derived from intact rock glaciers and characterized by low water temperatures, high EC, high sulfate, Mg and Ca, and partly high metal concentrations display a significantly lower biodiversity compared to high alpine creeks and lakes that are not influenced by water derived from permafrost.

In this contribution, we concentrate on nickel because: (1) Ni in drinking water is a toxic heavy metal; (2) Ni occurs in concentrations high above the upper limit for drinking water that is at 0.02 mg/L according to the Drinking Water Regulation (Trinkwasserverordnung – TWV 2023) of the Austrian Government; and (3) Ni-minerals are so far unknown from the rocks of the Ötztal Complex.

In the course of this study, thin sections of paragneiss and amphibolite rock samples from the rock glaciers Krummgampen, Wannenkar and Lazaun were prepared and the minerals were analyzed using the electron probe microanalysis, with respect to their Ni contents. Petrographic investigations show that the mineral assemblage (silicates and sulfides) is heavily altered. Sulfides for instance are almost completely replaced by goethite and silicates such as garnet, biotite and staurolite show replacement by chlorite. The results show that the sulfides, namely pyrrhotite contain Ni contents of up to 1.2 wt.% NiO, chalcopyrite on the other hand contains much lower Ni contents of up to 0.2 wt.% NiO. Silicate minerals contain Ni concentrations below 0.1 wt.% NiO. With respect to additional heavy elements (Mn, Zn) present in the waters, garnet contains up to 10 wt.% MnO and staurolite contains up to 1.7 wt.% ZnO. These data show that in the absence of evidence for other heavy element sources, the altered mineral assemblage in the rocks from the rock glaciers are the most obvious source of these elements.

Non-ideal, but how non-ideal?

Low-temperature calorimetry of the Al-F-titanite – titanite solid solution

P. Tropper¹, E. Dachs², U. Troitzsch³

¹University of Innsbruck, Institute of Mineralogy and Petrography, 6020 Innsbruck, Austria

²University of Salzburg, Chemie und Physik der Materialien, 5020 Salzburg, Austria

³Research School of Physics, Australian National University, Canberra, Australia
e-mail: peter.tropper@uibk.ac.at

Al-rich titanite [Ca(Ti,Al)(O,F,OH)SiO₄] has been the focus of many previous mineralogical studies, because Al is one of the most common and abundant substituents for Ti in natural titanite. Moreover, the substitution appeared to be pressure and temperature dependent and thus could be of interest for geothermobarometry. The two coupled substitution reactions that account for the formation of Al-bearing titanite are: $\text{Ti}^{4+} + \text{O}^{2-} = \text{Al}^{3+} + \text{F}^-$ and $\text{Ti}^{4+} + \text{O}^{2-} = \text{Al}^{3+} + \text{OH}^-$. Hence Al-rich titanite is made up of the three end-members CaTiOSiO₄ [titanite], CaAlFSiO₄, and CaAlOHSiO₄ (vuagnatite).

Tropper et al. (2018) measured the heat capacity (C_P) data of Al-F-bearing titanite that yielded the standard entropy S°_{298} of F-Al-titanite CaAlFSiO₄ (FAT). C_P of synthetic FAT was measured with relaxation calorimetry and differential scanning calorimetry between 5 and 764 K. The results yielded $S^\circ_{298.15}$ to be 115.4 ± 2.0 J/(mol·K) and subsequently the standard Gibbs free energy of formation from the elements, $\Delta_f G^\circ$, of CaAlSiO₄F to be between -2583 ± 3.0 and -2588 ± 3.0 kJ/mol, and the standard enthalpy of formation from the elements, $\Delta_f H^\circ$, to lie between -2728 ± 3.0 and -2733 ± 3.0 kJ/mol, depending on the thermodynamic data retrieval approach.

This study focusses on the determination of the entropy of mixing along the F-Al-titanite – titanite join. The following compositions (X_{Ti}) were measured: 0.18, 0.33, 0.63, 0.77, 0.82, 0.91. The corresponding values of $S^\circ_{298.15}$ are: 120.2, 127.27, 126.66, 128.43, 127.55, and 130.84 J/(mol·K) \pm 1.6-1.8 J/(mol·K) (2σ). Calculation of the excess entropy S^{ex} yielded a positive deviation from ideality. Due to the scatter of the data and the relatively large errors in S^{ex} , it is possible to use a symmetrical as well as an asymmetrical fit through the data. For simplicity, a regular model was fit through the data in accordance with the regular activity model proposed by Tropper et al. (2002). The corresponding values of the entropic Margules parameter W_S is 28 ± 16 J/(mol·K). In conjunction with data on W_V and estimates on W_H , this value will be another step closer to the comprehensive formulation of a non-ideal activity model for the system Al-F titanite – titanite.

Tropper P, Troitzsch U, Dachs E Benisek A (2018): Heat capacity measurements of CaAlSiO₄F from 5 to 850 K and its standard entropy. - Amer Miner 103, 1165-1168

Analysis of Vickers indentation tests by means of Atomic Force Microscopy (AFM)

P. Vivanco-Chávez¹, M. Klichowicz², H. Lieberwirth², F. Mertens¹, O. Popov², G. Heide³

¹*Institute for Physical Chemistry, Technische Universität Bergakademie Freiberg*

²*Institute for Mineral Processing Machines and Recycling Systems Technology, Technische Universität Bergakademie Freiberg*

³*Institute for Minealogy, Technische Universität Bergakademie Freiberg
e-mail: Patricia-Ilein.Vivanco-Chavez@chemie.tu-freiberg.de*

The study of the mechanical properties of materials such as fracture toughness (K_{IC}) and Vickers hardness (VH), at micro/nanometric scales is scarce and at the same time a challenge to determine them. Therefore, this research shows a new methodology of analysis and insight in detail regarding the elastic/plastic behaviour of investigated materials with Vickers indenters. In this research five samples were analysed: a fused silica as reference material, a synthetic quartz crystal (SQ_L and SQ_X) and finally quartz grains from granite and granodiorite. A possible tool for the verification of the recorded indentation depths is Atomic Force Microscopy (AFM). Using an AFM allows to measure with great accuracy such as the length of the cracks (l), the depth of residual indentation (h_f) and the indentation marks (d), allowing to determine K_{IC} and HV with greater accuracy, i.e. at the nanoscale.

Keywords: Microhardness; Vickers Indentation; Quartz; Atomic Force Microscopy, Radial Cracks; Cone Crack; Palmqvist Cracks

Background: The importance of realistic modelling of the mechanic behaviour of mineral materials has increased due to its demand and contributions to mineral processing optimization and mining. These models rely on the accurate characterisation of mechanical properties, e.g. fracture toughness (K_{IC}) which characterises the resistance to unstable crack propagation under the crack opening. Since the theory and application of this parameter are described in standard textbooks like Anderson (2017) and Gross & Seelig (2018), the focus is set on the properties which are relevant for minerals, as well as the characterisation of different types of crack morphology that was first observed and analysed by Cook & Pharr (1990).









In contrast to macroscopic measurement approaches, the microscopic fracture toughness is calculated from the size of the cracks, which can be observed as a result of indentation hardness testing with a Vickers pyramid (for details see Roebuck et al. 2008 and ISO 28079:2009). To date, this method has been applied to hard metals (Palmqvist, 1957), technical non-metallic materials like glasses and ceramics (Cook & Pharr, 1990; Moradkhani et al. 2013), and rocks and minerals (Swain & Lawn, 1976; Whitney et al. 2007; Han et al. 2020).

However, this approach presents some challenges as the measurement quality of this parameter is affected by the difficulty of implementing this method on natural minerals, i.e. not all minerals show regular cracks after indentation (Whitney et al. 2007), the type of crack can often only be assumed based on literature references since different crack systems (Glandus et al. 1991), and the crack length measurements via microscope have low accuracy. Therefore, in this study, AFM is used to analyze with high precision the indentation marks and cracks caused by micro indentation tests with a Vickers indenter, thus, increasing the accuracy of mechanical property (K_{IC}) calculation.

Methods: The investigation of microhardness and fracture toughness of mineral phases was carried out using a Shimadzu HMV-G21DT Micro Vickers Hardness Tester, in which each sample underwent 30 indentation tests with a maximum load of $F = 980.7 \text{ mN}$ and a 15-second holding time. Subsequently, the indentation marks were analyzed with Park NX10 AFM to scan the sample surfaces, where the indentation diagonals (d_i) and crack length (l) are determined, and the final depth of the residual hardness impression (h_f) measured on scales ranging from micrometres to a few nanometers.

Results: The following is a synthesis of the crack morphologies found in this study (Table 1) and a summary comparison of the fracture toughness (K_{IC}) of this study with other authors (Figure 1).

Table 1. Summary classification of the different morphologies in the indented samples (30 indentations for each sample).

| Sample | Cracks Morphology | | | | | | | |
|------------------|---|---|---|---|---|---|---|---|
| |  |  |  |  |  |  |  |  |
| | No cracks | PRC | SRC | PRC + SRC | PCC | PCC + SRC | PRC + SCC | PRC + SRC + SCC |
| FS | 5 (16.6%) | - | 2 (6.6%) | - | 3 (10%) | 4 (13.3%) | 10 (33.3%) | 6 (20%) |
| SQ _{II} | - | 25 (83.3%) | - | 5 (16.6%) | - | - | - | - |
| SQ _I | - | 5 (16.6%) | - | 25 (83.3%) | - | - | - | - |
| Q-Gr | - | 10 (33.3%) | - | 20 (66.6%) | - | - | - | - |
| Q-Bg | - | 3 (10%) | 7 (23.3%) | 20 (66.6%) | - | - | - | - |

PRC = Primary Radial Cracks; SRC = Secondary Radial Cracks; PCC = Primary Cone Cracks; SCC = Secondary Cone Cracks

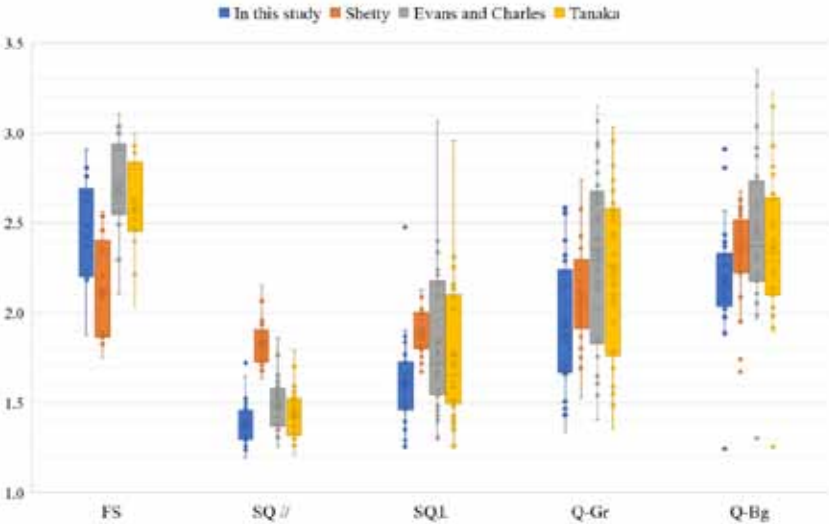


Figure 1. Comparison boxplot between the different K_{IC} values of the authors Deschamps et al. (2013), Tanaka (1987), Evans & Charles (1976) and this present study.

Conclusions:

- In this study, the characterization of the types of crack morphologies are both quantitatively and qualitatively determined (Table 1) and are consistent with models based on the literature review.
- Reconstruction of an indentation profile of the tested material based on the parameters of h_f and h_{max} is established, which is important to explain the elastic/plastic behaviour of the indented minerals.
- The fracture toughness (K_{IC}) values from this study agrees with the models of other authors (Figure 1), and this parameter is inversely proportional to the Vickers hardness (VH).

- Anderson TL (2017): Fracture mechanics: Fundamentals and applications. - Fourth ed, CRC Press Taylor & Francis Group: Boca Raton, Fla., London, New York, ISBN 9781498728133
- Roebuck B, Bennett E, Lay L, Morrell R (2008): Measurement good practice guide No. 9. - Palmqvist Toughness for Hard and Brittle Materials; Teddington, Middlesex, UK, TW11 0LW, ISBN 1368-6550
- Cook RF, Pharr GM (1990): Direct observation and analysis of indentation cracking in glasses and ceramics. - J Amer Ceram Soc 73, 787–817, doi:10.1111/j.1151-2916.1990.tb05119.x
- Evans AG, Charles EA (1976): Fracture toughness determinations by indentation. - J Amer Ceram Soc 59, 371–372, doi:10.1111/j.1151-2916.1976.tb10991.x
- Glandus JC, Rouxel T, Tai Q (1991). Study of the Y-TZP toughness by an indentation method. - Ceram Internat 17, 129–135, doi:10.1016/0272-8842(91)90041-W
- Gross D, Seelig T (2018): Fracture mechanics: With an introduction to micromechanics. - 3rd ed., Springer Internat Publ, Cham, ISBN 9783319710907.
- Han Q, Qu Z, Wang P, Bi G, Qu G (2020): Applications of micro-indentation technology to estimate fracture toughness of shale. - Materials (Basel) 13, doi:10.3390/ma13184208.
- International Organization for Standardization. ISO 28079 (2009): Hardmetals - Palmqvist toughness test (28079)
- Moradkhani A, Baharvandi H, Tajdari M, Latifi H, Martikainen J (2013): Determination of fracture toughness using the area of micro-crack tracks left in brittle materials by Vickers indentation test. - J Adv Ceram 2, 87–102, doi:10.1007/s40145-013-0047-z
- Palmqvist S (1957): Method att Bestamma Segheten hos Spread Material, Sarskit Hardmettaller. - Jernkontorets Annaler 141, 300–307
- Shetty DK, Wright IG, Mincer PN, Clauer AH(1985): Indentation fracture of WC-Co Cermets. - J Mater Sci 20, 1873–1882, doi: 10.1007/BF00555296
- Swain MV, Lawn BR (1976): Indentation fracture in brittle rocks and glasses. - Int J Rock Mechan Mining Sci Geomech Abstr 13, 311–319, doi:10.1016/0148-9062(76)91830-1
- Tanaka K (1987): Elastic/plastic indentation hardness and indentation fracture toughness: the inclusion core model. - J Mater Sci 22, 1501–1508. doi: 10.1007/BF01233154
- Whitney DL, Broz M, Cook RF (2007): Hardness, toughness, and modulus of some common metamorphic minerals. - Amer Mineral 92, 281–288, doi:10.2138/am.2007.2212

Petrological investigations on garnet-chlorite-mica schists of the Rossrugg and Hornkees (Zemmgrund, Zillertal)

S. Wagner¹, B. Zerobin², R. Köchl³, P. Tropper¹, G. Goldenberg²

¹*Institute of Mineralogy and Petrography, University of Innsbruck*

²*Department of Archaeologies, University of Innsbruck*

³*Department of History and European Ethnology, University of Innsbruck*
e-mail: simon.wagner@uibk.ac.at

Geologically, the Zemmgrund (Zillertal) is part of the Tauern Window and belongs tectonostratigraphically to the Venediger Duplex (Subpenninic Nappes). The garnet deposits occur locally on the Rossrugg and around the Hornkees glacier within ductile shear zones within the “Zentralgneisse”. Similar shear zones can be observed in other parts of the innermost Zillertal, for example, the Stilluptal. The garnet-bearing host-rocks can be described as chlorite-mica-schist, which formed during the alpine orogeny (Selverstone et al. 1991). Especially at the Rossrugg and Hornkees these garnets can reach sizes of several millimetres and are usually of good quality (few inclusions, beautiful red colour, etc.), which is why they were also used to produce garnet jewellery and are also very popular among mineral collectors.

The samples of the garnet-bearing chlorite-mica-schist have been taken directly from the historic mining site at the Rossrugg and the mineral site close to the Hornkees glacier. Both host rocks are mainly composed of Bt+Chl+Qz and show minor amounts of Fsp+Ms±Rt±Zrn±Ap±opaque phases. The garnets in this matrix show different sizes, often reaching several millimeters. Crack formation can also be observed depending on the thin section. The inclusion pattern of the garnets varies as well; typically, however, Chl+Ap+Zrn+Qz+Rt+Ilm can be found. Regarding their geochemical composition, garnets have been analysed with the help of μ -XRF, EPMA and LA-ICP-MS. Continuous zoning can be observed in all garnet samples, with the almandine component showing the largest proportions from 60 mol% (core) to 73 mol% (rim). The trace element distribution of Co, Zn, or Zr, for example, correlates with the pattern of the almandine component, whereas e.g., Ti shows a decreasing concentration from the core to the rim. The same can be observed for Y, whose distribution is already clearly visible in the distribution images generated with μ -XRF. HREEs, such as Yb or Lu, follow the same trend. The pressure and temperature of garnet formation have been calculated using *Thermocalc v.3.45* and the extension *TC_Comb* (Dolivo-Dobrovolsky 2023). The AveragePT calculations resulted in $T = 613 \pm 10$ °C and $P = 8.2 \pm 0.4$ kbar. Calculation of garnet isopleths using the program *Perplex* yielded garnet growth with decreasing pressures (approx. 8.9 kbar in the core and 7.7 kbar in the rim) and increasing temperatures (560 °C in the core and 590 °C in the rim). Additionally, pseudosection modelling [P-T, P-a(H₂O)] was done using *THERIAK-DOMINO* and the most current database *td-d62-mp50-05* (Tinkham 2022). The combination of geothermobarometry and thermodynamic modelling clearly shows that a (H₂O) greater than 0.6 must have been predominant. The obtained garnet ages (Lu-Hf-geochronology) of 32.5 Ma agree with the existing age data of the Alpine metamorphic event and correspond with the “Tauernkristallisation”.

Dolivo-Dobrovolsky D (2023): *TC_Comb* software

Selverstone J, Morteani G, Staude J-M (1991): Fluid channelling during ductile shearing: transformation of granodiorite into aluminous schist in the Tauern Window, Eastern Alps. - *J Metamorph Geol* 9, 419–431

Tinkham DK (2022): *td-ds62-mp50-05* database

Retrograde serpentinization and low-pressure metamorphic characteristics in the 3.8 Ga Isua Supracrustal belt, Greenland

J. Wolf¹, D. Sorger¹, S. Piazzolo², A.A.G. Webb³, T. Müller¹

¹*Geoscience Center Göttingen, Georg-August-University, Germany*

²*School of Earth and Environment, The University of Leeds, United Kingdom*

³*Division of Earth and Planetary Science and Laboratory for Space Research, University of Hong Kong, Hong Kong, China*
e-mail: j.wolf@stud.uni-goettingen.de

The Eoarchean Isua Supracrustal Belt (ISB) in West Greenland exposes one of the oldest rock records on Earth. Its tectonic setting is still subject of debate with interpretations ranging from plate tectonics to environments that are dominated by vertical tectonics. A first order question is the presence or absence of a metamorphic gradient within the belt. To that end, phase equilibria modeling combined with multiple geothermobarometric data convincingly suggested a homogeneous distribution of peak metamorphic conditions (550-600 °C; 0.8 - 1.0 GPa) (Ramírez-Salazar et al. 2021). However, recent studies of a dunite lens from the ISB suggested different metamorphic conditions varying from ultra-high pressure (Nutman et al. 2021) to low pressure deserpentinization (Guotana et al. 2022). In this study, we re-examine the petrography, mineral assemblages, reaction textures as well as the role of CO₂ in the metamorphism affecting ultramafic rocks from the specified lens B in the northwestern limb of the ISB. The texture of four different samples were analyzed using polarization microscopy, BSE imaging and EBSD measurements. Element x-ray maps and major element composition of major and accessory humite phases have been determined using EPMA. Phase equilibria modeling was done using the software package PerpleX to evaluate the role of CO₂.

Our petrographic observations show mineral assemblages of antigorite, olivine, magnesite, Ti-rich-humites and Fe-oxides. Antigorite (XMg = 0.99), magnesite, and Fe-oxide result from the breakdown reaction of olivine (XMg = 0.96). High forsterite content is interpreted to be the result of a hotter Archean mantle rather than deserpentinization. While the presence of accessory Ti-phases has been used as indicator for decompression through the breakdown reaction of Ti-chondrodite to form Ti-clinohumite, we present textural evidence of Ti-clinohumite being replaced by Ti-chondrodite pointing to a different reaction along a cooling path at lower pressures. The presence of carbonate instead of brucite highlights the role of CO₂ and its necessity to accurately describe phase relations for the metamorphic evolution of ultramafic rocks. Here, we present evidence from phase equilibria modeling, equally pointing to a simple cooling path at intermediate pressure conditions in agreement with metamorphic conditions obtained for the rest of the belt, rather than isothermal decompression from pressures higher than 2.0 GPa. The resulting lack of evidence for higher pressure conditions experienced by these mafic lenses thus removes a strong argument for the ISB to exhibit a metamorphic gradient, confirming the record of homogeneous metamorphic conditions within the belt.

- Guotana JM, Morishita T, Nishio I, Tamura A, Mizukami T, Tani K, Harigane Y, Szilas K, Pearson DG (2022): Deserpentinization and high-pressure (eclogite-facies) metamorphic features in the Eoarchean ultramafic body from Isua, Greenland. - *Geosci Front* 13, 101298, <https://doi.org/10.1016/j.gsf.2021.101298>
- Nutman AP, Scicchitano MR, Friend CRL, Bennett VC, Chivas AR (2021): Isua (Greenland) ~3700 Ma meta-serpentinite olivine Mg# and $\delta^{18}\text{O}$ signatures show connection between the early mantle and hydrosphere: Geodynamic implications. - *Precambrian Res.* 361, 106249, <https://doi.org/10.1016/j.precamres.2021.106249>
- Ramírez-Salazar A, Müller T, Piazzolo S, Webb AAG, Hauzenberger C, Zuo J, Haproff P, Harvey J, Wong TK, Charlton C (2021): Tectonics of the Isua Supracrustal Belt 1: P-T-X-d Constraints of a Poly-Metamorphic Terrane. - *Tectonics* 40, e2020TC006516. <https://doi.org/10.1029/2020TC006516>

Unravelling the formation history of the Maronia Skarn, NE Greece: Insights from melilite group minerals

M. Zeug¹, A. Repstock², P. Voudouris³, H. Gevorgyan⁴, H. Schleicher⁵

¹ Landesamt für Geologie und Bergwesen Sachsen-Anhalt,
Fliederwegkaserne 13, 06130 Halle, Saale, Germany

² Geological Survey and Geophysics, Sächsisches Landesamt für Umwelt,
Landwirtschaft und Geologie, Pillnitzer Platz 3, 01326 Dresden, Germany

³ Department of Mineralogy and Petrology, National and Kapodistrian University of Athens,
University Campus-Zografou, 15784, Athens, Greece

⁴ Institute for Mineralogy, TU Bergakademie Freiberg, Brennhausgasse 4, 09599 Freiberg

⁵ Mineralogisch-Petrographisches Institut, Universität Hamburg, Grindelallee 48, 20146 Hamburg, Germany
e-mail: manuela.zeug@sachsen-anhalt.de / manuela.zeug@univie.ac.at

The Maronia skarn is situated in the northern region of the Aegean Sea, approximately 25 km west of Alexandroupolis in northeastern Greece. During the Oligocene (29.8 Ma) the Maronia pluton (monzonite, quartz monzonite, monzogabbro) intruded into Mesozoic metasediments of the Circum Rhodope Belt (Schaarschmidt et al. 2021). This intrusive event led to the development of a remarkable skarn mineralisation within the western metamorphic aureole caused by the contact between the pluton and the adjacent marbles. The western contact aureole extends 3km in length and up to 100m in width.

Skarn zones between the pluton and the marble were identified based on mineral assemblages and the chemical composition of granditic garnet, which is present in each skarn zone. Garnet crystals of the western contact aureole of the Maronia skarn correspond to the grossular-andradite solid solution series. The Maronia skarn contains a variety of unusual and remarkable mineralisation, including (i) Ti-Zr-Cr-rich garnet crystals, which occurrence is possibly unique worldwide (Voudouris & Katerinopoulos 2004, Katerinopoulou et al. 2009), (ii) predominantly Ti-rich dark brown andradite crystals (2–6 wt% TiO₂) that contain subhedral to euhedral titanite crystals [CaTi(SiO₄)O] in the core, and (iii) andradite-rich garnet (2–8 wt% TiO₂) within a melilitic skarn that contain perovskite (CaTiO₃) in the core. The skarn mineral assemblages (e.g. Ti-rich garnet, melilite, perovskite) in both the endoskarn and the exoskarn indicate a development in a silica-undersaturated magmatic environment (cf. Russel et al. 1999).

Melilite group minerals are restricted to the exoskarn and refer to gehlenite (Ca₂Al[AlSiO₇])-åkermanite (Ca₂Mg[Si₂O₇]) solid solution series. Various stages of skarn formation can be identified based on the appearance of the melilite solid solutions, which are reflected in four different zones in the Maronia exoskarn. The first zone is fine-grained consisting of clinopyroxene, interstitial melilite, and andradite-rich garnet, which may contain perovskite cores. This fine-grained zone is assumed to be closest to the pluton. The adjacent zone consists of almost tabular, slightly rounded cube-shaped crystals associated with interstitial andradite-rich garnet (2–8 wt% TiO₂) with or without perovskite-cores (Fig. 1). These melilite crystals are closer in composition to gehlenite suggesting a formation of a high-temperature skarn (Deer et al. 1992; Katona et al. 2003; Marinacea et al. 2011, and references therein) at a formation temperature exceeding 900°C in the prograde stage of skarn formation (cf. Mposkos & Doryphoros 1993). In the following zone melilite crystals show zoning with a gehlenitic core and an åkermanitic rim indicating the initial retrograde stage (cf. Reverdatto et al. 1979). Next to the latter zone, melilite solid solutions are completely replaced by vesuvianite representing a late retrograde stage during the cooling down at temperatures below melilite stability (~ 675 °C, Mposkos & Doryphoros 1993). Results of the

present study show that melilite crystals can be used to reveal the different stages of Maronia skarn evolution.

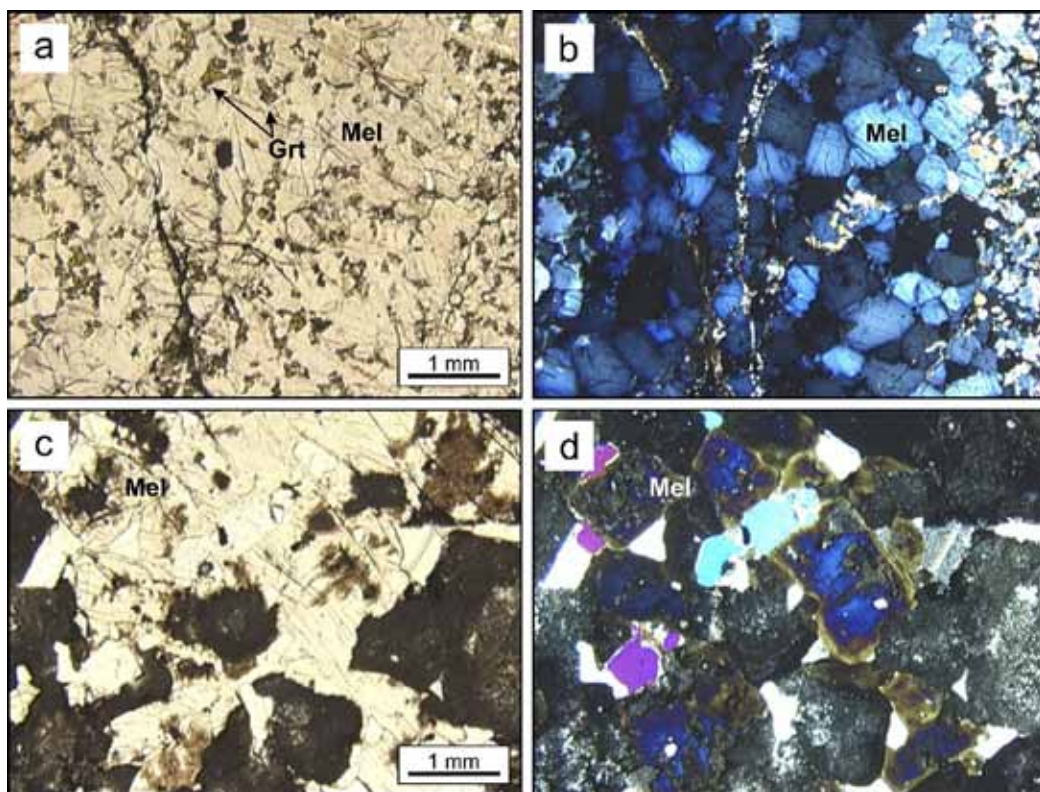


Figure 1. Plane-polarised (a and c) and cross-polarised (c and d) transmitted light photomicrographs of melilite zones in the Maronia skarn. The melilite in a and b is closer to the gehlenite endmember, suggesting a formation in the prograde stage. The melilite in c and d shows clear zonation of a gehlenite-rich core surrounded by an åkermanite-rich rim, which indicates an initial retrograde stage of skarn formation. Foto: M. Zeug

- Deer WA, Howie RA, Zussman J (1992): *An Introduction to the Rock-Forming Minerals* (second ed.). Longman, Hong Kong
- Katerinopoulou A, Katerinopoulos A, Voudouris P, Bieniok A, Musso M, Amthauer G (2009): A multi-analytical study of the crystal structure of unusual Ti–Zr–Cr-rich Andradite from the Maronia skarn, Rhodope massif, western Thrace, Greece. - *Miner Petrol* 95, 113–124
- Katona I, Pascal M-L, Fonteilles M, Verkaeren J (2003): The melilite (Gh50) skarns at Oravița, Banat, Romania: transition to gehlenite (Gh85) and to vesuvianite. *Can. Mineral.* 41, 1255–1270
- Marincea S, Dumitraș D-G, Ghineț C (2011) Gehlenite from three occurrences of high-temperature skarns, Romania: New mineralogical data
- Mposkos E, Doryphoros K (1993): High temperature skarns in the Maronia area (NE Greece). - *Bull Geol Soc Greece*, 23–35
- Reverdatto VV, Pertsev NN, Korolyuk VN (1979): P-T-Evolution and origin of zoning in melilite during the regressive stage of contact metamorphism in carbonate-bearing rocks. *Contrib Miner Petr* 70, 203–208
- Russell JK, Dipple GM, Lang JR, Lueck B (1999): Major-element discrimination of titanian andradite from magmatic and hydrothermal environments: an example from the Canadian Cordillera. *Europ J Miner* 11, 919–935
- Schaarschmidt A, Klemd R, Regelous M, Voudouris PC, Melfos V, Haase KM (2021) The formation of shoshonitic magma and its relationship to porphyry-type mineralisation: the Maronia pluton in NE Greece. *Lithos* 380–381, 105911
- Voudouris P, Katerinopoulos A (2004): New occurrences of mineral megacrysts in Tertiary magmatic-hydrothermal and epithermal environments in Greece. *Documenta Naturae* 151, 1–21